

# **Engineered Heart Tissues for Cardiovascular Disease Modeling**

**Beatriz Assunção Gamelas**

Thesis to obtain the Master of Science Degree in

## **Biological Engineering**

Supervisors: Dr. Marcelo Catarino Ribeiro  
Prof. Tiago Paulo Gonçalves Fernandes

### **Examination Committee**

Chairperson: Prof. Maria Margarida Fonseca Rodrigues Diogo  
Supervisors: Prof. Tiago Paulo Gonçalves Fernandes  
Members of the Committee: Prof. Carlos André Vitorino Rodrigues

**December 2020**



# Preface

The work presented in this thesis was performed at the Applied Stem Cell Technologies (AST) Group, Faculty of Science and Technology, of the University of Twente (Enschede, The Netherlands), during the period February-October 2020, under the supervision of Dr. Marcelo Catarino Ribeiro (Post Doc), and within the frame of the Erasmus+ programme. The thesis was co-supervised at Instituto Superior Técnico by Prof. Tiago Paulo Gonçalves Fernandes.

I declare that this document is an original work of my own authorship and that it fulfils all the requirements of the Code of Conduct and Good Practices of the Universidade de Lisboa.



# Acknowledgements

I want to start by expressing my gratitude to Prof. Dr. Robert Passier for welcoming me to the team and giving me the chance to develop a work I enjoyed so much. To Dr. Marcelo Ribeiro, thank you for all the knowledge, guidance, patience and advises throughout the entire process, I am sure they will be very useful throughout my entire personal and professional life. To Tom van Iddekinge, a huge thank you for all the help in the work developed, it wouldn't be possible without you. I would also like to thank the entire AST group for all the guidance and help provided throughout my entire internship.

To José, Tom Boonen, Eline and Luuk for all the help, making the lab fun, becoming my friends and making me laugh every day while "on the job". You really made me forget I was so far away from home in difficult times.

To my new family in The Netherlands, Ioana and Jacob, I couldn't have asked for better housemates. All the movies, series, walks, parties and laughs made me feel at home and I am so grateful I got to meet two wonderful and warm people I will adore and cherish for life. To Lucas, Eveline and Michael, my deepest gratitude for all the support and love you gave me.

A special thanks to Prof. Tiago Fernandes, for all the help, advise, encouragement and guidance during my internship.

To my family, specially my parents, grandparents and siblings, for being my safe haven, for making me who I am today and believing in me no matter what. It wouldn't be possible without your love, unconditional support and ability to motivate me to carry on in difficult moments.

To my friends from Aveiro, my oldest ones, who have been there through thick and thin and are a crucial part of this journey, a huge thank you for all the years we have been together. Ana, Joana, Marta, Morgana, Rafaela, Telma (because "É as pessoas que somos"), Zé, André, Rúben and Sara: you also helped shape who I am and I am sure we will be together for many years to come.

To my friends in Lisbon, there are no words to describe the times we've had together and how lucky I am to have met you. You made college one of the best experiences of my life and I will never forget all the support, laughs, movies and series marathons, study sessions (of course with a lot of procrastination), parties and help in tougher times. Chica, Clara, Irina, Madalena, Marta and Sofia, you have become my Lisbon family and I know we'll always be there for each other. My little Filipa, Daniela and Pedro, you have also helped me more than you know.

Finally, I would like to thank Ricardo for all the love, daily support and for motivating me to become the best version of myself every day.



## Abstract

Cardiovascular diseases are the leading cause of disability and death worldwide, representing a major economic burden in healthcare systems. Heart failure (HF) and hypertrophic cardiomyopathy (HCM) are amongst the most severe of these conditions and currently there is no effective cure for them. Although several animal or 2D models have been developed and used in preclinical drug trials, they lack accuracy when it comes to mimic the native 3D cardiac microenvironment, leading to failure in predicting disease phenotype and drug toxicity.

The urgent demand for new 3D *in vitro* models, coupled with human stem cell biology breakthroughs, have allowed the successful generation of engineered heart tissues (EHTs) and advanced the fields of disease modelling, drug development and regenerative medicine. Particularly, Human Induced Pluripotent Stem Cells (hiPSCs), when differentiated into cardiomyocytes (hiPSC-CMs), are the best stem cell type to recapitulate cardiomyocyte physiology.

In this project, a fibrin-based platform was used to simulate HCM by generating EHTs with isogenic hiPSC lines that only differed in a single nucleotide mutation in the MYBPC3 gene (the most common cause of HCM, this gene encodes for myosin binding protein C, crucial for sarcomere organisation and cardiac muscle contraction). Furthermore, the platform was used to simulate HF after long-term exposure of tissues composed by hiPSC-CMs to norepinephrine.

The platform was able to successfully replicate key aspects of both diseases, particularly contractile dysfunction that is also observed in human patients, which may help to find their pathomechanisms and new and efficient therapeutics.

**Keywords:** Engineered Heart Tissues, Cardiovascular Disease Modeling, Human Induced Pluripotent Stem Cells (hiPSCs), Hypertrophic Cardiomyopathy, Heart Failure.



## Resumo

Atualmente, as doenças cardiovasculares são a principal causa de morte a nível mundial, exercendo uma enorme pressão nos sistemas de saúde. A falência cardíaca e cardiomiopatia hipertrófica destacam-se como condições particularmente severas e até à data não há cura para ambas, apenas tratamentos paliativos. Embora vários modelos animais e 2D tenham sido desenvolvidos e utilizados em ensaios pré-clínicos para o desenvolvimento de novos fármacos, estes não replicam exatamente o ambiente cardíaco humano 3D, levando a falhas na previsão da eficácia desses fármacos e no fenótipo de doenças.

A necessidade crescente de novos modelos 3D *in vitro*, aliada aos avanços na área da biologia das células estaminais humanas, permitiu o desenvolvimento da engenharia de tecidos cardíacos como plataforma para modelação de doenças, desenvolvimento de fármacos e estratégias de medicina regenerativa. Particularmente, as células estaminais pluripotentes humanas induzidas (hiPSCs), quando diferenciadas em cardiomiócitos, são as que melhor replicam a fisiologia dos cardiomiócitos.

Neste projeto, recorreu-se a uma plataforma para modelar aspetos da cardiomiopatia hipertrófica, comparando tecidos cardíacos 3D gerados com linhas celulares isogénicas de hiPSCs, diferenciados em cardiomiócitos e apenas diferindo numa mutação no gene MYBPC3 (este gene codifica para uma proteína essencial na modelação da contração cardíaca). Adicionalmente, a plataforma foi utilizada para simular falência cardíaca, através de exposição prolongada dos tecidos cardíacos a noradrenalina.

Esta plataforma conseguiu modelar com sucesso aspetos-chave de ambas as condições, particularmente a disfunção cardíaca também observada em pacientes humanos, provando ser útil para a descoberta de patomecanismos e na descoberta de novas curas eficientes.

**Keywords:** Engenharia de Tecidos Cardíacos, Modelação de Doenças Cardiovasculares, Células Estaminais Pluripotentes Humanas Induzidas (hiPSC), Cardiomiopatia Hipertrófica, Insuficiência Cardíaca.



# Contents

<b>Abstract</b>	<b>iii</b>
<b>Resumo</b>	<b>v</b>
<b>List of Tables</b>	<b>ix</b>
<b>List of Figures</b>	<b>xi</b>
<b>Acronyms</b>	<b>xv</b>
<b>1 Introduction</b>	<b>1</b>
1.1 Cardiovascular diseases . . . . .	1
1.1.1 Overview . . . . .	1
1.1.2 Heart failure . . . . .	1
1.1.3 Hypertrophic cardiomyopathy . . . . .	2
The role of MYBPC3 in hypertrophic cardiomyopathy . . . . .	3
1.2 Disease models . . . . .	4
1.2.1 Pharmacology and <i>in vivo</i> models for heart failure and hypertrophic cardiomyopathy	4
1.2.2 <i>In vitro</i> models for heart failure and hypertrophic cardiomyopathy . . . . .	5
Models using human Pluripotent Stem Cells (hPSCs) . . . . .	5
2D vs. 3D models . . . . .	6
hiPSC-CMs maturation . . . . .	6
1.2.3 3D Cardiac Tissue Engineering Models . . . . .	8
Strategies for Engineered Heart Tissues . . . . .	8
EHTs as a platform for numerous studies . . . . .	13
1.2.4 modeling cardiovascular diseases with EHTs . . . . .	14
Heart Failure . . . . .	14
Hypertrophic cardiomyopathy and the role of MYBPC3 in this disease . . . . .	15
<b>2 Project Purposes</b>	<b>17</b>
<b>3 Materials and Methods</b>	<b>19</b>
3.1 Design and Fabrication of the PDMS Anchoring System . . . . .	20
3.1.1 Preparation of the PDMS and Replica Moulding . . . . .	20
3.1.2 PDMS Cantilevers Painting . . . . .	21
3.1.3 PDMS Cantilevers Plating . . . . .	22
3.1.4 PDMS Part Air Plasma Treatment . . . . .	23
3.2 Generation of Fibrin-based Engineered Heart Tissues . . . . .	23
3.2.1 hiPSC-CMs and hiPSC-FBs used for EHT making . . . . .	23

3.2.2	Making of the casting mould . . . . .	24
3.2.3	Generation of the EHTs . . . . .	25
3.2.4	Maintenance of the EHTs and Drug Adding . . . . .	26
3.3	Monitoring contractile function of EHTs and Data Analysis . . . . .	26
3.4	Fluorescence-Activated Cell Sorting Analysis (FACS) . . . . .	27
3.5	Statistical Analysis . . . . .	27
<b>4</b>	<b>Results and Discussion</b>	<b>29</b>
4.1	MYBPC3 Assay . . . . .	30
4.1.1	Horse serum-based experiments . . . . .	30
4.1.2	Serum-free Experiments . . . . .	34
	FACS Analysis and its Implications . . . . .	34
	Comparison between EHTs generated with the healthy and mutated cell lines . . .	39
4.2	Drug Induced Heart Failure Model . . . . .	41
<b>5</b>	<b>Conclusions and Future Perspectives</b>	<b>49</b>
	<b>Bibliography</b>	<b>50</b>
<b>A</b>	<b>Appendix A: Preparation of the CM High Gluc+TDI Medium</b>	<b>57</b>
<b>B</b>	<b>Appendix B: Preparation of the CM Low Ins+Low Gluc+TDI+Lact Medium</b>	<b>59</b>
<b>C</b>	<b>Appendix C: Calculation Formula for Contraction Force Based on Pillar Deflection</b>	<b>61</b>
<b>D</b>	<b>Appendix D: Drug Induced Heart Failure Assay- Measurements for Tissues from Experiments 1 and 2 before and after incubation with norepinephrine</b>	<b>63</b>

# List of Tables

4.1	Contraction force, contraction velocity and relaxation velocity obtained for EHTs made with the different cell lines when supplemented with CM Low Ins+Low Gluc+TDI+Lact+HS Medium, with the respective units. . . . .	30
4.2	Contraction force per area obtained for EHTs made with the different cell lines when supplemented with CM Low Ins+Low Gluc+TDI+Lact+HS Medium, with the respective units. . . . .	31
4.3	Contraction/Relaxation time at 10% and 90% obtained for EHTs made with the different cell lines when supplemented with CM Low Ins+Low Gluc+TDI+Lact+HS Medium. All the values are in milliseconds. . . . .	33
4.4	FACS analysis results reflecting the content of cardiomyocytes (% CM) from each batch of cells used to generate the different groups of EHTs from the FLB cell line and the MYBPC3 mutant line. This cardiomyocyte content is crucial to know the success rate of lactate purification treatment. . . . .	34
4.5	Contraction force of EHTs generated in each group with the FLB and MYBPC3 mutant cell lines. All values are in $\mu\text{N}$ . . . . .	35
4.6	Contraction velocity of EHTs generated in each group with the FLB and MYBPC3 mutant cell lines. All values are in $\mu\text{N/s}$ . . . . .	36
4.7	Relaxation velocity of EHTs generated in each group with the FLB and MYBPC3 mutant cell lines. All values are in $\mu\text{N/s}$ . . . . .	37
4.8	CT10, CT90, RT10, RT90 of EHTs generated in each group with the FLB and MYBPC3 mutant cell lines. All values are in milliseconds. . . . .	38
4.9	Contraction force, contraction velocity and relaxation velocity obtained for EHTs made with the different cell lines supplemented with CM Low Ins+Low Gluc+TDI+Lact Medium, with the respective units. . . . .	39
4.10	Contraction/Relaxation time at 10% and 90% obtained for EHTs made with the different cell lines supplemented with CM Low Ins+Low Gluc+TDI+Lact Medium. All the values are in milliseconds. . . . .	41
4.11	Contraction force values for EHTs from both experiments. All values are in $\mu\text{N}$ . . . . .	43
4.12	Contraction velocity values for EHTs from both experiments. All values are in $\mu\text{N/s}$ . . . . .	44
4.13	Relaxation velocity values for EHTs from both experiments. All values are in $\mu\text{N/s}$ . . . . .	44
4.14	CT10, CT90, RT10, RT90 values for EHTs from Experiment 1. All values are in milliseconds. . . . .	46
4.15	CT10, CT90, RT10, RT90 values for EHTs from Experiment 2. All values are in milliseconds. . . . .	47
A.1	Formulation of the CM High Gluc Medium with all its components discriminated, along with suppliers for ordering and the quantities to add for a final volume of medium of 1000 mL. . . . .	57

B.1	Formulation of the CM Low Ins Medium with all its components discriminated, along with suppliers for ordering and the quantities to add for a final volume of medium of 1000 mL.	59
D.1	Contraction force values of tissues from Experiments 1 and 2, before and after daily drug administration for 7 days. All values are in $\mu\text{N}$ .	64
D.2	Contraction velocity values of tissues from Experiments 1 and 2, before and after daily drug administration for 7 days. All values are in $\mu\text{N/s}$ .	64
D.3	Relaxation velocity values of tissues from Experiments 1 and 2, before and after daily drug administration for 7 days. All values are in $\mu\text{N/s}$ .	65
D.4	CT10 values of tissues from Experiments 1 and 2, before and after daily drug administration for 7 days. All values are in milliseconds.	66
D.5	CT90 values of tissues from Experiments 1 and 2, before and after daily drug administration for 7 days. All values are in milliseconds.	67
D.6	RT10 values of tissues from Experiments 1 and 2, before and after daily drug administration for 7 days. All values are in milliseconds.	68
D.7	RT90 values of tissues from Experiments 1 and 2, before and after daily drug administration for 7 days. All values are in milliseconds.	69

# List of Figures

1.1	Overview of the structural and functional differences when comparing a healthy heart and one that suffers from diastolic or systolic heart failure. . . . .	2
1.2	Overview of the structural differences when comparing a healthy heart and one that suffers from hypertrophic cardiomyopathy. . . . .	3
1.3	Comparison between the myocardial cellular arrangement of a <b>(A)</b> healthy heart and <b>(B)</b> a heart that suffers from hypertrophic cardiomyopathy. . . . .	3
1.4	Schematic representation of MYBPC. . . . .	4
1.5	Schematic illustration of the different methods that promote hiPSC-CMs maturation, by recapitulating the <i>in vivo</i> microenvironment. . . . .	7
1.6	Schematic illustration of different casting moulds for hydrogel encapsulation techniques, in order to develop EHTs. . . . .	9
1.7	Exposing the PDMS surface to a reactive air plasma introduces polar silanol groups, which makes it more hydrophilic and suitable for experiments. . . . .	10
1.8	Schematic representation of fibrin gel formation, catalysed by thrombin. Thrombin promotes the release of fibrinopeptides (FpA and FpB), which in turn allows the interaction and assembly of the fibrinogen chains, leading to the formation of the first protofibrils. Fibrin-hydrogel is formed by lateral aggregations between protofibrils. . . . .	11
1.9	Schematic illustration of two methods to harvest CMs in culture and generate 3D tissues: enzymatic treatment, which causes the disruption of proteins in the ECM and damage of the cells; cell sheet technology, where temperature reduction causes the detachment of intact monolayers of cell to cell connections, with ECM included. 3D cardiac tissues are developed by stacking the sheets on top of each other. . . . .	12
1.10	Schematic illustration of the decellularisation/recellularisation technique of a heart. . . . .	13
1.11	Schematic illustration of the necessary steps to generate an EHT and the different fields that benefit from this 3D construct. . . . .	14
1.12	Schematic illustration of the different disease models developed, in the last years, to study hypertrophic cardiomyopathy phenotypes, with their respective advantages, disadvantages and readouts. . . . .	16
3.1	Bottom view of two wells in a standard 12-well culture plate, where three engineered heart tissues have been generated per well, cultured between two PDMS flexible cantilevers. . . . .	19
3.2	Schematic representation of the PDMS part that anchors the fibrin-based miniaturised EHTs. . . . .	20
3.3	Photograph of the Teflon mould after solidification in the oven, which enables the fabrication of thirty PDMS parts at a time. . . . .	21
3.4	Photographs of a PDMS part after being taken out of the Teflon mould, cut and trimmed. . . . .	21
3.5	Photographs of a PDMS part after the tip of the pillars has been painted black and cured in the oven. . . . .	22

3.6	Top view ( <b>top picture</b> ) and bottom view ( <b>center picture</b> ) of the plater that allows to make the plates for each pillar. The <b>bottom picture</b> shows a close-up of the bottom part. . . . .	22
3.7	Photographs of different perspectives of a PDMS part after plating. . . . .	23
3.8	Photographs of the PMMA holder ( <b>left picture</b> ) and of the Teflon spacer ( <b>center picture</b> ). . . . .	24
3.9	Photograph of the agarose mould after solidification. . . . .	25
3.10	Exemplary contraction pattern of an EHT displaying contraction force over time with pacing at 1,5 Hz. . . . .	27
4.1	Bottom view of an engineered heart tissue cultured between the two PDMS cantilevers. . . . .	29
4.2	Comparison between <b>(A)</b> contractile force, <b>(B)</b> contraction velocity and <b>(C)</b> relaxation velocity of the engineered heart tissues generated with the FLB (control) and the MYBPC3 mutant cell lines. . . . .	30
4.3	Comparison between force per area of the engineered heart tissues generated with the FLB (control) and the MYBPC3 mutant cell lines. . . . .	31
4.4	Relaxation velocity of the engineered heart tissues generated with the FLB (control) and the MYBPC3 mutant cell lines if the maximum of the dataset (an outlier value) is removed from the statistical analysis. . . . .	32
4.5	Contraction time at <b>(A)</b> 10% and <b>(B)</b> 90% and relaxation time at <b>(C)</b> 10% and <b>(D)</b> 90% for tissues generated with the FLB (control) and the MYBPC3 mutant cell lines. . . . .	33
4.6	Contraction force obtained for the EHTs generated in each group with the <b>(A)</b> FLB cell line and <b>(B)</b> MYBPC3 mutant cell line. . . . .	35
4.7	Contraction velocity obtained for the EHTs generated in each group with the <b>(A)</b> FLB cell line and <b>(B)</b> MYBPC3 mutant cell line. . . . .	36
4.8	Relaxation velocity obtained for the EHTs generated in each group with the <b>(A)</b> FLB cell line and <b>(B)</b> MYBPC3 mutant cell line. . . . .	36
4.9	Contraction time at 10% obtained for the EHTs generated in each group with the <b>(A)</b> FLB cell line and <b>(B)</b> MYBPC3 mutant cell line. . . . .	37
4.10	Contraction time at 90% obtained for the EHTs generated in each group with the <b>(A)</b> FLB cell line and <b>(B)</b> MYBPC3 mutant cell line. . . . .	37
4.11	Relaxation time at 10% obtained for the EHTs generated in each group with the <b>(A)</b> FLB cell line and <b>(B)</b> MYBPC3 mutant cell line. . . . .	38
4.12	Relaxation time at 90% obtained for the EHTs generated in each group with the <b>(A)</b> FLB cell line and <b>(B)</b> MYBPC3 mutant cell line. . . . .	38
4.13	Comparison between <b>(A)</b> contractile force, <b>(B)</b> contraction velocity and <b>(C)</b> relaxation velocity of the engineered heart tissues generated with the FLB (control) and the MYBPC3 mutant cell lines. . . . .	39
4.14	Contraction time at <b>(A)</b> 10% and <b>(B)</b> 90% and relaxation time at <b>(C)</b> 10% and <b>(D)</b> 90% for EHTs generated with the FLB (control) and the MYBPC3 mutant cell lines. . . . .	40
4.15	Top view of the wells used to culture EHTs in CM Low Ins+Low Gluc+TDI+Lact Medium to study the effects of three different NE concentrations: 10 $\mu$ M, 50 $\mu$ M and 100 $\mu$ M, when compared to control tissues. . . . .	42
4.16	Contraction force obtained after incubating the tissues for 7 days with the different drug concentrations (10 $\mu$ M, 50 $\mu$ M and 100 $\mu$ M) when compared to control tissues, for <b>(A)</b> Experiment 1 and <b>(B)</b> Experiment 2. . . . .	42
4.17	Contraction velocity values obtained after incubating the tissues for 7 days with the different drug concentrations (10 $\mu$ M, 50 $\mu$ M and 100 $\mu$ M) when compared to control tissues, for <b>(A)</b> Experiment 1 and <b>(B)</b> Experiment 2. . . . .	43

4.18	Relaxation velocity obtained after incubating the tissues for 7 days with the different drug concentrations (10 $\mu$ M, 50 $\mu$ M and 100 $\mu$ M) when compared to control tissues, for <b>(A)</b> Experiment 1 and <b>(B)</b> Experiment 2. . . . .	44
4.19	Contraction time at 10% obtained after incubating the tissues for 7 days with the different drug concentrations (10 $\mu$ M, 50 $\mu$ M and 100 $\mu$ M) when compared to control tissues, for <b>(A)</b> Experiment 1 and <b>(B)</b> Experiment 2. . . . .	45
4.20	Contraction time at 90% obtained after incubating the tissues for 7 days with the different drug concentrations (10 $\mu$ M, 50 $\mu$ M and 100 $\mu$ M) when compared to control tissues, for <b>(A)</b> Experiment 1 and <b>(B)</b> Experiment 2. . . . .	45
4.21	Relaxation time at 10% obtained after incubating the tissues for 7 days with the different drug concentrations (10 $\mu$ M, 50 $\mu$ M and 100 $\mu$ M) when compared to control tissues, for <b>(A)</b> Experiment 1 and <b>(B)</b> Experiment 2. . . . .	46
4.22	Relaxation time at 90% obtained after incubating the tissues for 7 days with the different drug concentrations (10 $\mu$ M, 50 $\mu$ M and 100 $\mu$ M) when compared to control tissues, for <b>(A)</b> Experiment 1 and <b>(B)</b> Experiment 2. . . . .	46
D.1	Contraction force obtained 10 days after culturing <b>(before)</b> and after incubating the tissues for 7 days with norepinephrine <b>(after)</b> . From left to right, the graphs depict Control, 10 $\mu$ M, 50 $\mu$ M and 100 $\mu$ M tissues, from Experiment 1 (top row) and Experiment 2 (bottom row). .	63
D.2	Contraction velocity obtained 10 days after culturing <b>(before)</b> and after incubating the tissues for 7 days with norepinephrine <b>(after)</b> . From left to right, the graphs depict Control, 10 $\mu$ M, 50 $\mu$ M and 100 $\mu$ M tissues, from Experiment 1 (top row) and Experiment 2 (bottom row). . . . .	64
D.3	Relaxation velocity obtained 10 days after culturing <b>(before)</b> and after incubating the tissues for 7 days with norepinephrine <b>(after)</b> . From left to right, the graphs depict Control, 10 $\mu$ M, 50 $\mu$ M and 100 $\mu$ M tissues, from Experiment 1 (top row) and Experiment 2 (bottom row). . . . .	65
D.4	Contraction time at 10% obtained 10 days after culturing <b>(before)</b> and after incubating the tissues for 7 days with norepinephrine <b>(after)</b> . From left to right, the graphs depict Control, 10 $\mu$ M, 50 $\mu$ M and 100 $\mu$ M tissues, from Experiment 1 (top row) and Experiment 2 (bottom row). . . . .	66
D.5	Contraction time at 90% obtained 10 days after culturing (before) and after incubating the tissues for 7 days with norepinephrine (after). From left to right, the graphs depict Control, 10 $\mu$ M, 50 $\mu$ M and 100 $\mu$ M tissues, from Experiment 1 (top row) and Experiment 2 (bottom row). . . . .	67
D.6	Relaxation time at 10% obtained 10 days after culturing <b>(before)</b> and after incubating the tissues for 7 days with norepinephrine <b>(after)</b> . From left to right, the graphs depict Control, 10 $\mu$ M, 50 $\mu$ M and 100 $\mu$ M tissues, from the Experiment 1 (top row) and Experiment 2 (bottom row). . . . .	68
D.7	Relaxation time at 90% obtained 10 days after culturing <b>(before)</b> and after incubating the tissues for 7 days with norepinephrine <b>(after)</b> . From left to right, the graphs depict Control, 10 $\mu$ M, 50 $\mu$ M and 100 $\mu$ M tissues, from the Experiment 1 (top row) and Experiment 2 (bottom row). . . . .	69



# Acronyms

*2D* Two-Dimensional.

*3D* Three-Dimensional.

*ATP* Adenosine Triphosphate.

*CICR* Calcium Induced Calcium Release.

*CM* Cardiomyocyte.

*CT* Contraction Force.

*CT10* Contraction Time at 10%.

*CT90* Contraction Time at 90%.

*CV* Contraction Velocity.

*CVD* Cardiovascular Disease.

*DEX* Dexamethasone.

*DMEM* Dulbecco's Modified Eagle Medium.

*ECM* Extracellular Matrix.

*EHM* Engineered Heart Myocardium.

*EHT* Engineered Heart Tissue.

*ESC – CMs* Embryonic Stem Cell- derived cardiomyocytes.

*FACS* Fluorescence-Activated Cell Sorting Analysis.

*HCM* Hypertrophic Cardiomyopathy.

*HF* Heart Failure.

*HOCM* Hypertrophic Obstructive Cardiomyopathy.

*HS* Horse Serum.

*HighGluc* High Glucose.

*ICD* Implantable Cardioverter-Defibrillator.

*IGF – 1* Insulin-like Growth Factor 1.

*Lact* Lactate.

*LowGluc* Low Glucose.

*LowIns* Low Insulin.

*MLCK* Myosin Light Chain Kinase.

*MSC* Mesenchymal Stem Cell.

*MYBPC* Myosin Binding Protein C.

*NE* Norepinephrine.

*PDMS* Polydimethylsiloxane.

*PEB* Protein Extraction Buffer.

*PMMA* Poly(methyl methacrylate).

*RT10* Relaxation time at 10%.

*RT90* Relaxation time at 90%.

*RV* Relaxation Velocity.

*SEM* Standard Error of the Mean.

*SNS* Sympathetic Nervous System.

*T3* Triiodothyronine.

*TCA* Tricarboxylic Acid Cycle.

*TDI* T3 hormone + Dexamethasone + IGF-1.

*fps* frames per second.

*hESC* human Embryonic Stem Cell.

*hPSC* Human Pluripotent Stem Cell.

*hiPSC* human induced Pluripotent Stem Cell.

*hiPSC – CM* human induced Pluripotent Stem Cell- derived Cardiomyocytes.

*hiPSC – FBs* human induced Pluripotent Stem Cell-derived fibroblasts.

*mRNA* messenger RNA.

# Chapter 1

## Introduction

### 1.1 Cardiovascular diseases

#### 1.1.1 Overview

Cardiovascular disease (CVD) is a broad term for conditions that affect the heart or blood vessels, in what concerns their structure and/or function <sup>[1]</sup>. There are many different types of CVDs, such as peripheral arterial disease, coronary or congenital heart disease, angina, arrhythmia, pericarditis or hypertrophic cardiomyopathy. In spite of the heart's ability to trigger compensatory mechanisms in some of these CVDs, if not properly aided or treated, these types of diseases often lead to heart failure and even death.

Although the underlying mechanisms differ depending on the disease, there are some common risk factors that can increase the chances of a person develop a CVD, such as high cholesterol, high blood pressure, diabetes, smoking, obesity, lack of exercise or a family history of CVDs <sup>[1]</sup>.

According to the World Health Organization, CVDs are the primary cause of global deaths (about 31%), taking an estimated 17,9 million lives each year, with a high prevalence in the male gender when compared to the female one <sup>[2]</sup>. Particularly in Europe, in 2017, approximately 3,9 million people died due to CVDs annually, which accounts for 45% of all deaths <sup>[3]</sup>. Due to these numbers, cardiovascular healthcare constitutes a significant proportion of total health care expenditure of most countries worldwide <sup>[4]</sup>.

#### 1.1.2 Heart failure

Heart failure (HF) is a clinical syndrome caused by functional and structural defects in the myocardium, resulting in the inability of blood ejection or ventricular filling. Thus, its primary features are the heart's inability to pump sufficient blood to meet the metabolic demands of the body (which may lead to the disruption of all major body functions) <sup>[5]</sup> or stiffening of the heart muscle (which reduces or prevents blood flow to the heart) <sup>[6]</sup>.

Some of the major pathogenic mechanisms that cause HF are genetic mutations, accelerated apoptosis, abnormal myocyte calcium cycling or ischemia-related dysfunction <sup>[5]</sup>. The most common cause for this illness is reduced left ventricular myocardial function, but dysfunction of the endocardium, pericardium, myocardium, great vessels or heart valves alone or in combination is also associated with heart failure.

This illness can be classified as predominantly right ventricular (impeding blood pumping to the lungs so it can collect oxygen), left ventricular (preventing the body from getting enough oxygen-rich blood) or

biventricular, based on the location of the deficit, as well as systolic or diastolic. Regarding the time of onset, it may be an acute (short-term) or chronic (ongoing) condition [7].

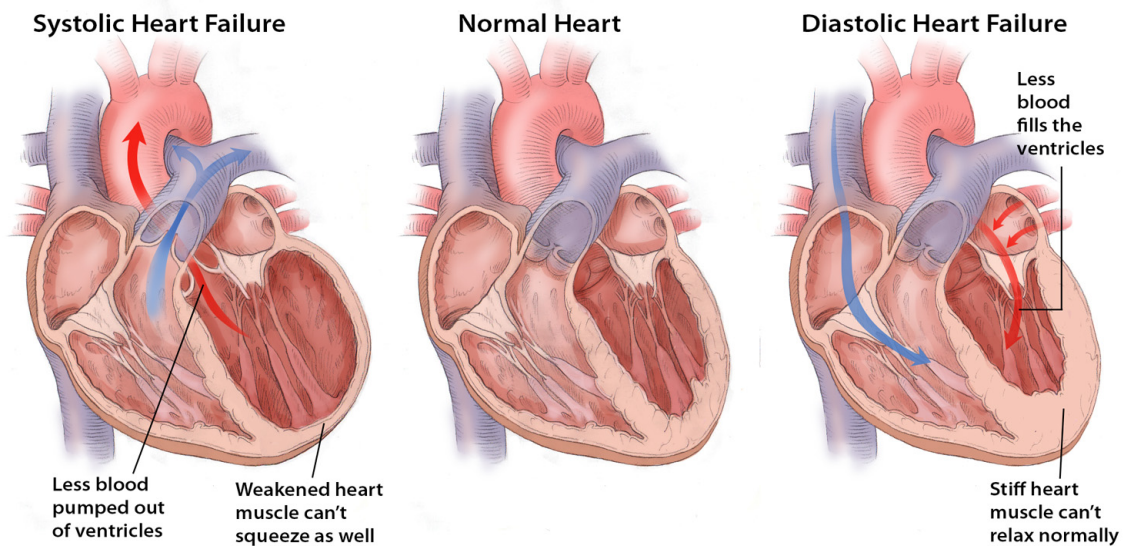


Figure 1.1: Overview of the structural and functional differences when comparing a healthy heart and one that suffers from diastolic or systolic heart failure [8].

In Europe, in 2015, this condition was the leading cause of hospitalisation in people over the age of 65 and, overall, approximately 15 million people lived with it. These circumstances exert a serious economic toll on patients and in healthcare systems [9].

The treatment of this illness depends on its severity and cause, and most approaches focus on disease management rather than curing heart failure, since there is presently no cure for it. However, most mild cases can be prevented with behavioural and lifestyle changes, such as exercising more often, medication, a healthy diet or by avoiding smoking [5].

### 1.1.3 Hypertrophic cardiomyopathy

Hypertrophic cardiomyopathy (HCM) is the most common genetically inherited cardiomyopathy, characterized by abnormal thickening of certain parts of the heart muscle (such as the septum, apex and right or left ventricles) and mitral valve changes due to cardiomyocyte (CM) enlargement.

Commonly, thickening of the myocardium occurs at the septum, the muscular wall that separates the right and left side of the heart. A thickened septum causes a narrowing that can reduce or block the blood flow, from the left ventricle to the aorta, forcing the ventricles to pump harder to overcome this narrowing. This type of condition is called hypertrophic obstructive cardiomyopathy (HOCM).

When stiffness occurs in the left ventricle, pressure inside the heart increases and this particular chamber becomes smaller and is incapable to relax normally and fill with blood, which results in a lower pumping of oxygen-rich blood to the rest of the muscles and organs. Another consequence of this thickening is the disruption of the proper function of the mitral valve, causing outflow obstruction and leakage of the blood back to the left atrium [10].

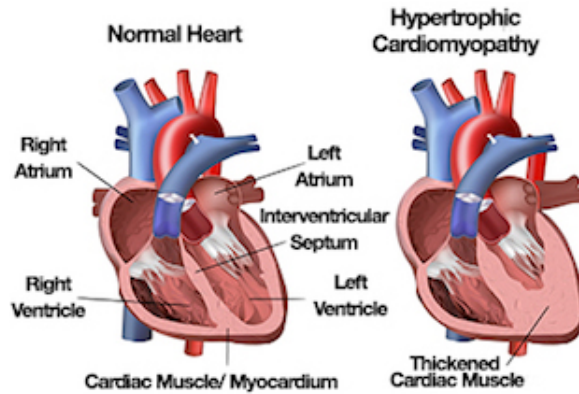


Figure 1.2: Overview of the structural differences when comparing a healthy heart and one that suffers from hypertrophic cardiomyopathy <sup>[11]</sup>.

In patients with HCM, it is possible to observe cardiac histological changes, since there is evident hypertrophy, irregularity and disarray of the cardiomyocytes, instead of being parallel and organised (Figure 1.3), along with interstitial fibrosis of varying degrees. As a possible consequence of this disarray, the electric signals that travel through the lower chambers of the heart become abnormal, leading to arrhythmias <sup>[12]</sup>.

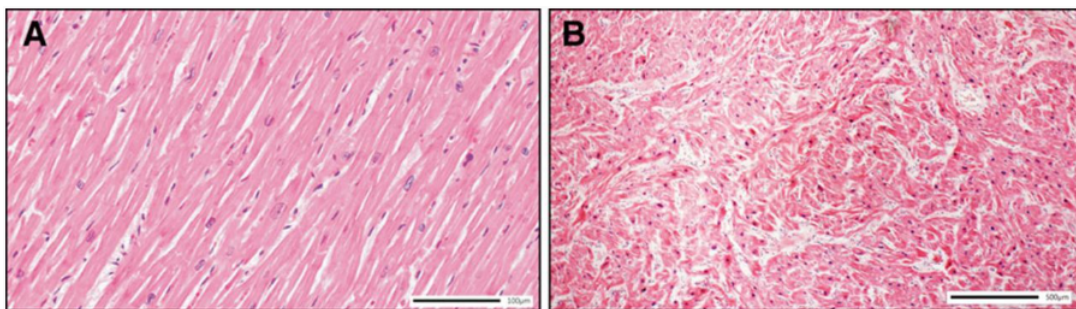


Figure 1.3: [adapted] Comparison between the myocardial cellular arrangement of a **(A)** healthy heart and **(B)** a heart that suffers from hypertrophic cardiomyopathy <sup>[12]</sup>.

By 2018, it was estimated that approximately 20 million people worldwide, from over 122 countries, suffered from HCM <sup>[13]</sup>. Although the majority of patients show no symptoms and consequent disturbances in their lives, others may experience serious arrhythmias, shortness of breath and inability to exercise. Furthermore, HCM is also an important cause of sudden cardiac death, particularly in adolescents, young adults and athletes <sup>[12]</sup>.

HCM is not a curable disease and the primary goals of treatment are to reduce symptoms and prevent sudden death.

### The role of MYBPC3 in hypertrophic cardiomyopathy

Hypertrophic cardiomyopathy is the most common monogenic cardiac disease and is usually caused by a mutation in one of the genes that encode a protein from the sarcomere, Z-disc or intracellular calcium modulators. Some of the most common disease genes for HCM are MYL2, MYL3, TPM1, ACTC1 or MYH7 <sup>[14]</sup>. However, mutations in cardiac myosin binding protein C (MYBPC), encoded by the MYBPC3 gene are the most common cause of HCM <sup>[15]</sup>. MYBPC3 mutations are inherited in an autosomal dominant manner, although *de novo* mutations may also occur.

Most of MYBPC3 variations lead to premature termination codons responsible for mRNA (messenger RNA) degradation and consequent reduction in MYBPC synthesis in HCM patient hearts [15].

MYBPC is a flexible, rod-like protein, that is a key component of the heart's basic contractile unit, the sarcomere. Within it, MYBPC's C-terminal C10 domain strongly binds to the myosin filament backbone and its N-terminal domains bind to either the actin filament or myosin head, to control calcium-activated sliding, that powers cardiac muscle contractility (Figure 1.4). Thus, MYBPC is crucial for sarcomere organisation and its phosphorylation increases the availability of myosin heads for interaction with actin, thus enhancing and modulating cardiac muscle contraction [15].

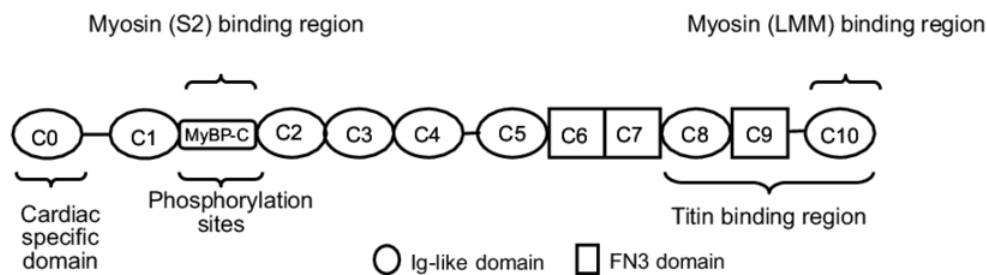


Figure 1.4: [adapted] Schematic representation of MYBPC [16].

For sarcomeric genes, the majority of the mutations identified are single nucleotide substitutions and, for most genes, it is believed that the consequent mutant protein incorporated into the sarcomere exerts a poisoned peptide effect (antimorphic mutations). The only exception is the MYBPC3 gene, in which the mutations are usually insertions or deletions that lead to a truncated protein, that consequently loses its function. Thus, in this case, HCM appears to be caused by a haploinsufficiency mechanism [17].

When it comes to Z-disk or calcium modulators genes, the specific mechanism is yet to be clarified, since most mutations are single substitutions, but it is not clear whether the illness is caused by haploinsufficiency or negative dominance.

Several studies suggest that mutations in the MYBPC3 gene, with a consequent abnormality in MYBPC, lead to a higher myofibrillar  $Ca^{2+}$  sensitivity, with a consequent defect in intracellular  $Ca^{2+}$  handling, phosphorylation of some proteins and sarcoplasmic reticulum  $Ca^{2+}$  reuptake. Since higher  $Ca^{2+}$  sensitivity is the constant molecular malformation in HCM, it is deduced that MYBPC3 mutations increase myofibrillar  $Ca^{2+}$  sensitivity, and this condition is necessary and sufficient to increase the probability of arrhythmias and induce HCM [14][18].

## 1.2 Disease models

### 1.2.1 Pharmacology and *in vivo* models for heart failure and hypertrophic cardiomyopathy

As aforementioned, both HF and HCM have no cure yet and treatments only delay disease progress, ease symptoms or prevent death. For HF, primary treatments consist of pharmacological approaches, mainly with beta-blockers or angiotensin-converting enzyme inhibitors [7]. As for HCM, medication to slow the heart rate, relax the heart muscle (so that the heart can pump more efficiently) or control the heart rhythm may be an option, but surgical options are also included, such as a septal myectomy (where a part of the thickened septum is removed) or an implantable cardioverter-defibrillator (ICD), which is implemented like a pacemaker that continuously monitors a patient's heartbeat and delivers electrical shocks when arrhythmias occur and to restore a normal heart rhythm [10].

Nowadays, most of the preclinical trials (which help predict proarrhythmic side effects of drugs), engineered cardiac models developed for cardiac repair purposes and disease modeling or genetic causation studies are performed using animal models, since *in vivo* interventions carry unacceptably high risks for humans.

Models using small animals such as mice allow larger sample sizes, are generally cheaper and less space-demanding, offer a greater variety of transgenic models and the procedure is relatively simple requiring little instrumentation. However, small mammals have distinct ion channels, much higher heart rates and the small size of their organs also pose constraints on experiments.

As an alternative, large animal models, using dogs, pigs, sheep (in cases of heart failure<sup>[19]</sup>) or cats (in cases of hypertrophic cardiomyopathy<sup>[20]</sup>) have also been developed to study these diseases, since they bear a closer resemblance to human cardiovascular physiology. Nevertheless, these models are subjected to stricter regulations, have higher costs, labor, maintenance and inherent ethical and cultural issues.

For both small and large animal models, there are naturally crucial physiological and genomic differences when compared to the human heart and, as a consequence, the models fail to predict accurately the toxicity of drugs for cardiomyocytes or the disease phenotype.

Hence, in order to reduce morbidity and mortality rates, as well as the pressure in healthcare systems associated to heart failure and hypertrophic cardiomyopathy, it is essential to invest in the development and improvement of dependable engineered cardiac *in vitro* models, capable of mimicking the physiology and structure of the human heart for drug development, disease modeling and cardiac repair, as well as other clinical applications.

## 1.2.2 *In vitro* models for heart failure and hypertrophic cardiomyopathy

### Models using human Pluripotent Stem Cells (hPSCs)

The rising need for new *in vitro* models that mimic the human heart, coupled with the advancement of human stem cell biology, have had a significant impact in drug development, disease modeling and regenerative medicine fields, with more accurate results in terms of resemblance and prediction, when compared to animal models.

In the last decade, the primary goal was to discover the optimal source of functional and beating cardiomyocytes in order to develop a reliable *in vitro* cardiac model. Initially, early cardiac tissue depended on primary cells isolated from multiple species or immortalized human cell lines.

Nowadays, these models make use of differentiated pluripotent stem and progenitor cells. Similarly, Mesenchymal Stem Cells (MSCs), bone marrow and endogenous cardiac stem cells were vastly used for this purpose, but their suboptimal capability for cardiac differentiation and low yield have limited their clinical use<sup>[21][22]</sup>. Today, the best *in vitro* cardiac models make use of human Pluripotent Stem Cells (hPSCs), including human Embryonic Stem Cells (hESCs) and human induced Pluripotent Stem Cells (hiPSCs), since these two stem cell types are the ones that best recapitulate human CM physiology (when it comes to molecular, mechanical, metabolic, ultrastructural and electrophysiological properties) and pathology<sup>[23]</sup>.

In spite of the huge potential of hESCs (since these cells can specialize in all cell types), there are still lots of ethical issues when it comes to their embryo origin, which limits their application worldwide<sup>[24]</sup>.

Thus, hiPSCs have been the primary go-to tool when it comes to *in vitro* cardiac models. Furthermore, human induced Pluripotent Stem Cell-derived cardiomyocytes (hiPSC-CMs) were also found to recapitulate phenotypic characteristics caused by genetic mutations. Using genome-editing methods,

such as CRISPR, libraries of disease-specific CMs can be generated, making these cells a valuable source for drug testing, disease modeling, gene therapy and personalized medicine [23] [22].

Since a large number of disease often result in failure of one or multiple organs with a complex pathophysiology, *in vitro* models also provide the chance of studying the interaction between different cell types and manipulate tightly regulated mechanisms, mimicking organ to organ interaction [22].

## **2D vs. 3D models**

Nowadays, *in vitro* cardiac models are conducted using two-dimensional (2D) or three-dimensional (3D) cultures. Each one of these models has advantages and disadvantages when used in certain essays, making it essential to decide beforehand which organotypic characteristics and parameters are to be included in a particular project.

Standard 2D *in vitro* cardiac systems consist of adherent cells on flat surfaces, such as multi-well plates, flasks or petri dishes and are a successful technique to inspect cells in established conditions or expand cell lines. These models possess ample literature available, offer the possibility of comparison with previous studies, are relatively simple and less time consuming to handle, study and offer the option to use relatively effortless methods of analysis [25].

Even though 2D models have helped to expose several cellular mechanisms that take place in the human heart, they do not accurately mimic what happens in the native cardiac 3D microenvironment. The human heart is composed of non-myocytes and cardiomyocytes with specific cellular interaction, anisotropic tissue structure, extracellular matrix (ECM) network, circulation and vascularization. As soon as 2D cell cultures are expected to respond to drugs, signaling modifiers or toxins, the results are misleading, due to their lack of ability to recapitulate biological cell interactions and mechanical dynamic of the *in vivo* microenvironment [23].

Furthermore, hiPSC-CMs obtained with 2D cultures resemble immature cardiomyocytes, with decreased force of contraction, lower expression of specific cardiac genes, morphological (such as random sarcomere structures) and electrophysiological (mainly affecting calcium handling) differences, when compared to mature cardiomyocytes [26].

Although not as standardised, 3D *in vitro* models have proven to overcome some of these limitations and have enormous potential when it comes to tissue engineering, cardio-toxicology and drug development [25]. In spite of some obstacles, such as the higher cost, reproducibility, difficulty related to manual handling or obtaining data at a cellular or sub-cellular level when compared to 2D models, researchers are working towards improving these models due to their enormous potential to replicate the 3D cardiac native environment and act as a platform for numerous studies [25].

## **hiPSC-CMs maturation**

Since one of the unresolved issues, when it comes to *in vitro* models using hiPSCs, is that hiPSC-CMs often remain immature when compared to adult cardiomyocytes [27], several methods have been proven effective in promoting hiPSC-CMs maturation. These techniques are essential to guarantee that these cell types can be fully utilized for pharmacological and toxicological screening, as well as cardiovascular disease modeling along with reliable results. The introduction of 3D cultures that resemble the *in vivo* cardiac physiological conditions has been a major step forward, but this alone is not enough to mimic the complex cardiac *in vivo* environment, therefore different combinations of several strategies are being under scrutiny (Figure 1.5).

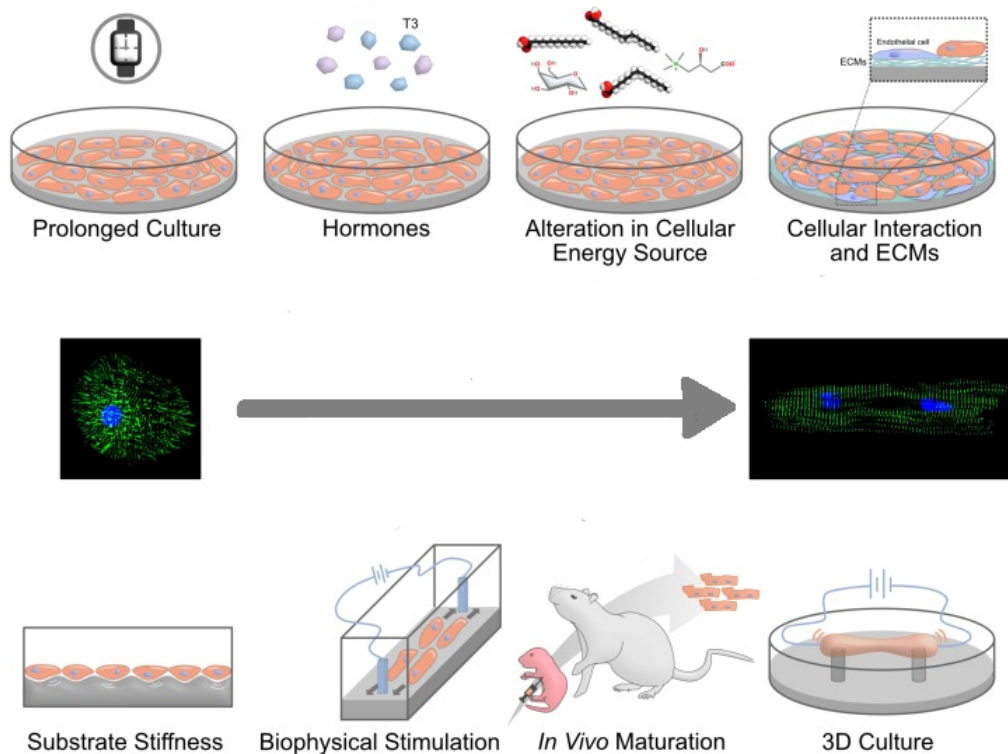


Figure 1.5: [adapted] Schematic illustration of the different methods that promote hiPSC-CMs maturation [27], by recapitulating the *in vivo* microenvironment.

Of the methods displayed in the figure, there are two important ones that require further explanation: alteration in cellular energy source and the addition of hormones or soluble factors.

- **Alteration in cellular energy source**

When cultured in a medium with glucose, hiPSC-CMs rely mostly on glycolysis to meet its metabolic demands. However, culturing these cells in a non-glucose medium enriched with galactose or fatty acids forces them to shift to oxidative phosphorylation for ATP generation. Since CM maturation *in vivo* has been associated to a transition from an embryonic-like glycolytic to an adult-like oxidative metabolism [28], adapting hiPSC-CMs to a non-glucose medium, enriched with galactose or fatty acids, aids in their *in vitro* maturation.

In addition, in a glucose-depleted or low glucose culture medium supplemented with lactate, cardiomyocytes are able to use the lactate in Krebs cycle metabolism to obtain ATP and survive, unlike non-CMs, which allows to purify a culture and enrich it with hiPSC-CMs and eliminate non-CMs [29].

Nevertheless, after CMs adaptation to the new energetic source, whether galactose, fatty acids or lactose, glucose should not be dismissed from the culture medium, since these cells also rely on the glycolytic pathway, *in vivo*, to produce ATP.

- **Addition of soluble factors**

When it comes to the addition of certain soluble factors, triiodothyronine (T3) hormone, dexamethasone (DEX) and insulin-like growth factor 1 (IGF-1) provide important biochemical cues to promote hPSC-CM *in vitro* maturation.

T3 hormone is known to play an essential role in cardiac development and cardiovascular physiology, by enhancing the expression of several cardiac genes involved in the maturation of cardiomyocytes' electrophysiological properties and calcium handling. T3-treated hiPSC-CMs actually show

a higher degree of maturation, exhibiting a larger cell size, longer sarcomere length, increased maximal mitochondrial respiration capacity, higher contractile force generation and enhanced calcium handling properties <sup>[30]</sup>.

A major limitation of hiPSC-CMs use is the lack of t-tubule formation. T-tubules are organized invaginations in the cardiomyocyte sarcolemma, critical for the coordinated "calcium induced calcium release" (CICR) that underlies systematic excitation-contraction coupling in human ventricular myocardium. Reduced t-tubule formation contributes to deficient excitation-contraction coupling in HF and may be the cause for ventricular arrhythmias. When treated with a combination of T3 hormone and dexamethasone (a glucocorticoid essential for maturation of fetal heart structure and function), cultured hiPSC-CMs develop an extensive functional t-tubule network, leading to uniform CICR and efficient excitation-contraction coupling, characteristic of healthy adult ventricular myocardium. Thus, this combination aids in hiPSC-CMs maturation <sup>[31]</sup>.

Lastly, IGF-1 has a critical role in cardiomyocyte growth, proliferation, metabolism and survival, by activating specific signaling pathways such as the phosphoinositide 3-kinase/Akt (PI 3-kinase/Akt) *in vitro*. A carefully regulated IGF-1 signaling is then required for the proper maturation and development of the heart, making this growth factor a potential precursor for the promotion of hPSC-differentiated cardiomyocytes maturation *in vitro* <sup>[32]</sup>.

### 1.2.3 3D Cardiac Tissue Engineering Models

#### Strategies for Engineered Heart Tissues

Keeping in mind the goal to mimic normal tissue organization *in vitro* and the study of cell to cell interactions and heart muscle function, under normal and pathological states, several methods have been developed to generate 3D cardiac tissues. Tissue generation can be accomplished by pursuing two different strategies: by engineering the 3D organization with the aid of chemical or technical means or by taking advantage of the ability of cardiomyocytes to beat spontaneously and internally assemble and form 3D organized structures <sup>[25]</sup>.

This last strategy (the most commonly used), coupled with techniques that help to shape certain constructs with the wished geometry, size or other characteristics allow the development of engineered heart tissues (EHTs).

The EHT model was conceived in the 2000s and, since then, a lot of different EHT production systems have been developed, coupled with other technologies such as microfluidics, micro patterns or adapted microscopes and software for live imaging. Nowadays, some of the most common techniques to produce EHTs are hydrogel encapsulation, prefabricated matrices, cell sheet technology and recellularisation of decellularised heart tissues <sup>[33]</sup>.

With the intent to better reproduce the composition of the human heart and cellular interaction, most of EHT protocols have currently standardised the addition of non-myocytes (such as fibroblasts, smooth muscle or endothelial cells) to tissues, when compared to protocols using only purified cardiomyocytes. Furthermore, these cell types have also shown to stimulate contractile force generation <sup>[22]</sup> (which also aids in cardiac maturation, as expressed in Figure 1.5).

In spite of some disadvantages, such as the large number of cells per tissue required, the necessity of intense manual labour, frailness, uneven distribution of cells or limited diffusion of nutrients and oxygen, EHTs are still a better option in terms of viability and invariability of results when compared to the other 3D cell culture model used, spheroids, to perform several assays, such as direct force measurement <sup>[25]</sup>.

Although this does not recapitulate the natural *in vivo* cardiac environment, most EHTs models still rely on the supplementation of the maintenance medium with horse serum (HS), usually at 10% (v/v),

since HS increases cardiomyocyte viability and contractile activity by providing nutrients, hormones and growth factors, improving the duration of culture time [34].

- **Hydrogel Encapsulation**

Presently, the most used technique to produce *in vitro* EHTs is through hydrogel encapsulation, a relatively simple technology that only requires cells (cardiomyocytes and non-cardiomyocytes), a casting mould, an anchoring support and a hydrogel. The hydrogel restrains the cells during gelling time in the casting mould, which provides the intended 3D organ-like form; the anchoring system allows the cells to fix and establish mechanical load between the anchoring points, causing the cardiomyocytes to align parallel to the force lines, mimicking their *in vivo* behaviour and leading to an improved cardiac tissue generation and maturation [35].

Hydrogel encapsulation creates an environment where cells can interact with each other and create an ECM, resembling accurately *in vivo* conditions. Furthermore, it allows standardized force measurements, miniaturisation and automatisation [33], with smaller formats suitable for optimization of maturation protocols and drug treatment, and larger formats applicable for regenerative therapies [25].

Casting moulds are a crucial component for this technique, since they determine the conformation and size of the 3D tissue in development. The mould must be designed in order to be biologically relevant for the final purpose of the tissue in question. Throughout the years, a lot of different conformations have been developed (Figure 1.6), with the aid of 3D precise printing approaches and multifunctional synthetic polymers.

For example, one of the first hydrogel-based methods was developed by Eschenhagen et al. in 1997, by generating plane collagen-based EHTs using Velcro-covered rods as casting moulds (Figure 1.6 - [A]) [36]. Using a different hydrogel, fibrin, Hansen et al. was able to develop mini EHTs on polydimethylsiloxane (PDMS) flexible racks (Figure 1.6 - [C]) [37].

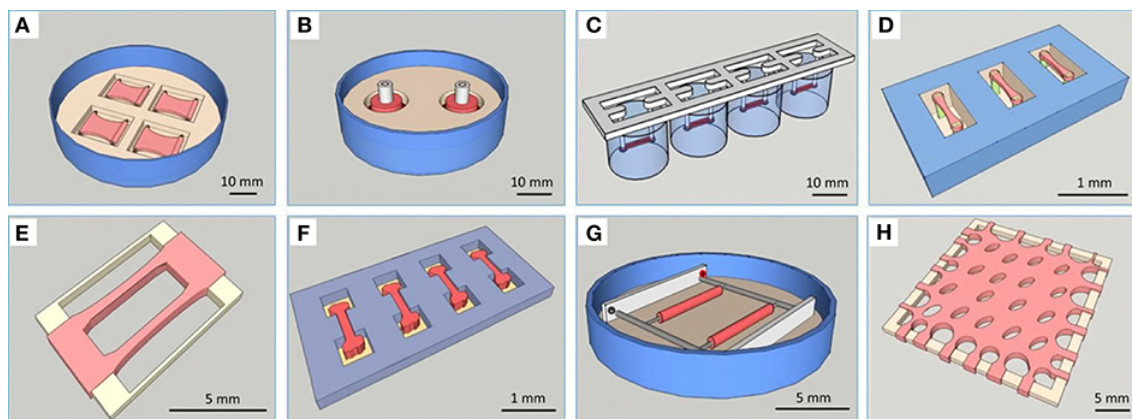


Figure 1.6: [adapted] Schematic illustration of different casting moulds for hydrogel encapsulation techniques, in order to develop EHTs [25]. [A] plane collagen-based EHTs on Velcro-covered rods; [B] ring collagen-based EHTs; [C] fibrin-based mini-EHTs on PDMS racks; [D] collagen/fibrin-based cardiac micro tissues on fluorescent pillars; [E] fibrin-based cardiobundles on PDMS frame; [F] micro heart muscle; [G] collagen-based cardiac biowires; [H] fibrinogen/matrigel-based cardiac patch.

The most commonly used fabrication material, whether to be a part of the casting mould or anchoring system, is PDMS. This synthetic polymer is easy to fabricate and customise, nontoxic, biocompatible, chemically stable, optically clear, hyperelastic (can undergo large deformations before rupture and when subjected to a tensile force can return easily to its initial state once the load

is removed), cures at low temperatures and inexpensive. For these reasons, PDMS has been the material of choice for creating organ-on-chip microfluidic platforms and a part of mechanical or electrochemical sensors, electronic components and biomedical equipment [38].

In spite of these advantages, this polymer has a high hydrophobic nature that can limit the attachment and spreading of cells and can easily entrap air bubbles during its fabrication, which may cause elastic deformations or scatter the light. To address these issues, the PDMS surface may be coated with proteins (such as fibronectin) or undergo an air plasma treatment, which enhance its hydrophilic properties (Figure 1.7).

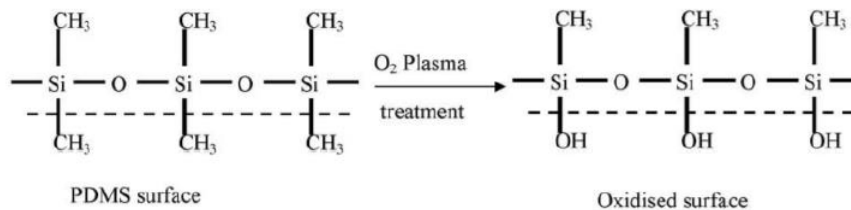


Figure 1.7: Exposing the PDMS surface to a reactive air plasma introduces polar silanol groups, which makes it more hydrophilic and suitable for experiments [38].

When it comes to hydrogels, both natural (such as collagen, gelatin, laminin, matrigel or fibrin) and synthetic ones (such as polyacrylamide, polylactide or polyethylene glycol) may be used, since they are capable of replicating native tissue biochemical and biomechanical environment, due to their viscoelastic and soft nature. Overall, natural hydrogels are most commonly used, since they are non-cytotoxic and present better cell affinity and biocompatibility than synthetic polymers, but are less versatile when it comes to tailoring physical and chemical properties to meet necessary requirements, such as degradation rate, water content or mechanical load. Therefore, a beneficial strategy may include the combination of both natural and synthetic hydrogels, to maximize their advantages [39].

Collagen, particularly subtype I, is the primary constitute of myocardial connective tissue, with versatile and strong biomechanical properties to meet the complex functional and structural needs of the heart. Due to its high biocompatibility and minor inflammatory responses, collagen I is one of the most used natural hydrogels in tissue engineering. However, this gel presents some disadvantages, such as low stiffness, slow gelation time that may lead to cells being flush away before encapsulation, architecture highly dependent on temperature, batch-to batch variability and low long-term viability [40].

Matrigel, another natural hydrogel frequently used, is an assortment of ECM proteins extracted from Englebreth-Holm-Swarm tumors in mice. It consists of laminin, collagen IV, enactin and growth factors, closely resembling the native ECM. Besides being cytocompatible, Matrigel enables faster vascularisation, compared to other natural hydrogels, making it advisable to develop tissues *in vitro* [41][39].

Lastly, fibrin is also a natural, non-cytotoxic and biodegradable gel that is produced in the human plasma blood from which it can be purified. When compared to collagen, this hydrogel has a faster gelation time, leading to a more homogeneous cellular distribution, higher softness that contributes to cardiomyocytes with higher motility and provides a more flexible environment. Furthermore, fibrin can also be synthesised *in vitro* by combining fibrinogen and thrombin, under the catalysis of calcium ions (Figure 1.8) [42].

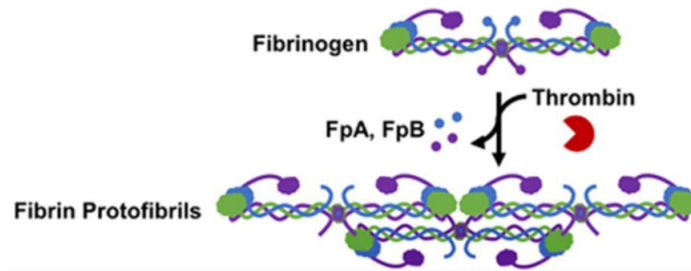


Figure 1.8: [adapted] Schematic representation of fibrin gel formation, catalysed by thrombin. Thrombin promotes the release of fibrinopeptides (FpA and FpB), which in turn allows the interaction and assembly of the fibrinogen chains, leading to the formation of the first protofibrils. Fibrin-hydrogel is formed by lateral aggregations between protofibrils <sup>[42]</sup>.

Although fibrin has been gradually substituting collagen I in many assays, this hydrogel has a rapid degradation (fibrinolysis) rate, which may lead to loss of the supporting matrix before cell encapsulation. In order to slow down this degradation, an antifibrinolytic agent like aprotinin must be added to the fibrin-based gel culture medium <sup>[39]</sup>.

After cell culturing, natural hydrogels provide biochemical aids to the encapsulated cells, enabling the establishment of novel cell to cell interactions and spreading on the surface. Coupled with hydrogel degradation by increased production of ECM proteins, cells get closer to each other and within few days they start to beat synchronously and coherently as single cell clusters.

- **Prefabricated Matrices**

Prefabricated matrices or scaffold-based techniques make use of prefabricated porous materials, with cardiomyocytes embedded in them. These platforms provide structure for cells/tissue to grow, may deliver biomolecules, such as cytokines and growth factors and allow nutrient and oxygen diffusion. Their primary goal is to mimic the mechanical characteristics of native cardiac tissue (since these properties may alter the phenotypical disposition of the seeded cells) and they must be thick enough to contract with proper strength and in synchronisation with cardiomyocytes <sup>[33]</sup>.

A major advantage of this method is the ability, through 3D printing techniques, to manipulate and engineer the intended 3D form, according to the purpose of the study. Various materials have been tested, both natural and synthetic, such as alginate, collagen, gelatin sponges, polyglycolic acid or polyglycerol sebacate and the choice of the material is crucial, since it will affect cells function, force of contraction or migration, amongst other properties. Although synthetic materials offer higher durability and strength when compared to natural polymers, a biodegradable natural polymer is preferably used, keeping in mind that the disintegrated products must be non-cytotoxic <sup>[33] [35]</sup>.

- **Cell Sheet Technology**

This is a new scaffold-free approach (which straightaway diminishes concerns such as biocompatibility of materials), where cardiomyocytes are cultured on standard petri dishes and overtime show a tendency to detach from their surface as an intact monolayer. The dishes are coated with a temperature-sensitive polymer, making them hydrophobic and cell adhesive at 37°C. By lowering the temperature, culture cells, along with the ECM, begin to detach as an intact monolayer, unlike the results obtained with enzymatic treatment (Figure 1.9). By pilling 2D cell layers, 3D cell constructs are obtained, due to cell to cell interactions and since the ECM and intercellular connections between neighbouring CMs are preserved <sup>[33]</sup>.

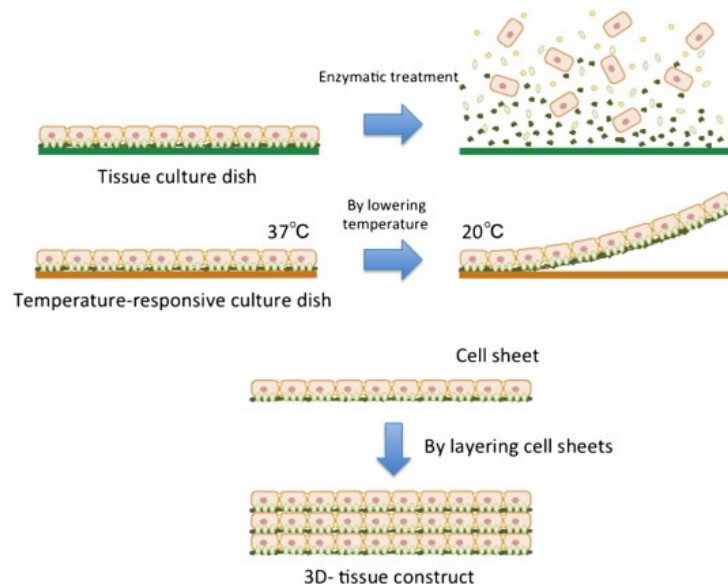


Figure 1.9: Schematic illustration of two methods to harvest CMs in culture and generate 3D tissues: enzymatic treatment, which causes the disruption of proteins in the ECM and damage of the cells; cell sheet technology, where temperature reduction causes the detachment of intact monolayers of cell to cell connections, with ECM included. 3D cardiac tissues are developed by stacking the sheets on top of each other [43].

This technique is adequate for cardiac repair applications, but it still presents some bottlenecks, such as frailness and difficult in handling. Furthermore, monolayers are not attached and prevent the connection of force transducers for functional analysis and testing, making it unsuitable for disease modeling and drug screening applications. To overcome this issue, mixed cell sheets using endothelial cells, fibroblasts and cardiomyocytes are being used to improve sheet thickness and better mimic the native *in vivo* environment [33] [35].

- **Recellularisation of Decellularised Heart Tissues**

This process makes use of the whole heart itself to supply for the 3D structure of the tissue. Cells are washed away by perfusion or immersion/agitation (infusion of decellularisation agents through the organ vasculature or immersing the organ into decellularisation, respectively), only leaving the ECM and decellularised scaffold structure of the heart. Then, the organ is recellularised through the blood vessels with cardiac cells and the ECM, addition of growth factors and electrical stimulation aid the cells to attach, grow, multiply and beat [33] (Figure 1.10).

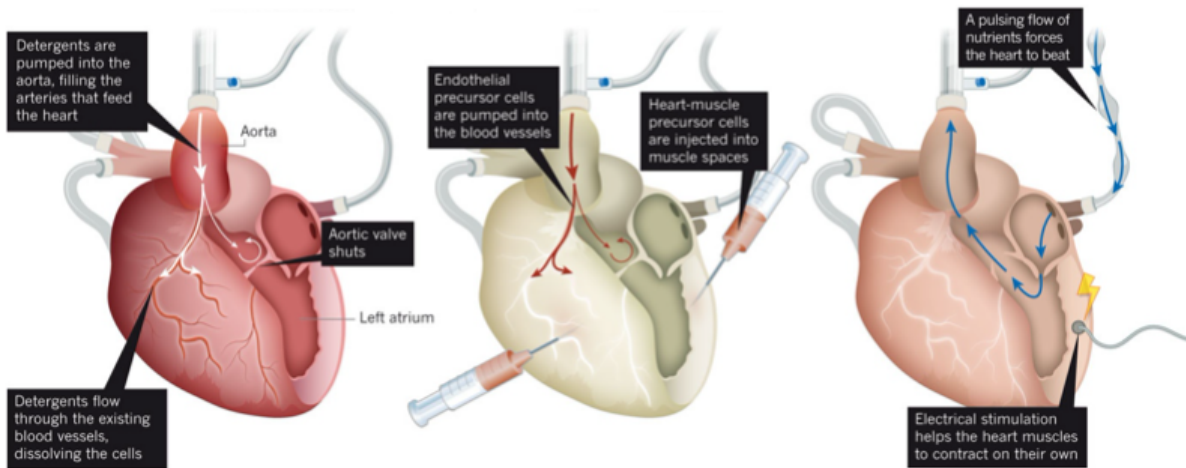


Figure 1.10: [adapted] Schematic illustration of the decellularisation/recellularisation technique of a heart. Firstly, a pump pushes decellularisation agents through a tube running into the heart's aorta and blood vessels, stripping away DNA, lipids, sugars and almost all the cellular material of the heart (**left picture**); leaving only the ECM that holds the heart together, a mixture of cardiac, endothelial precursor and muscle progenitor cells is then injected, recellularising the organ (**center picture**); with the help of electrical stimulation and pumping of nutrients through the aorta, the heart becomes functional (**right picture**)<sup>[44]</sup>.

Although optimisation of decellularisation protocols and introducing cardiac cells back in the matrix with high efficiency and precise positioning of specific cell types into their corresponding specific organ compartment has been problematic, researchers have been improving this methodology and it is currently pursued using different types of animal and even human hearts. Furthermore, studies have shown successful regeneration of decellularised human heart muscle using hiPSC-CMs. By injecting them into the left ventricular wall, cardiac muscle tissue demonstrated functional contraction after 14 days, which shows this technique is promising for regeneration and potentially enables patient-specific disease modeling and therapeutic discovery<sup>[45]</sup>.

### EHTs as a platform for numerous studies

Several years ago, the only way to study pathological molecular mechanisms occurring in failing hearts involved primarily invasive methods, such as biopsies. Since biopsies from cardiac tissues come with the risk of perforation and the amount of material is often not enough for substantial molecular analyses, several technological breakthroughs, during the last decades, have allowed researchers to noninvasively study cardiac function in detail.

New EHT strategies have been continuously developed and improved in order to achieve an efficient, reliable and scalable technique that replicates the 3D native cardiac environment. At first, EHTs were generated using standardised cell lines, such as the HL-1 or immortalized cardiomyocytes, since these cells proliferate indefinitely, but some of these cell lines only resemble CMs to some extent and may possess tumor-like properties. As an alternative, it is possible to use primary CMs isolated from chicken embryos, neonatal mice or rats, but animal cell-based models cannot truly recapitulate human physiology and a large number of animals is required to acquire a large amount of cells<sup>[22]</sup>.

The introduction of human Embryonic Stem Cells and human induced Pluripotent Stem Cells, coupled with metabolic maturation techniques for hiPSC-CMs and gene editing tools in EHT technologies allows to generate reliable 3D human constructs that can be examined in a controllable setting, suitable to study physiological and pharmacological properties of cardiac tissue *in vitro*, as well as disease

modeling. Furthermore, the use of hiPSC-CMs enables to conduct patient-specific *in vitro* studies and investigate the underlying mechanism of certain genetic mutations and their causality in pathophysiology of cardiac dysfunctions, improving diagnosis and decision-making regarding treatment strategies [22] [46].

Figure 1.11 summarizes the important steps that lead to EHT development and its primary applications.

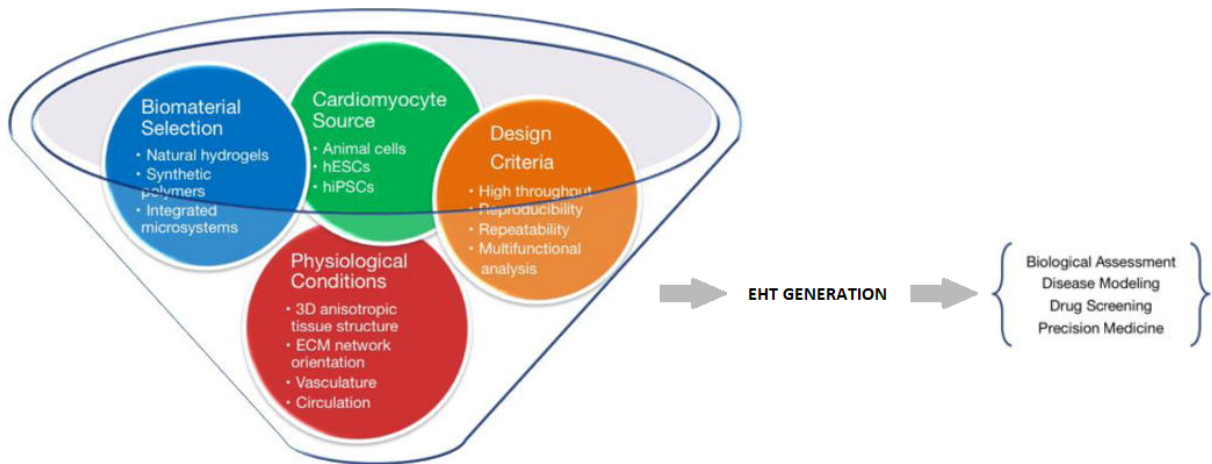


Figure 1.11: [adapted] Schematic illustration of the necessary steps to generate an EHT and the different fields that benefit from this 3D construct [23].

## 1.2.4 modeling cardiovascular diseases with EHTs

Due to the massive number of people worldwide affected by some form of cardiovascular disease, drug discovery and development is a crucial yet demanding road. The different phases between drug discovery and commercialisation may take up to several years and are very costly, so EHTs offer an important alternative for disease modeling, in order to discover underlying biological pathways of specific CVDs and to improve disease diagnosis (by identifying specific disease-associated genes and genotype-phenotype biomarkers) [23].

Since most heart diseases have an indirect (impact on ion channels) or direct (impact on sarcomeric proteins) effect on cardiomyocyte force production, researchers have been focusing on developing and improving the ability to measure and analyse contractile force, with a standardised and reproducible approach [46].

### Heart Failure

HF is amongst the most predominant cardiovascular conditions and therefore the need for a reliable platform that allows to devise new drugs for each condition or understand exactly the effect of already know ones, as well as pharmacological screening and efficacy testing of different drug concentrations, has risen substantially.

An important substance to be studied, together with its effects in the human heart, is norepinephrine (NE). Norepinephrine, also know as noradrenaline, functions as an hormone and is the main neurotransmitter used by the Sympathetic Nervous System (SNS) as a response to exercise, stress and in a "fight-or-flight" situation (when the body is subjected to acute threat). NE increases heart rate, contractility and blood pumping to other organs. It also triggers vasoconstriction with subsequent raise in blood pressure and helps to break down fat to increase blood sugar levels to supply more energy to the body.

As a prescribed medicament, NE is used to treat hypotension (low blood pressure) secondary to septic shock or in life-threatening situations that require cardiopulmonary resuscitation [47].

HF is characterised by an intricate interaction of several neurohormonal mechanisms that are activated in order to try to support cardiac output due to impaired function. The SNS is the most important among these mechanisms and, in patients with heart failure, its outflow and activity raises notoriously, instantly restoring cardiac function. However, prolonged SNS activity may exert harmful consequences on cardiovascular function and structure by promoting pathological myocardial remodeling, an essential feature in myocardial failure [48]. Since NE is the major transmitter of the SNS, extended SNS activity results in the increase of plasma norepinephrine, which has been associated to cardiomyocytes' hypertrophy and apoptosis, downregulation of several "adult" genes implicated in excitation-contraction coupling and changes in the extracellular matrix composition, all known to have an important role in causing heart failure [48].

Several models, when subjected to long administration of NE, using neonatal rat cardiomyocytes, ESC-CMs (Embryonic Stem Cell derived cardiomyocytes) or hiPSC-CMs, have demonstrated the previously described effects and contractile dysfunction, providing a simulation of the HF phenotype [49] [50] [51]. Since they can accurately recapitulate native cardiac tissue drug-induced changes in contraction rate and morphology, EHTs using hiPSC-CMs may prove crucial for understanding the exact action mechanisms of NE in human cardiomyocytes and its repercussions, at a given range of concentrations.

### **Hypertrophic cardiomyopathy and the role of MYBPC3 in this disease**

Over the last few years, several disease models have been developed to study HCM, but the complexity of this disease, as well as the heterogeneity of clinical symptoms and wide spectrum of mechanisms by which it occurs make it difficult to study its causality and progression. The main HCM models that have been generated include *in silico* approaches, myofibrils derived from skinned hearts (where tissue/cell derived skinned myofibril preparations are placed between force transducers and length motors, in solutions with different  $Ca^{2+}$  concentrations to trigger contraction/relaxation) or purified actin/myosin proteins (where the movement of fluorescently labeled actin filaments over a layer of random oriented myosin molecules, immunoadsorbed to an antibody-coated surface, is recorded). The main approaches generated are expressed in Figure 1.12, along with their main outputs and positive or negative aspects. Regardless of each model intricacy at several degrees, all of them have contributed to a deeper molecular perception of HCM hallmarks and development [52].

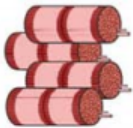
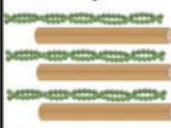
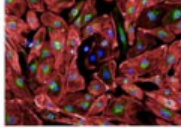
	Intact heart muscle strips	Isolated cardiomyocytes	Myofibrils from tissue/cells	Purified actomyosin	Animal models	hPSC-CMs
<b>Disease model</b>						
<b>Advantages</b>	Physiological relevance Pharmacological predictivity	Amenable to measurements of subcellular functions	Direct access to myofilament function Simple logistics (allows sample freezing)	Higher sample availability (heterologous systems) Direct assessment of actin–myosin interactions	Whole organ/organism studies Genetically tractable Easily available cell and tissue samples	Unlimited source of cardiomyocytes Recaptures patient genotype Gene editing enables isogenic controls
<b>Disadvantages</b>	Demanding logistics Limited sample availability	Limited sample availability Lack of proliferative ability in culture Lack of 3D architecture	Preparation artefacts Limited sample availability	Over-simplistic (nonrepresentative of whole sarcomere) Preparation artefacts (causing contradictory results)	Species differences relative to human Time-consuming genetic manipulation	Immaturity relative to human adult cardiomyocytes Lack of multicellular cardiac composition and neurohormonal control
<b>Main readouts</b>	Histology: fibrosis, myocyte enlargement, and disarray Pharmacological responses (e.g., $\beta$ -blockers)	Electrophysiology Single-cell transcriptomics	Calcium sensitivity Isometric tension ATP consumption Energy cost of contraction	Kinetics of contraction ATPase activity Surrogate of force generation	Histology: fibrosis, disarray Contraction parameters and calcium sensitivity (integrated in EHTs)	High-throughput molecular and functional phenotyping Genetic causation (isogenic controls)

Figure 1.12: [adapted] Schematic illustration of the different disease models developed, in the last years, to study hypertrophic cardiomyopathy phenotypes, with their respective advantages, disadvantages and readouts [52].

Although MYBPC3 mutations are the most recurrent genetic cause of HCM (as aforementioned in 1.1.3), the molecular mechanisms and temporal relationship linking these mutations to the pathogenesis and development of the disease remain elusive.

Several researchers have been studying the effects of MYBPC3 mutations. For example, Dutsch et al. generated EHTs using cardiac cells of mice with a MYBPC3-targeted knock-in, that exhibited typical aspects of human HCM when compared to EHTs generated with wild-type cardiac cells [53].

The creation of models using hiPSC-CMs has also been growing in the past years. For instance, Helms et al. harnessed patient and gene-edited MYBPC3-mutant iPSC-CMs to explore the effects of this mutation in early evolution stage modeled by iPSC-CMs, and seeded them onto row-micropatterned PDMS substrates, generating 2D anisotropic cardiac tissues [15]. In another study, Ma et al. developed a cardiac tissue model consisting of filamentous 3D matrices populated with healthy hiPSC-CMs or from MYBPC3-mutant hiPSC-CMs, to study the differences in contraction output under mechanical overload [54]. Lastly, Cohn et al. used 3D cardiac microtissues to compare healthy and mutated hiPSC-CMs, to study the hypercontractility effects of MYH7 and MYBPC3 mutations [55].

Since HCM is a disease with known genetic cause, it is an excellent candidate for stem cell modeling, since the application of genome-editing technologies to hiPSCs allows for limitless isogenic sets of heart cells in that only differ in a single mutation, allowing to discover new pathomechanisms and paving the way to urgent and more efficient HCM therapeutics [52].

## Chapter 2

# Project Purposes

Cardiovascular diseases remain, to this day, the main cause of incapacity and death worldwide, representing a considerable economic burden in healthcare systems. Among the most severe types of cardiovascular conditions, two stand out due to the appalling number of people affected by them globally: heart failure and hypertrophic cardiomyopathy. Heart failure is a condition characterised by functional and structural defects in the myocardium, leading to impaired blood pumping to meet the metabolic demands of the body for blood and oxygen or stiffening of the heart muscle, which reduces or prevents blood flow to the heart.

The second disease, hypertrophic cardiomyopathy, is distinguished by abnormal thickening of certain parts of the heart muscle, prevalently the septum, due to cardiomyocytes enlargement and disarray. This irregular thickening leads to arrhythmias and reduction or blockage of blood flow to the rest of the organs. HCM is the most common monogenic cardiac disease and mutations in cardiac myosin binding protein C (MYBPC), encoded by the MYBPC3 gene, are the most frequent cause of HCM. This protein is crucial for sarcomere organisation and aids in cardiac muscle contraction. The molecular mechanisms and sequence of events that links this mutation to the pathogenesis and evolution of this disease remains unknown.

Presently, there is no cure for these two conditions and treatments focus on the alleviation of symptoms or prevention of disease progress. Since *in vivo* interventions bring undesirably high risks for humans, some animal models have been developed and used in preclinical drug trials, but there are evident physiological and genomic differences when compared to the human heart, that lead to model failure to predict exactly drug toxicity and disease phenotype. Furthermore, 2D cultures have helped to expose several cellular mechanisms that take place in the human heart, but lack accuracy when it comes to mimic the native 3D cardiac microenvironment.

The emergent demand for new *in vitro* models that mimic the human heart, coupled with human stem cell biology breakthroughs, have had a critical impact in disease modeling, drug development and regenerative medicine fields. Human induced Pluripotent Stem Cells (hiPSCs) have been the primary go-to tool for *in vitro* cardiac models, since this stem cell type is the one that best recapitulates cardiomyocyte physiology when differentiated into human induced Pluripotent Stem Cell-derived cardiomyocytes (hiPSC-CMs). By coupling hiPSC-CMs with metabolic maturation protocols and addition of non-myocytes (such as fibroblasts or endothelial cells), it is possible to produce 3D engineered heart tissues (EHTs) that closely mirror the native human cardiac environment. Furthermore, when coupled with genome-editing methods, hiPSC-CMs are able to simulate phenotypic characteristics caused by genetic mutations, enabling the creation of libraries of disease-specific CMs and the study of their underlying mechanism and influence in pathophysiology.

By using an EHT platform developed by staff of the AST group of the University of Twente in The

Netherlands, this project has two primary goals. The first one is to verify if the platform was able to model elements of HCM by generating EHTs with healthy hiPSC-CMs or with a mutation in the MYBPC3 gene (co-cultured with a population of hiPSC-FBs (human induced Pluripotent Stem Cell- derived fibroblasts)) and assessing the differences in important parameters, such as contraction force.

The second motivation of this work is to simulate heart failure after long-term exposure of EHTs (co-cultured with hiPSC-CMs and hiPSC-FBs) to a specific range of concentrations of norepinephrine (main neurotransmitter used by the Sympathetic Nervous System (SNS), known to increase heart rate, contractility and precursor of several mechanisms associated to heart failure due to extended SNS activity).

The success of this platform may pave the way to find these diseases pathomechanisms and to discover new and efficient therapeutics.

## Chapter 3

# Materials and Methods

All of the disease modeling experiments conducted throughout this report made use of an EHT platform already designed by staff from the Applied Stem cell Technologies (AST) group of the University of Twente in The Netherlands. This platform allows the generation of fibrin-based miniaturised EHTs in a standard 12-well culture plate. In each well, a PDMS part with six flexible cantilevers enables the generation and analysis of three 3D tissues, since each tissue is cultured between two cantilevers, as shown in Figure 3.1. These cantilevers provide anchoring during tissue culture to resist axial gel compaction and facilitate cell alignment by applying an auxotonic load.

After the heart tissues have been properly formed, their contraction force is reflected by the cantilevers distance of deflection and may be further tracked in real time by automated video optical recording with an inverted microscope.

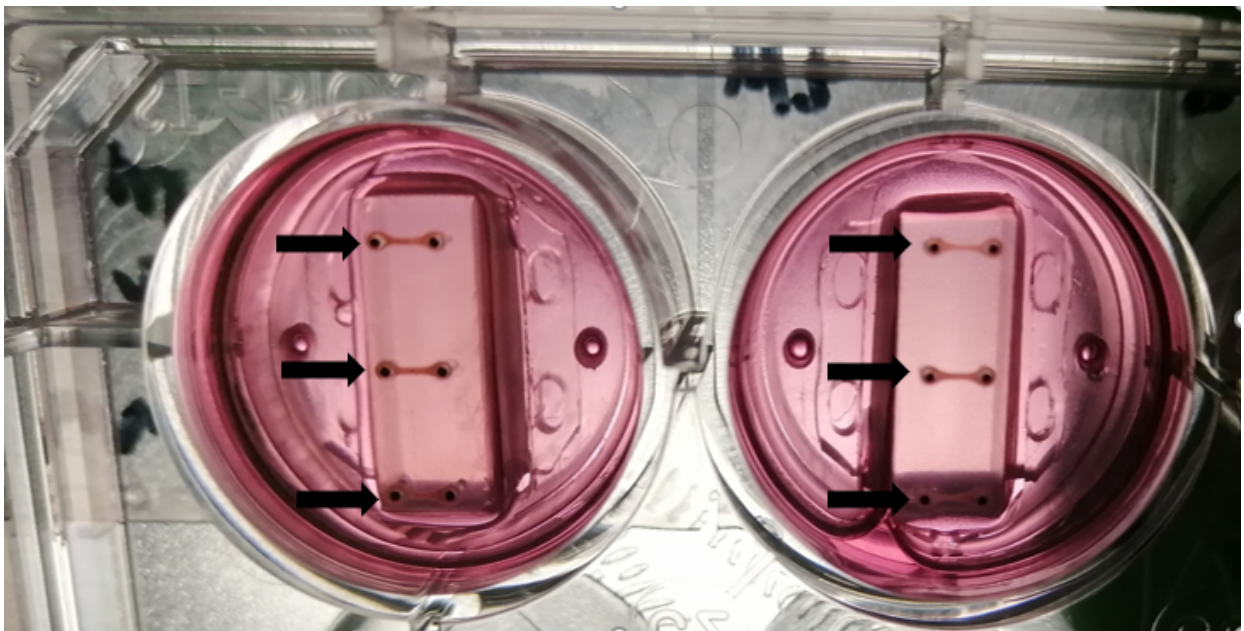


Figure 3.1: Bottom view of two wells in a standard 12-well culture plate, where three engineered heart tissues have been generated per well, cultured between two PDMS flexible cantilevers. Each tissue is pinpointed by a black arrow.

### 3.1 Design and Fabrication of the PDMS Anchoring System

A crucial piece of this EHT platform is the PDMS part, that anchors tissues culture. As explained in Section 1.2.3 -"Hydrogel Encapsulation", PDMS is an optically transparent soft elastomer, easy to customise and its surface provides a good structure for cell attachment. Its properties allow the cantilevers (or pillars) to rapidly return to its initial state after being subjected to a tensile force. Thus, once a cardiac tissue is cultured between the pillars, relevant parameters such as force of contraction or contraction/relaxation time can be assessed by knowing the distance of deflection between cantilevers.

This PDMS part was designed to fit in a well of a standard 12-well culture plate and is depicted in Figure 3.2. Each cantilever has a radius of 0,25 mm, with each tip painted with black PDMS and a small PDMS circle (referred to as plate) around it. The purpose of the black tip and of the plates will be explained in subsequent Sections 3.1.2 and 3.1.3, respectively.

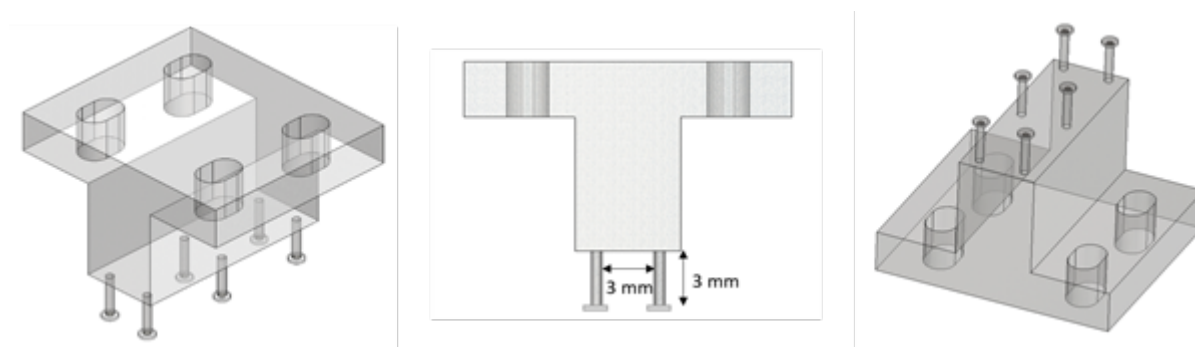


Figure 3.2: Schematic representation of the PDMS part that anchors the fibrin-based miniaturised EHTs. Both **left** and **center pictures** are bottom views and the **right picture** is a top view. All the views were obtained through SolidWorks ®Software.

In the next Sections, the different steps that lead to the fabrication of this PDMS part will be thoroughly described and the final result will be shown.

#### 3.1.1 Preparation of the PDMS and Replica Moulding

The PDMS elastomer is obtained by mixing two components, the PDMS base (a viscous silicone liquid) and the curing agent, that works as a catalyst for the cross-linking of PDMS when mixed with the base (Sylgard™ 184 Silicone Elastomer Kit, Dow Corning®, Midland, MI, USA) in a 10:1 ratio (w/w). This mixture is degassed in a vacuum desiccator until there are no more air bubbles and poured into a Teflon mould, naturally adapting its shape to the desired features. This mould with PDMS also undergoes degassing, to make sure that there are no entrapped air bubbles that can prevent the correct making of the cantilevers.

Lastly, the degassed Teflon mould with PDMS is cured at 65°C overnight in an oven (Quincy Lab Inc. Model 10), to ensure proper cross-linking and solidification of the polymer. This mould allows to fabricate thirty PDMS parts at a time, which is extremely advantageous in terms of fabrication output (Figure 3.3).

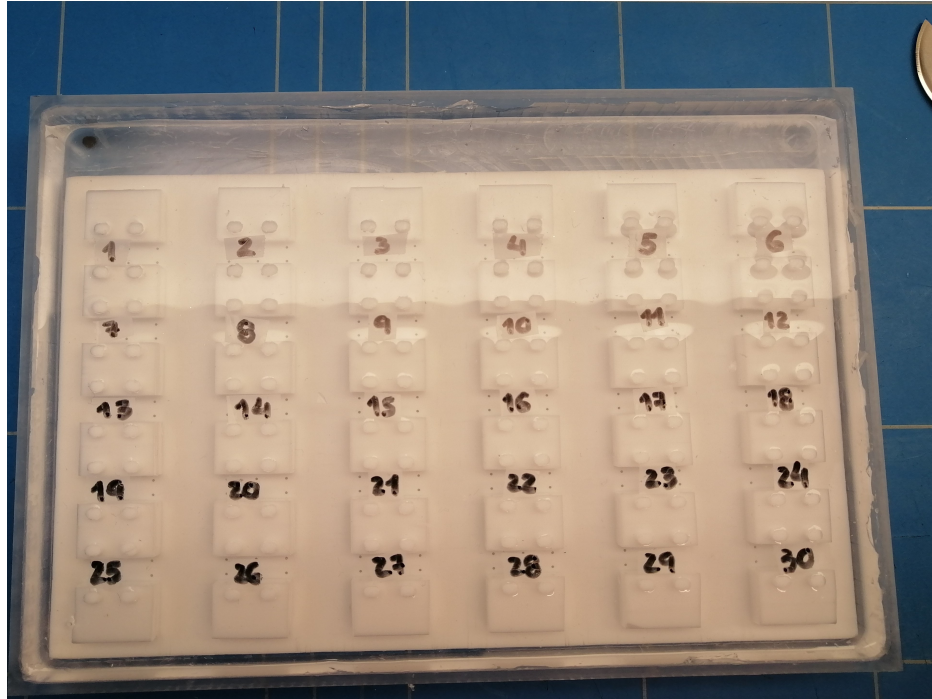


Figure 3.3: Photograph of the Teflon mould after solidification in the oven, which enables the fabrication of thirty PDMS parts at a time.

### 3.1.2 PDMS Cantilevers Painting

Once the Teflon mould is out of the oven, the leftovers of PDMS are removed and the PDMS parts are taken out of the mould, cut and trimmed until they have the desired shape (Figure 3.4). At this point, it is essential to verify that the cantilevers have formed properly.

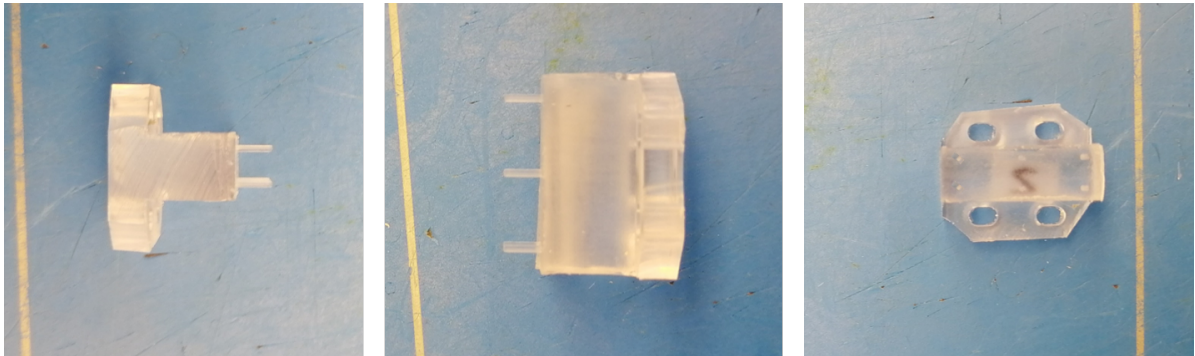


Figure 3.4: Photographs of a PDMS part after being taken out of the Teflon mould, cut and trimmed. From both side view (**left and center pictures**) and top view (**right picture**), it is possible to observe that the pillars formed properly and have an even height.

The painting step of the tip of the pillars is a crucial one, since it allows to track the position of the cantilevers at any given moment under the microscope during repetitive cycles of contraction and aids the measurement of their deflection with an analysis software. Thus, the tip of each pillar is painted with black PDMS. This is accomplished by pouring the black PDMS (mixture of carbon black (Vulcan @XC 72R) and 45 mL of PDMS) onto a glass slide (Thermo Fisher Scientific) to obtain an even layer of paint and carefully dipping just the tip of the cantilevers, in order to form an even black circle. The painted PDMS parts are then cured in the oven, at 65 °C, for two hours. The final result is shown in Figure 3.5.

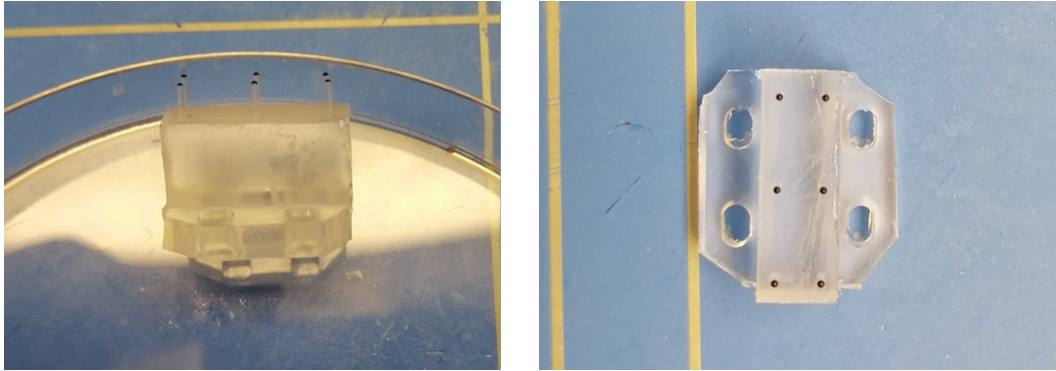


Figure 3.5: Photographs of a PDMS part after the tip of the pillars has been painted black and cured in the oven. From both side view (**left picture**) and top view (**right picture**), it is possible to notice that only the very tip is painted (so there is no leakage of black paint along the height of the pillar) and that it has an even black circle.

### 3.1.3 PDMS Cantilevers Plating

The final step in the fabrication of the PDMS parts is the plating. Since the tissue is cultured around two pillars, it is necessary to have a small PDMS circle (a plate) attached to each black tip of the cantilevers, that anchors the tissue and prevents it from falling to the bottom of the well when suspended upside-down. These plates are made with the aid of a plater.

The plater consists of two parts (a bottom part with small holes with the exact size intended for each plate and a top part that anchors the PDMS parts) that are assembled together and where the PDMS parts can be positioned and adjusted so that each black tip of the pillars is centered in the small hole (Figure 3.6).

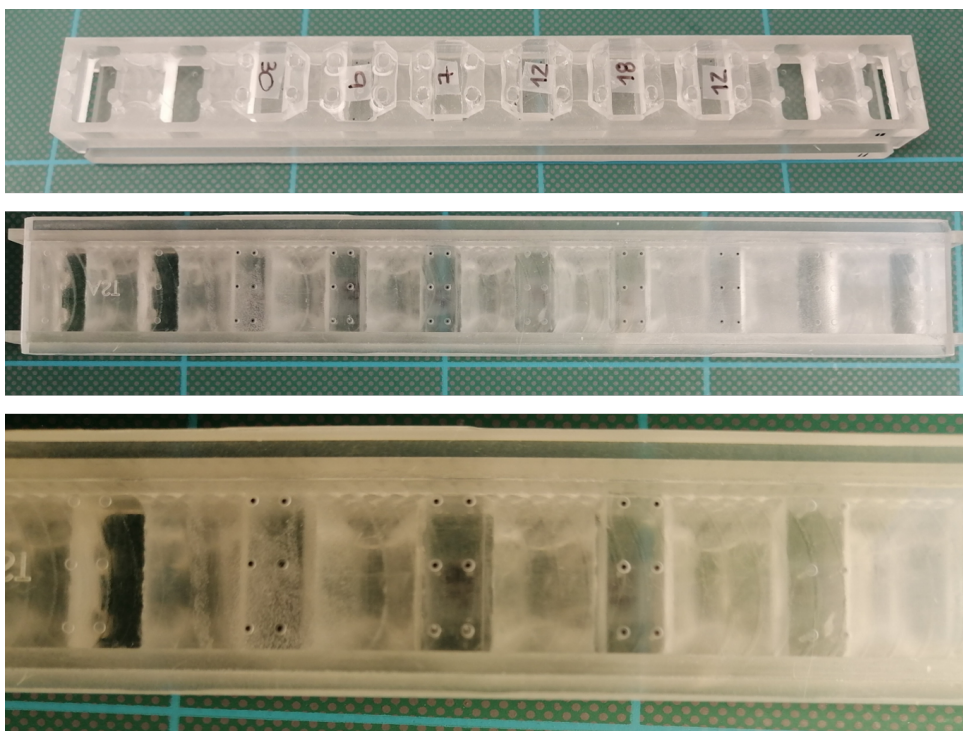


Figure 3.6: Top view (**top picture**) and bottom view (**center picture**) of the plater that allows to make the plates for each pillar. The **bottom picture** shows a close-up of the bottom part, where each tip of the cantilevers is positioned in their respective hole.

After placing each PDMS part in the top part, PDMS is poured into the holes of the bottom part with the help of a small plastic pipette tip, the excess of PDMS is scraped off with a glass slide and the plater goes into the oven at 65°C, to cure the plates for two hours. The final PDMS part is shown in Figure 3.7. Each plater allows to plate ten PDMS parts at a time (beneficial in terms of fabrication output and time saving).

After curing, it is important to verify that all plates formed appropriately and are well centered, to later prevent the growing tissue from falling.

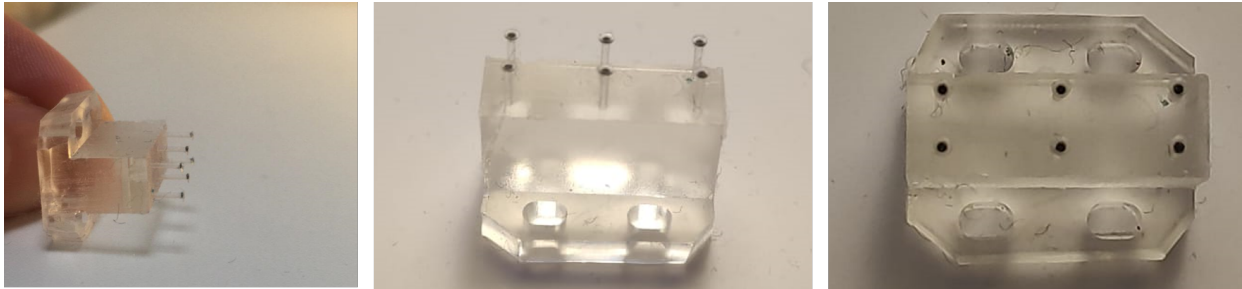


Figure 3.7: Photographs of different perspectives of a PDMS part after plating. The black tip of each pillar must be centered in the plates to guarantee proper anchoring of the tissue.

### 3.1.4 PDMS Part Air Plasma Treatment

As mentioned in Section 1.2.3 -"Hydrogel Encapsulation", air plasma treatment aids to enhance the hydrophilic properties of PDMS surfaces to facilitate cell attachment. Since the goal is for the cells to spread around the pillars and not to attach to them, at least 24 hours before experiments the PDMS parts are subjected to this treatment, so that partial or full hydrophobicity may be recovered.

Thus, PDMS parts inside a petri dish (Greiner-Bio One™) with the lid open are placed at the chamber of a plasma cleaner (Femto Science Inc., CUTE Model), where they are subjected to two low pressure cycles (the first one with the pillars facing upwards and the second one with the PDMS part on the side). Afterwards, the petri dish is covered with the lid and sealed with sealing film (Parafilm®) until further use.

This plasma treatment not only affects the hydrophilicity of the PDMS parts, but also cleans its surfaces and removes organic contaminants, assuring the needed sterilisation when working with cell cultures.

## 3.2 Generation of Fibrin-based Engineered Heart Tissues

### 3.2.1 hiPSC-CMs and hiPSC-FBs used for EHT making

All of the experiments were conducted using hiPSC-CMs and hiPSC-FBs (human induced Pluripotent Stem Cell-derived fibroblasts) previously differentiated by members of the AST group of the University of Twente.

The human induced pluripotent stem cell line FLB, formerly described by Bellin et al. 2013 [56], was used to generate cardiomyocytes *in vitro*. This cell line also allowed to engineer an isogenic cell line that only differs in a heterozygous mutation c.2373insG in the MYBPC3 gene (this guanine nucleotide insertion leads to a frameshift that creates an alternative splice donor site and consequently skipping of exon 25) for the corresponding assay.

For the serum-based experiments in the aforementioned assay, the hiPSC-CMs were cultured for four days in a medium with 15 mM of glucose and T3 hormone + Dexamethasone + IGF-1 (combination hereon known as TDI) (see Appendix A- "Preparation of the CM High Gluc+TDI Medium") and then frozen down.

For the experiments without horse serum in the MYBPC3 assay and for the drug induced heart failure model, these hiPSC-CMs were purified for four days (also to eliminate non-CMs) in a medium containing low insulin (Low Ins), TDI and lactate (Lact) (see Appendix B-"Preparation of the CM Low Ins+Low Gluc+TDI+Lact Medium", but without the glucose adding step) and then recovered for three days in a medium with low insulin, low glucose, TDI and lactate, henceforth addressed as CM Low Ins+Low Gluc+TDI+Lact Medium (see Appendix B-"Preparation of the CM Low Ins+Low Gluc+TDI+Lact Medium") before being frozen down.

All of the tissues were made directly from these frozen hiPSC-CMs and using 5% of hiPSC-FBs (also frozen).

As described in Section 1.2.2-"Addition of soluble factors", supplementing the medium with TDI promotes *in vitro* maturation of hPSC-CMs into a more adult-like state.

### 3.2.2 Making of the casting mould

Prior to experiments, it is necessary to produce the casting moulds that will shape the tissue. These casting moulds are made in a 12-well plate (Greiner-Bio One™) by pipetting 1.2 mL of a previously warmed (to 37°C) working solution of 10% agarose into each well. After pipetting, a Teflon spacer (formerly autoclaved at 121°C) is placed from above, supported by a PMMA holder (Poly(methyl methacrylate)) (previously sterilised using the plasma treatment), to shape the agarose (Figure 3.8).



Figure 3.8: Photographs of the PMMA holder (**left picture**) and of the Teflon spacer (**center picture**). By positioning the spacer in the holder and placing it on the well with agarose, the spacer shapes the casting mould according to desired specifications.

The positioning of each Teflon spacer must be done as soon as possible, since agarose solidifies very fast. The 12-well plate is then covered with a lid, sealed with sealing film and placed in a -20°C freezer for agarose solidification for one hour. After solidification, the Teflon spacers are removed and the 12-well plate may be stored in the -4°C fridge until further use.

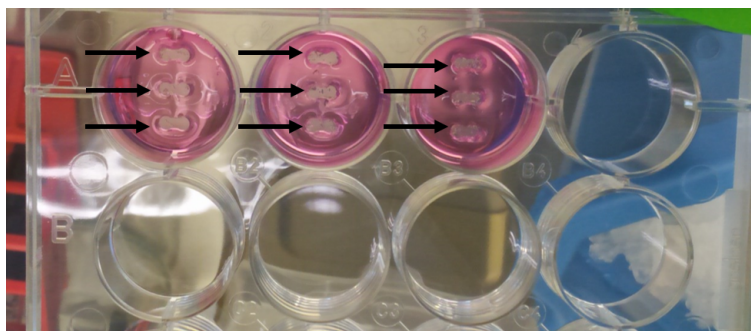


Figure 3.9: Photograph of the agarose mould after solidification. Each well allows to culture three tissues that will be confined in the shape produced by the Teflon spacer (pinpointed with the black arrows).

### 3.2.3 Generation of the EHTs

For the following protocol, it is important to mention that when medium supplementation is referred, the medium utilised for the serum based experiments in the MYBPC3 assay is the CM Low Ins+Low Gluc+TDI+Lact Medium supplemented with 10% (v/v) of horse serum (Gibco™, Life Technologies), hereon mentioned as CM Low Ins+Low Gluc+TDI+Lact+HS Medium. For the MYBPC3 experiments without HS in the MYBPC3 assay and for the drug induced heart failure model, the medium used is the CM Low Ins+Low Gluc+TDI+Lact Medium. Furthermore, all of the possible steps were conducted in a laminar flow hood (Telstar) to provide a UV sterile environment.

The procedure begins with the thawing of the cells. The vials containing the cells (stored in liquid nitrogen towers) are warmed in a water bath (37 °C) until the cell suspension is liquid and then pipetted into a 15 mL tube. To clean any leftover of cells, 1 mL of DMEM (Dulbecco's Modified Eagle Medium) (Gibco™, Life Technologies) is added to the vial and transferred to the 15mL tube. Afterwards, 4 mL of DMEM/mL of cell suspension are added dropwise (to prevent osmotic shock) to this tube, since it is a source of vitamins, salts and amino acids.

The tube with the cell suspension + DMEM is centrifuged at 1100 rpm for 3 minutes, followed by removal of the supernatant and resuspension of the cell pellet in 1 mL of medium. 10 µL of the cell resuspension are then mixed in an Eppendorf with the appropriate volume of Trypan Blue solution to dilute the cells (at 0.4%, Gibco™, Life Technologies) for counting, using a counting chamber (Marienfeld Superior™). The counting step is crucial and determines how many wells of EHTs are made, since each well must have at least 800K hiPSC-CMs.

After assessing how many hiPSC-CMs are available, hiPSC-FBs are added to the tube with the cardiomyocytes. The volume of hiPSC-FBs added corresponds to 5% of the amount of hiPSC-CMs. Then, the tube with this cell suspension undergoes centrifugation at 1100 rpm for 3 minutes. The supernatant is then removed and the cell suspension is supplemented with the proper volume of medium to address the final volume of cell suspension necessary to generate the EHTs.

To produce a fibrin-based hydrogel, the following components were mixed in an Eppendorf placed on ice: 100 µL/mL of Matrigel (1:10 dilution (v/v)) (Corning ®); 250 µg/mL of aprotinin (1:100 dilution (v/v)) (Sigma-Aldrich ®); 20 mg/mL of fibrinogen in NaCl 0.9% (1:10 dilution (v/v)); two times concentrated medium, known as 2X Medium (1:10 dilution (v/v)). Considering that the fibrinogen is dissolved in a saline solution, the 2X Medium helps to restore the isotonic conditions of the medium.

The appropriate amount of this mixture is added to the cell suspension and, as shortly before seeding as possible, 100 U/mL of thrombin (dilution 1:150 (v/v)) (Sigma-Aldrich ®) is added to the cell suspension as well (since the polymerisation reaction starts immediately).

Finally, 15  $\mu\text{L}$  of this reconstitution mixture are quickly pipetted into each mould with the tissue shape and the PDMS parts, properly placed in the PMMA holders, are positioned in the well. After waiting 8-10 minutes for the fibrin-based hydrogel to form properly, 1 mL of medium is added to each well and the 12-well plate is placed in the incubator (Sanyo) at 37°C and 5%  $\text{CO}_2$ .

Using this protocol, all tissues compacted and the onset of spontaneous beating is observed between 3-5 days after casting.

### **3.2.4 Maintenance of the EHTs and Drug Adding**

Usually, the EHTs are made on Tuesdays or Thursdays and cell culture medium is changed every other day. Tissues are fed by replacing 1 mL of medium with the same volume of fresh medium, always guaranteeing that medium is not pipetted out below tissue line, since until day 10 they are fragile and can break.

For the drug modeling assay, tissues are fed as aforementioned until day 10. Then, norepinephrine is added to each well at the desired concentration every day until day 17.

The NE (Sigma-Aldrich®) concentrations that were tested were 10  $\mu\text{M}$ , 50  $\mu\text{M}$  and 100  $\mu\text{M}$ . For this purpose, 500  $\mu\text{L}$  of a 10 mM stock of NE were diluted in 5 mL of medium, to create a solution with a concentration of 1  $\mu\text{M}$ . Of this solution, 20  $\mu\text{L}$ , 100  $\mu\text{L}$  and 200  $\mu\text{L}$  were pipetted into each well to test the effects of NE at a concentration of 10  $\mu\text{M}$ , 50  $\mu\text{M}$  and 100  $\mu\text{M}$ , respectively.

## **3.3 Monitoring contractile function of EHTs and Data Analysis**

Tissue formation and contraction is monitored using an inverted microscope (Nikon Eclipse Ts2). This microscope is connected to a computer (Dell) with Nikon's NiS Elements Software installed and allowed to obtain all the micrographs that will later be presented in Chapter 4- "Results and Discussion".

Contractile function of the tissues is measured using an inverted microscope with an enclosed incubator to control temperature and humidity (37°C and 5%  $\text{CO}_2$ ). The tissues were paced at 1,5 Hz and image acquisition was done at 100 frames per second (fps) with 2x magnification.

For each contraction, a software program allowed to track the cantilevers position as a function of time, by analysing the change in distance between the centroids of the moving black tips. Then, force development is calculated based on PDMS pillars deflection and their elasticity/geometry (the formula used for this calculation is presented in Appendix C). Figure 3.10 displays an example of an EHT variation of contraction force over time. Other relevant parameters, such as contraction/relaxation velocity, were also obtained, by knowing how long tissues took to achieve a fully relaxed or contracted state.

To prevent any interference in these analysis, the EHTs are gently transferred to a new 12-well plate where each well is supplemented with 2 mL of fresh medium, prior to measurements.

For the MYPBC3 assay, EHTs are measured 10 days after cultured. For the drug induced heart failure experiments, tissues are measured before drug adding and after 7 days of being incubated with the drug. The initial measurements are the base line to see how tissue behaviour evolves after drug administration.

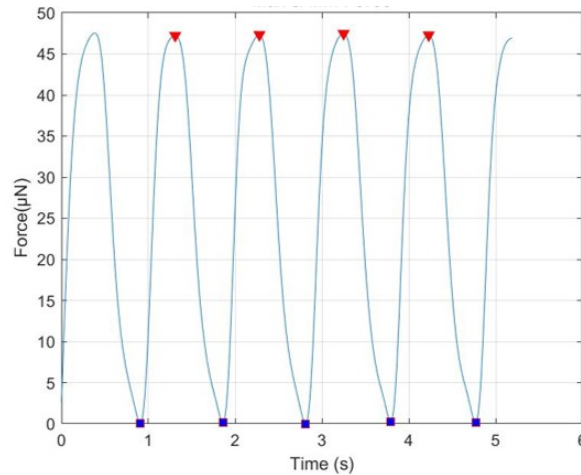


Figure 3.10: Exemplary contraction pattern of an EHT displaying contraction force over time with pacing at 1,5 Hz.

### 3.4 Fluorescence-Activated Cell Sorting Analysis (FACS)

Troponin FACS analysis was conducted in order to ascertain the cardiomyocyte content of each batch of cells purified by lactate treatment before frozen. For this purpose, leftovers of these cells used to generate EHTs are first collected (maintaining the requirement of 800K cells/well), fixated and permeabilised with the aid of the FIX and Perm Cell Fixation and Permeabilisation Kit (Thermo Fisher Scientific, GAS003/4). In a tube, cells are centrifuged at 1100 rpm for 3 minutes, the supernatant is removed, cells are washed with 1 mL of Protein Extraction Buffer (PEB) (Thermo Fisher Scientific) and undergo new centrifugation under the same conditions. Afterwards, cells are resuspended with 100 µL of Reagent A (Fixation Medium) of the Kit and incubated for 15 minutes at room temperature. After incubation, cells are washed again with 3 mL of PEB and centrifuged for 5 minutes at 1563 rpm and the supernatant is removed.

To aid permeabilisation, 100 µL of Reagent B (Permeabilisation Medium) of the Kit is added to the cell suspension. The content of the tube is split into two different tubes: 50 µL for negative control and 50 µL stained with Cardiac Troponin T Antibody- VioBlue conjugated (Miltenyi Biotec, 130-120-542) (4.5 µL of antibody are added to the 50 µL of cell suspension, with a final dilution of 1:11 (v/v)). These tubes are then vortexed for 5 seconds and incubated for 30 minutes in the dark at room temperature, so that antibody staining is effective.

Lastly, the antibody incubated cell suspension is washed with 3 mL of PEB, centrifuged for 5 minutes at 1563 rpm, the supernatant is removed and samples are analysed (both the ones stained with antibody and the negative controls) in a flow cytometer (MACSQuant VYB, Miltenyi Biotec) after resuspension in 1 mL of PEB.

### 3.5 Statistical Analysis

Statistical analysis was performed using GraphPad Prism software 9.0. Data in the text are expressed as mean ± SEM (standard error of the mean). Data in box plots are represented with the whiskers as the minimum and maximum of all of the respective data. For all experiments, differences between parameters were analysed with a Welch's t-test and a 95% confidence interval. In the drug induced heart failure experiments, differences between control and different groups were analysed by one-

way ANOVA (comparison between the mean of control and the mean obtained for each concentration in different parameters) followed by Dunnett's (all compared with control) *post hoc* multiple comparisons. A p-value (\*) < 0.05 was considered statistically significant.

## Chapter 4

# Results and Discussion

In this chapter, the results obtained for each experiment setup will be analysed and discussed. After casting, the cells started to spread out longitudinally along the force lines of the tissue, compacted and formed a coherently beating EHT within 3-5 days. The cantilevers not only anchored the EHTs, but also presented a rigid external structure to mimic *in vitro* cardiac tissue afterload. EHTs formation progress and spontaneous beating patterns were observed throughout time. If tissues homogeneously distributed around the pillars without rupture, then their formation was considered successful. The used EHT platform allowed to culture three tissues per well (Figure 3.1) and Figure 4.1 shows the outlook of an engineered heart tissue.

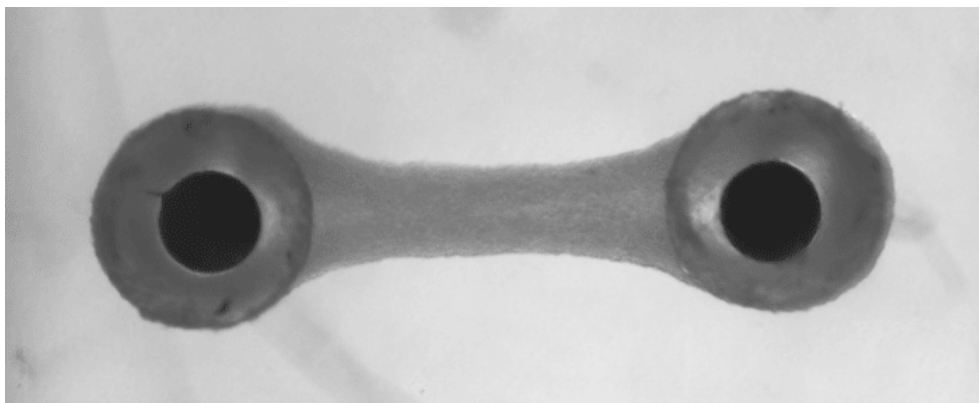


Figure 4.1: Bottom view of an engineered heart tissue cultured between the two PDMS cantilevers.

Through automated video optical recording, tissue behaviour was monitored and important parameters such as contraction force (CF), contraction velocity (CV), relaxation velocity (RV), contraction time at 10% or 90% (CT10 and CT90, respectively) and relaxation time at 10% and 90% (RT10 and RT90, respectively) were obtained and compared for each condition.

Across all experiments, it was possible to validate that tissues can be generated from previously differentiated and frozen CMs. This brings a major advantage in terms of workflow since differentiating hiPSCs is a time-consuming process and helps decreasing batch to batch variability (advantageous when it comes to comparing results).

All tissues were successfully generated and maintained with a medium with lactate and a physiologically relevant glucose concentration of 4.5 mM <sup>[57]</sup>. As described in Section 1.2.2, the addition of lactate is relevant for CMs since they can use it as a source to obtain ATP through Krebs cycle metabolism. However, non-CMs do not possess this ability, so the addition of glucose is necessary to maintain the fibroblasts and also allows the CMs to produce ATP through the glycolytic pathway.

The incorporation of fibroblasts aided to recapitulate more accurately the *in vivo* composition and cellular interaction in the human heart, increasing the mechanical integrity, connectivity and contractile force of tissues.

## 4.1 MYBPC3 Assay

The first goal of the project was to compare the behaviour between EHTs generated with cardiomyocytes containing a mutation in the MYBPC3 gene and EHTs produced with healthy cardiomyocytes, to see if the platform allowed HCM modeling. As explained in Section 1.1.3, mutations in MYBPC are the most common cause of HCM and this protein has a leading role in sarcomere organisation and cardiac muscle contraction, since it is involved in regulating the positions of myosin and actin for interaction, acting as a brake on cardiac contraction. Thus, it is essential to try to understand the effects of this mutation on contraction force and other relevant parameters, such as contraction/relaxation speed.

### 4.1.1 Horse serum-based experiments

As aforementioned in Section 1.2.3, horse serum helps to extend the duration of CMs culture time and increases their contractile activity and viability. Hence, EHTs were generated and maintained with a medium supplemented with 10% (v/v) of HS. After 10 days of culturing, the contractile function of 9 EHTs generated with the FLB line (control) and 11 EHTs made with the isogenic MYBPC3 mutant line was monitored. The results of the different parameters obtained are showed and compared for each cell line in the next figures and tables.

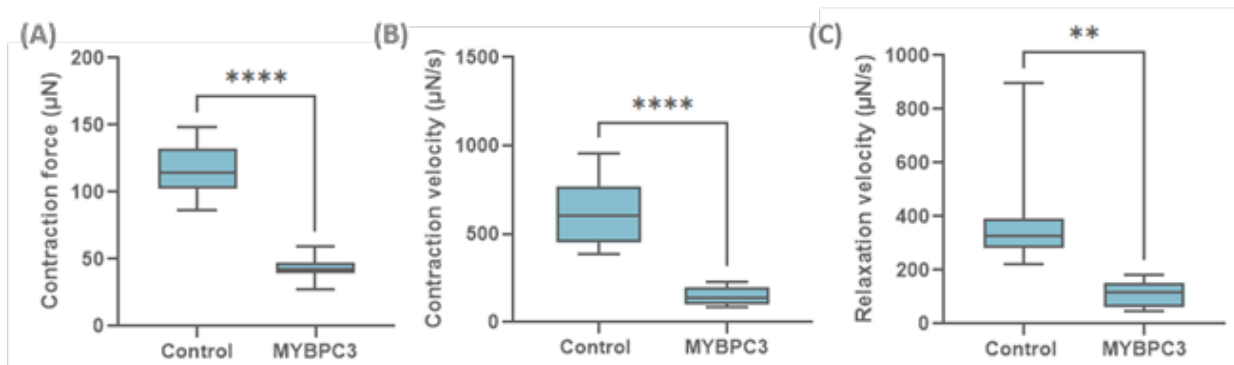


Figure 4.2: Comparison between **(A)** contractile force, **(B)** contraction velocity and **(C)** relaxation velocity of the engineered heart tissues generated with the FLB (control) and the MYBPC3 mutant cell lines, obtained after 10 days of generation in CM Low Ins+Low Gluc+TDI+Lact+HS Medium. \*\*\*\* $p \leq 0.0001$ ; \*\* $p \leq 0.01$ .

Table 4.1: Contraction force, contraction velocity and relaxation velocity obtained for EHTs made with the different cell lines when supplemented with CM Low Ins+Low Gluc+TDI+Lact+HS Medium, with the respective units.

	Control	MYBPC3
<b>Contraction Force (µN)</b>	117.3 ± 5.94	43.32 ± 2.46
<b>Contraction Velocity (µN/s)</b>	642.2 ± 58.8	153.1 ± 15.0
<b>Relaxation Velocity (µN/s)</b>	387.4 ± 66.6	115.5 ± 13.3

Contraction force was obtained with the aid of the formula of Appendix C, using the deflection of

the pillars. By knowing how long it takes for each tissue to completely contract or relax, contraction or relaxation speed can be ascertained, respectively. As shown in Figure 4.2 and Table 4.1, there are substantial differences between isogenic tissues in the three evaluated parameters, especially in contraction force and contraction velocity.

When it comes to contraction force, EHTs generated with mutant cardiomyocytes showed significantly lower values, with a force decrease of 63.1% when compared to healthy ones. A study conducted by Birket et al., 2015 performed single-cell contractility measurements, using serum-free conditions and TDI medium, and compared three different patient derived hiPSC-CMs with the same MYBPC3 mutation as the one studied in this project against CMs derived from two hiPSC lines generated from healthy controls (measurements were made at day 25 of differentiation). Mutant CMs exerted appreciably less force at single-cell level (an averaged decrease of 46.9%), with an average traction force of  $0.44 \pm 0.01 \mu\text{N}$  for the three HCM cell lines when compared to  $0.84 \pm 0.02 \mu\text{N}$  for the healthy controls [58]. As aforementioned, this decrease in CF generation from healthy to mutated tissues was also observed in the used 3D platform, naturally with a higher order of greatness. Since a 3D microenvironment is always preferable compared to 2D single cell CM cultures (due to a better degree of recapitulation of the human *in vivo* environment) and single-cell measurements may offer a very low level of sensitivity to detect defects in function (and even control cells may function far from their full dynamic range [58]), this EHT platform offers an advantage to model and study the consequences of MYBPC3 mutations, particularly when it comes to contraction force differences.

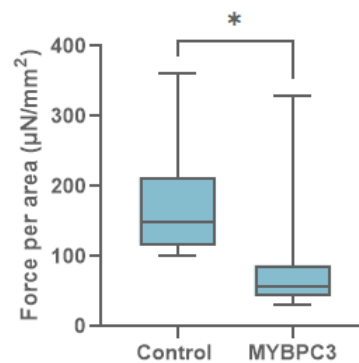


Figure 4.3: Comparison between force per area of the engineered heart tissues generated with the FLB (control) and the MYBPC3 mutant cell lines, obtained after 10 days of generation in CM Low Ins+Low Gluc+TDI+Lact+HS Medium. \* $p \leq 0.05$ .

Table 4.2: Contraction force per area obtained for EHTs made with the different cell lines when supplemented with CM Low Ins+Low Gluc+TDI+Lact+HS Medium, with the respective units.

	Control	MYBPC3
<b>Force per area</b> ( $\mu\text{N}/\text{mm}^2$ )	$173.4 \pm 25.7$	$87.42 \pm 26.8$

As shown in Figure 4.3 and Table 4.2, control EHTs displayed a force per area significantly higher than mutated ones, that translates into a 49.6% difference. In a study conducted by van Dijk et al., 2009 comparisons were made between human cardiac samples from 11 patients carrying a MYBPC3 mutation and 13 nonfailing donors. Force measurements in mechanically isolated and permeabilised cardiomyocytes demonstrated a notable reduction of 42% in maximum force-generating capacity in MYBPC3 mutants ( $20.2 \pm 2.7 \text{ kN}/\text{m}^2$ ) when compared to healthy patients ( $34.5 \pm 1.1 \text{ kN}/\text{m}^2$ ) [16]. In another study described by Witjas-Paalberends et al., 2013, where force measurements were conducted in the same conditions as the previous mentioned study, the same effect was observed when comparing

13 healthy cardiac samples ( $36 \pm 2 \text{ kN/m}^2$ ) versus 21 MYBPC3 mutant carriers ( $26 \pm 1 \text{ kN/m}^2$ ), which represents a 28% decrease in CF generation [59].

Even though results obtained with the EHT platform are still significantly smaller (a difference of  $10^3$  in order of magnitude) than the ones observed with human heart samples (indicating that additional maturation steps for the hiPSC-CMs are necessary), the model portrays impaired contractile function between healthy CMs and MYBPC3 mutant CMs.

In previous studies, it has been reported that loss of MYBPC affects the kinetics of contraction and relaxation [16] [60]. This effect is observed in Figure 4.2 and Table 4.1-(B) and (C), since MYBPC3 mutant EHTs contract 75.5% slower than FLB EHTs. Mutated CMs also achieved a relaxed state slower than control CMs, with a 71.2% speed reduction. Figure 4.2- (C) shows an outlier value (the maximum of the dataset) for the control line of  $895.50 \mu\text{N/s}$ . Nevertheless, if this value is disregarded of the statistical analysis, relaxation speeds are still notably different (Figure 4.4), with mutant CMs relaxing 65.6% slower than healthy ones (the mean value for the mutant CMs would alter to  $323.90 \pm 20.6 \mu\text{N/s}$ ).

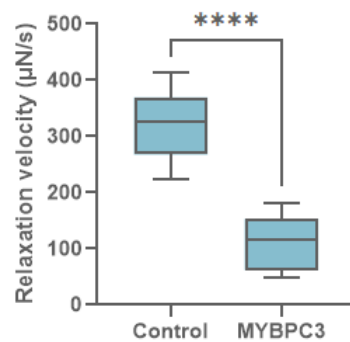


Figure 4.4: Relaxation velocity of the engineered heart tissues generated with the FLB (control) and the MYBPC3 mutant cell lines if the maximum of the dataset (an outlier value) is removed from the statistical analysis. The decrease of relaxation speed in EHTs with the mutant cell line is even more significant when compared to EHTs with the healthy cell line. \*\*\*\* $p \leq 0.0001$ .

A study conducted by Cohn et al., 2019 using 3D cardiac microtissues (a mixture hiPSC-CMs derived from the PGP1 cell line and then purified with a lactate treatment, fibroblasts and an ECM slurry) growing between two PDMS cantilevers (similar to the used platform in this project) set out to compare the effect of MYBPC3 mutations (two different ones, a truncation mutation known as Trp792ValfsX41 and a missense mutation addressed as R502W) in isogenic iPSC models. When compared to controls, both MYBPC3 mutations showed an increase in maximum contraction velocity, which is not consistent with what is observed in the present model. These disparities are due to the difference of mutations studied, since different mutations lead to different consequences in the MYBPC3 gene and therefore can cause distinct phenotypes. [55].

In the next figures are presented the time that tissues took to achieve 10% and 90% of contraction and relaxation. In certain pathological conditions, these parameters are important for comparison with healthy states and usually, tissues generated with diseased cell lines take longer to reach 10% or 90% of both contraction and relaxation.

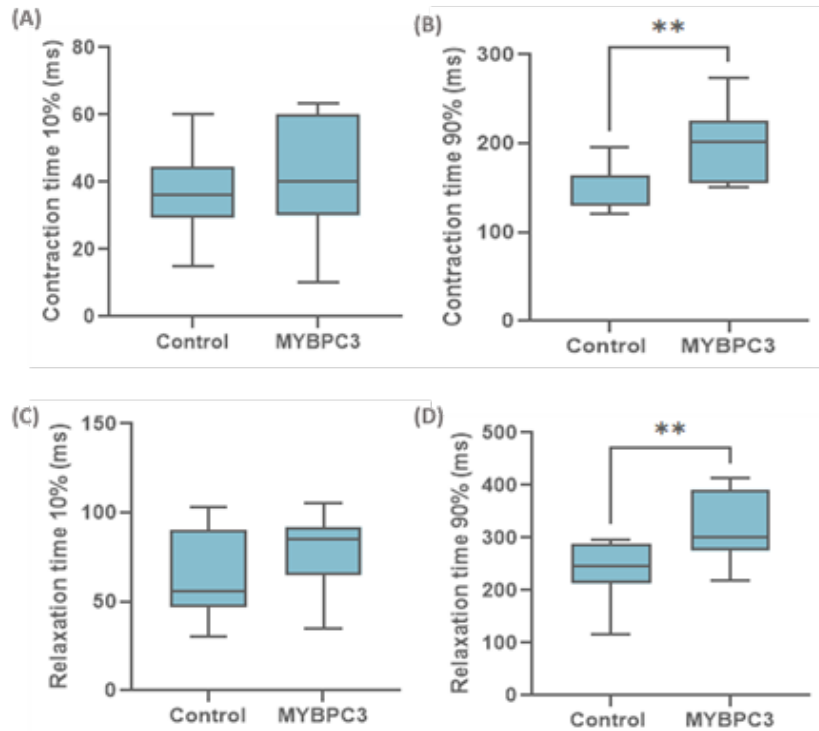


Figure 4.5: Contraction time at (A) 10% and (B) 90% and relaxation time at (C) 10% and (D) 90% for tissues generated with the FLB (control) and the MYBPC3 mutant cell lines, obtained after 10 days of culturing in CM Low Ins+Low Gluc+TDI+Lact+HS Medium.  $**p \leq 0.01$ .

Table 4.3: Contraction/Relaxation time at 10% and 90% obtained for EHTs made with the different cell lines when supplemented with CM Low Ins+Low Gluc+TDI+Lact+HS Medium. All the values are in milliseconds.

	Control	MYBPC3
<b>CT10</b>	37.22 ± 3.96	41.08 ± 4.77
<b>CT90</b>	144.3 ± 8.31	195.0 ± 12.4
<b>RT10</b>	65.84 ± 7.94	78.42 ± 6.47
<b>RT90</b>	240.9 ± 17.9	322.8 ± 19.9

As expected, the mutant MYBPC3 cell line took more time to achieve the mentioned parameters of contraction and relaxation. Figures 4.5- (A) and (C) and Table 4.3 indicate that both tissues generated with healthy CMs or mutated CMs achieved 10% of contraction or relaxation in similar times with mutated tissues reaching CT10 and RT10 9.38% or 16.0% slower than healthy ones, respectively.

However, the differences between cell lines are evident for CT90 and RT90 (Figures 4.5- (B) and (D) and Table 4.3). Tissues generated with mutant CMs reached 90% of contraction 26.0% slower than FLB CMs. As for relaxation, MYBPC3 mutant tissues achieved RT90 25.4% slower than control tissues. The increase observed for CT90 and RT90 in MYBPC3 mutant EHTs is a consequence of lower contraction and relaxation speeds, respectively.

In the previously mentioned assay led by Cohn et al., there was no significant changes in contraction time between control and mutant cell lines (approximately 320 ms, higher than both CT10 and 90 for FLB and MYBPC3 cell lines used for the current project, which can again be justified by the difference in mutations studied) but the time to achieve half of relaxation was also notably prolonged for the mutant cell lines when compared to control (approximately 350 ms *versus* 200 ms) [55], which is also closely

portrayed in the present model by the RT90 parameter and further supports that impaired relaxation is a consequence of HCM thick-filament mutations.

#### 4.1.2 Serum-free Experiments

Since the cells that were used to generate EHTs from the previously discussed experiments were not purified, it was not certain if the contraction disparities observed were due to the differences in CM content from each batch of cells used to generate the EHTs or to the different cell composition between FLB and MYBPC3 mutant lines. Therefore, previous experiments were repeated using lactate treated cells (cultured as explained in section 3.2.1) and without HS. Although HS is a standard additive in mediums as a source of hormones, nutrients and growth factors, it can affect CMs morphology, growth and differentiation and batch to batch variabilities may influence results [34]. Furthermore, HS contains undefined molecules that generate unclear effects in cells.

After 3 days of culturing, the EHTs generated with the FLB cell line showed spontaneous beating patterns (although not as strong as the ones in tissues generated with HS), unlike the ones made with the MYBPC3 mutant cell line. In fact, the latest only started to show some slight twitching after 5 days, not consistent contractions.

Nevertheless, all of them were maintained until measuring day and contractile function of 21 FLB EHTs and 21 MYBPC3 mutant EHTs was tracked. Before presenting the results obtained for FLB and MYBPC3 mutant EHTs, it is important to know the results of the FACS analysis and ascertain the impact of cardiomyocyte content in different contractile parameters.

#### FACS Analysis and its Implications

The efficacy of purification through lactate treatment was evaluated and quantified through FACS analysis. As mentioned in Section 1.2.2, lactate treatment allows to purify a culture of cells and enrich it with hiPSC-CMs, since they are capable of using lactate to obtain ATP, unlike non-CMs.

This analysis was performed after collecting lactate treated cells that were used to make EHTs, without compromising the requirement of 800K cells/well, to evaluate the cardiomyocyte purity of each batch of cells. The 42 EHTs generated and compared (21 from the FLB line and 21 from the MYBPC3 line) were cultured in three different occasions, with Group 1 comparing 9 EHTs of each cell line, Group 2 comparing 7 EHTs with CMs from the FLB line and 9 EHTs with CMs from the MYBPC3 mutant cell line and Group 3 comparing 3 EHTs from the FLB line and 5 from the MYBPC3 line. Cardiomyocyte content of each batch of cells used to generate these tissues is shown in Table 4.4.

Table 4.4: FACS analysis results reflecting the content of cardiomyocytes (% CM) from each batch of cells used to generate the different groups of EHTs from the FLB cell line and the MYBPC3 mutant line.

This cardiomyocyte content is crucial to know the success rate of lactate purification treatment.

	Group 1		Group 2		Group 3	
	FLB	MYBPC3	FLB	MYBPC3	FLB	MYBPC3
number of tissues (n)	9	9	7	9	5	3
% CM	67	48	86	50	36	50

These results showed that cell purification in a glucose depleted medium supplemented with lactate for four days (CM Low Ins+TDI+Lact Medium), followed by recovery in the same medium with addition of 4.5 mM of glucose (CM Low Ins+Low Gluc+TDI+Lact Medium) did not achieve the expected purity levels. MYBPC3 mutant cell line attained a steady purity of CMs around 50% for its three different cell batches, while the FLB cell line content varies greatly between its batches.

Lactate-based enrichment can generate purity yields up to 80-99% in hESC-CMs and hiPSC-CMs (for example, protocols developed by Tohyama et al., 2013 or Fuerstenau-Sharp et al., 2015) when these cells are maintained in a glucose-depleted medium supplemented with lactate for seven days [29] [61]. Moreover, these protocols describe that this lactate method was applied to cells on day 20 to 30 of differentiation (Tohyama et al., 2013) or on day 16 to day 18 of differentiation (Fuerstenau-Sharp et al., 2015).

Since FLB and MYBPC3 mutant derived CMs were subjected to lactate treatment after only 13 or 14 days of differentiation, a possible strategy to implement in the future and increase CM content would be to differentiate cells a few more days before culturing them with lactate (to avoid undifferentiated hiPSCs) and extend the lactate treatment to seven days instead of four days, since adding glucose may allow non-CMs to proliferate as well.

Ideally, comparison between the different parameters obtained for EHTs generated with the FLB and mutant cell lines would be done with FLB and mutated EHTs that had a close content of cardiomyocytes, so that the contraction output would be similar and to confirm results robustness. FACS analysis showed that this prerequisite was not achieved, since cardiomyocyte content varies for the two different cell lines in all groups.

To ascertain the impact of this CM content disparity in generated EHTs, a thorough comparison analysis was conducted for the different parameters obtained for each cell line, in the different groups. These results are shown from Figures 4.6 to 4.12 and from Tables 4.5 to 4.8. Results related to force per area were not available for all datasets.

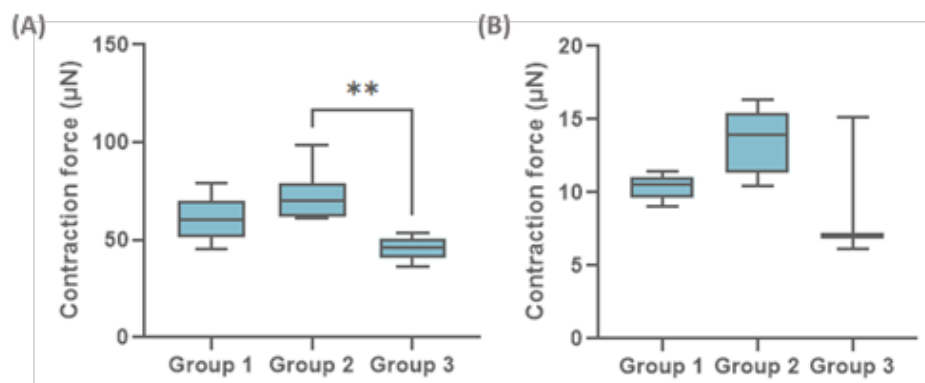


Figure 4.6: Contraction force obtained for the EHTs generated in each group with the (A) FLB cell line and (B) MYBPC3 mutant cell line.  $**p \leq 0.01$ .

Table 4.5: Contraction force of EHTs generated in each group with the FLB and MYBPC3 mutant cell lines. All values are in µN.

Group 1		Group 2		Group 3	
FLB	MYBPC3	FLB	MYBPC3	FLB	MYBPC3
60.38 ± 3.41	10.39 ± 0.25	72.30 ± 4.62	13.40 ± 0.67	45.84 ± 2.56	9.455 ± 2.35

Cardiomyocyte content for the three batches of the MYBPC3 mutant cell line was around 50% and Figure 4.6- (B) showed that there were no significant differences in contraction force across the three groups (Table 4.5 also indicates that mutant EHTs contracted with a force variance between 9,455 and 13,40 µN). However, FLB cell batches reflected that higher CM contents translate into higher contraction forces. In fact, EHTs from Group 2 had the highest CM purity (86%) and contracted stronger than the ones from Group 1 and 3 (relatively to this latest group, Figure 4.6- (A) depicts a significant contraction

force reduction of 36.0% when compared to Group 2).

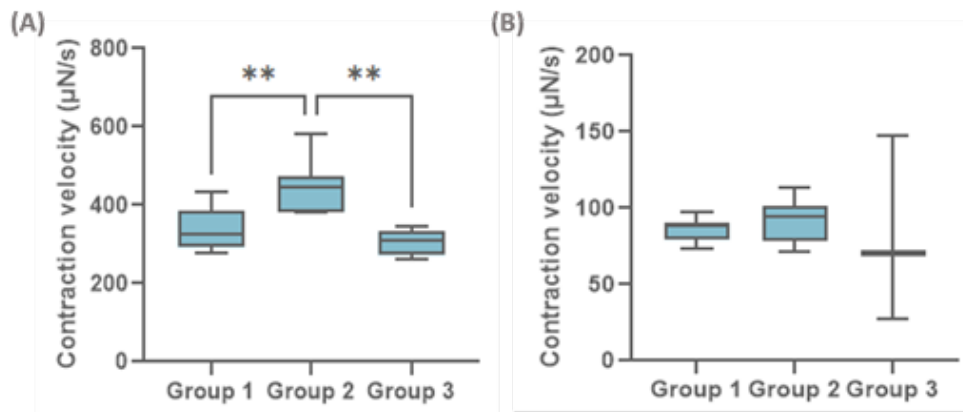


Figure 4.7: Contraction velocity obtained for the EHTs generated in each group with the (A) FLB cell line and (B) MYBPC3 mutant cell line.  $**p \leq 0.01$ .

Table 4.6: Contraction velocity of EHTs generated in each group with the FLB and MYBPC3 mutant cell lines. All values are in  $\mu\text{N/s}$ .

Group 1		Group 2		Group 3	
FLB	MYBPC3	FLB	MYBPC3	FLB	MYBPC3
338.2 $\pm$ 17.2	85.90 $\pm$ 2.30	445.9 $\pm$ 25.2	91.80 $\pm$ 4.42	304.3 $\pm$ 13.2	81.91 $\pm$ 28.8

As for contraction velocity, EHTs composed by MYBPC3 mutant cells showed no notable difference across all groups, with speeds varying between 81.91 and 91.80  $\mu\text{N/s}$ . For FLB cells, contractile velocity varied greatly between batches (values range from 304.3 to 445.9  $\mu\text{N/s}$ ) and the higher the CM content, the faster tissues contracted. EHTs from Group 2 contracted 24.2% and 31.8% than the ones from Group 1 and Group 3, respectively.

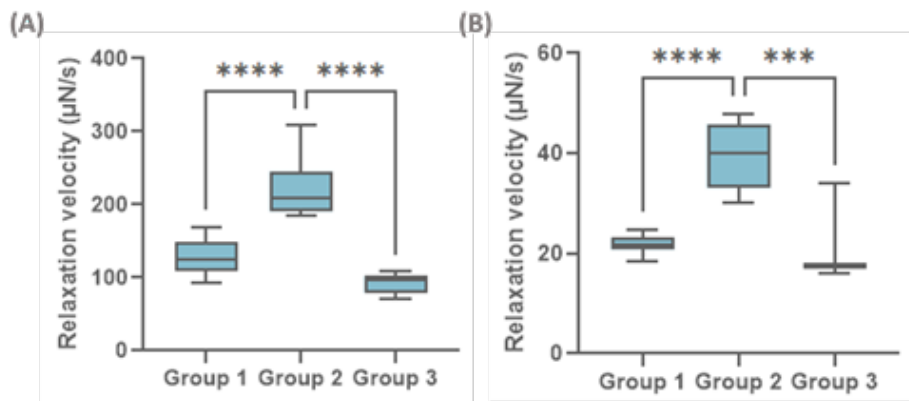


Figure 4.8: Relaxation velocity obtained for the EHTs generated in each group with the (A) FLB cell line and (B) MYBPC3 mutant cell line.  $***p \leq 0.001$ ;  $****p \leq 0.0001$ .

Table 4.7: Relaxation velocity of EHTs generated in each group with the FLB and MYBPC3 mutant cell lines. All values are in  $\mu\text{N/s}$ .

Group 1		Group 2		Group 3	
FLB	MYBPC3	FLB	MYBPC3	FLB	MYBPC3
$128.2 \pm 7.47$	$21.76 \pm 0.58$	$221.8 \pm 15.1$	$39.14 \pm 2.05$	$92.10 \pm 5.56$	$22.63 \pm 4.72$

When it comes to relaxation velocity, Figure 4.8 exhibits significant differences for both MYBPC3 cell batches (in spite of their close CM content, EHTs from Group 2 relaxed 44.4% and 42.2% faster than the ones from Group 1 and Group 3, respectively) and FLB cell batches. For the latest, tissues from Group 2 reached a relaxed state faster than the other two groups (42.2% than Group 1 and 58.8% than Group 3), which may also be a consequence of a higher CM content.

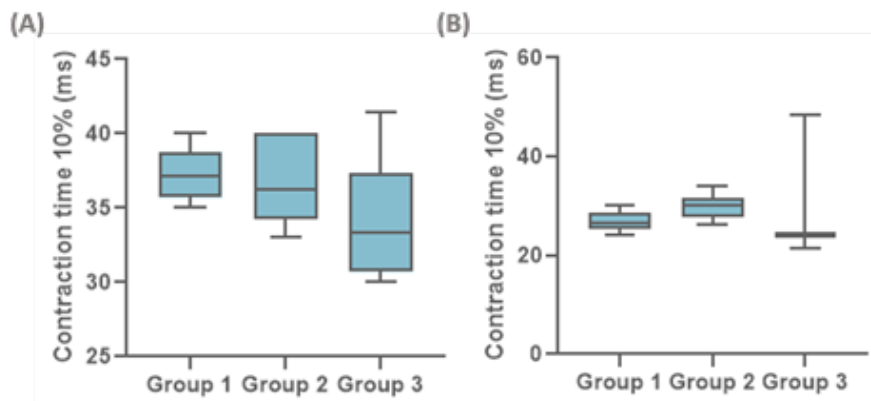


Figure 4.9: Contraction time at 10% obtained for the EHTs generated in each group with the (A) FLB cell line and (B) MYBPC3 mutant cell line.

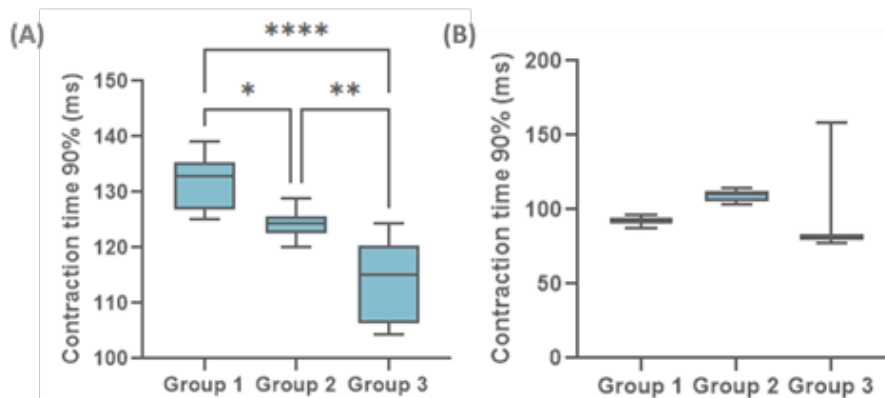


Figure 4.10: Contraction time at 90% obtained for the EHTs generated in each group with the (A) FLB cell line and (B) MYBPC3 mutant cell line. \* $p \leq 0.05$ ; \*\* $p \leq 0.01$ ; \*\*\*\* $p \leq 0.0001$ .

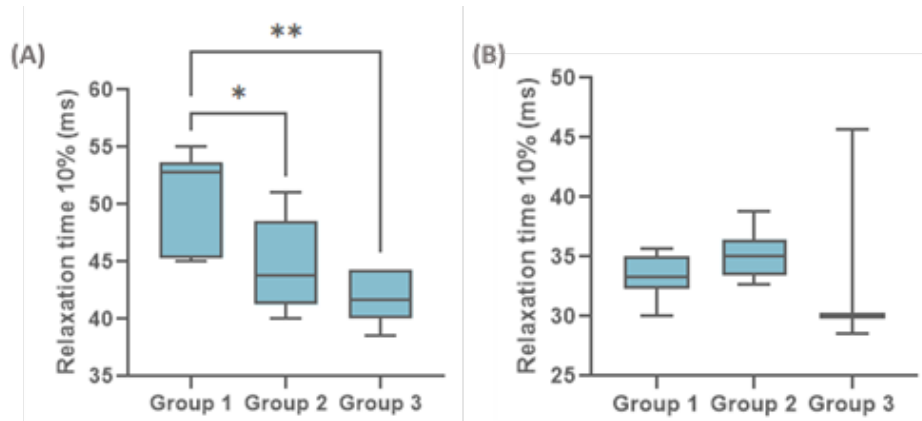


Figure 4.11: Relaxation time at 10% obtained for the EHTs generated in each group with the (A) FLB cell line and (B) MYBPC3 mutant cell line. \* $p \leq 0.05$ ; \*\* $p \leq 0.01$ .

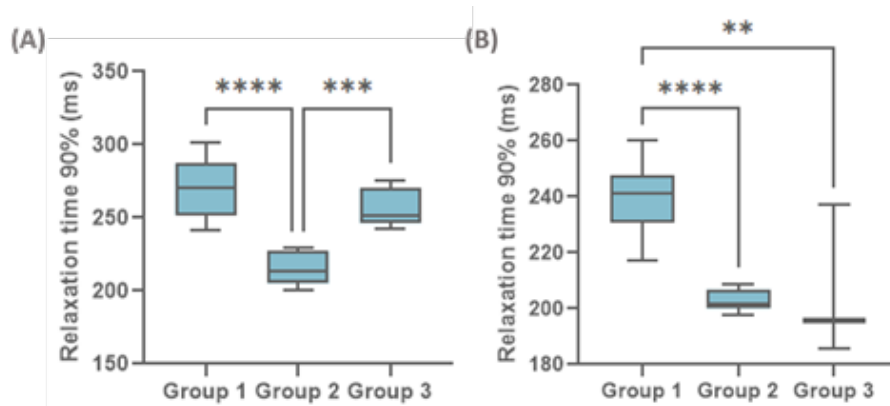


Figure 4.12: Relaxation time at 90% obtained for the EHTs generated in each group with the (A) FLB cell line and (B) MYBPC3 mutant cell line. \*\* $p \leq 0.01$ ; \*\*\* $p \leq 0.001$ ; \*\*\*\* $p \leq 0.0001$ .

Table 4.8: CT10, CT90, RT10, RT90 of EHTs generated in each group with the FLB and MYBPC3 mutant cell lines. All values are in milliseconds.

	Group 1		Group 2		Group 3	
	FLB	MYBPC3	FLB	MYBPC3	FLB	MYBPC3
<b>CT10</b>	37.38 ± 0.55	26.95 ± 0.58	36.54 ± 0.93	30.03 ± 0.77	33.90 ± 1.77	31.43 ± 7.03
<b>CT90</b>	131.9 ± 1.51	92.29 ± 0.86	124.3 ± 0.95	108.9 ± 1.19	113.8 ± 3.08	105.7 ± 21.6
<b>RT10</b>	50.41 ± 1.29	33.38 ± 0.55	44.62 ± 1.36	35.21 ± 0.59	42.10 ± 0.95	34.76 ± 4.48
<b>RT90</b>	271.0 ± 6.22	239.2 ± 3.94	214.7 ± 3.71	202.7 ± 1.20	256.9 ± 5.22	206.2 ± 12.9

Figure 4.9 shows no notable differences for the CT10 parameter for both cell lines across batches. For MYBPC3 mutant cell line, there were also no significant differences in the time that tissues took to achieve 90% of contraction and 10% of relaxation. However, and in spite of the similar CM content across batches, the three groups of EHTs got to 90% of relaxation in very distinct times (varying from 202.7 to 271.0 ms).

As for the FLB cell line, Group 3 of EHTs (the one with lowest CM purity) was the one that took the least amount of time to achieve CT90, RT10 and RT90. However, the group of EHTs with the highest purity (Group 2) was not the slowest to reach all of them, so there is no evident impact of CM content in these parameters.

All of these results revealed that CM content has a notable impact on EHTs contraction output. The FLB line proved that a higher CM content translates into a more significant contraction force, contraction velocity and relaxation velocity.

As for the differences in cell composition between FLB and MYBPC3 lines, it is important to notice that even though CM content was higher for mutated EHTs than healthy ones in Group 3 (50% *versus* 36%, respectively), healthy EHTs still showed significantly higher contraction force (Table 4.5:  $45.84 \pm 2.56$  *versus*  $9.455 \pm 2.35$   $\mu\text{N}$ ), contraction velocity (Table 4.6:  $304.3 \pm 13.2$  *versus*  $81.91 \pm 28.8$   $\mu\text{N/s}$ ) and relaxation velocity (Table 4.7:  $92.10 \pm 5.56$  *versus*  $22.63 \pm 4.72$   $\mu\text{N/s}$ ) when compared to mutated EHTs.

Since contraction output was more significant for healthy EHTs than mutated EHTs, regardless of the CM content of each batch of cells, the next section focus on the comparison between the combined parameters obtained for healthy tissues and mutant ones in the three groups.

### Comparison between EHTs generated with the healthy and mutated cell lines

The results obtained for 21 tissues produced with the FLB cell line and 21 tissues generated with the MYBPC3 mutant cell line, in three different occasions and supplemented with Low Ins+Low Gluc+TDI+Lact Medium, are present in the next figures and tables. Results related to force per area for each tissue were not available for all datasets.

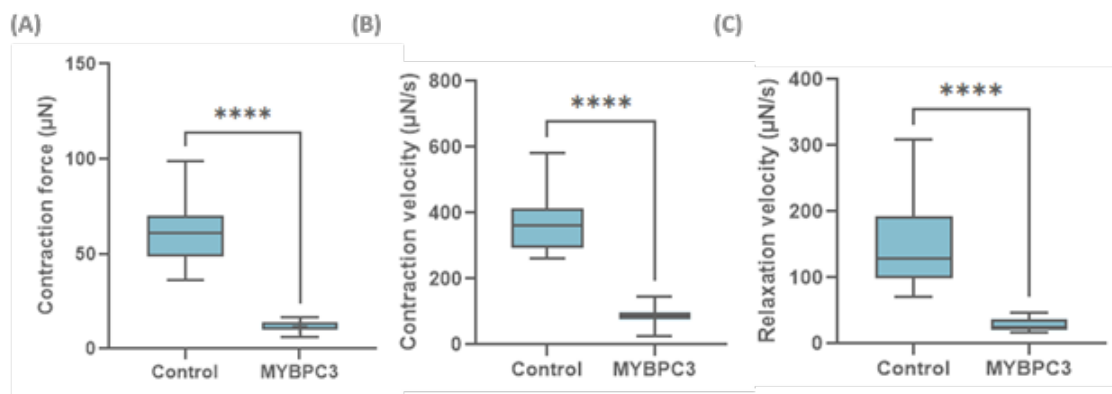


Figure 4.13: Comparison between (A) contractile force, (B) contraction velocity and (C) relaxation velocity of the engineered heart tissues generated with the FLB (control) and the MYBPC3 mutant cell lines, obtained after 10 days of generation in CM Low Ins+Low Gluc+TDI+Lact Medium. \*\*\*\* $p \leq 0.0001$ .

Table 4.9: Contraction force, contraction velocity and relaxation velocity obtained for EHTs made with the different cell lines supplemented with CM Low Ins+Low Gluc+TDI+Lact Medium, with the respective units.

	Control	MYBPC3
<b>Contraction Force (<math>\mu\text{N}</math>)</b>	$60.89 \pm 3.09$	$11.55 \pm 0.58$
<b>Contraction Velocity (<math>\mu\text{N/s}</math>)</b>	$366.0 \pm 17.2$	$87.86 \pm 4.70$
<b>Relaxation Velocity (<math>\mu\text{N/s}</math>)</b>	$150.8 \pm 12.9$	$29.33 \pm 2.17$

Tissues composed of healthy cardiomyocytes exhibited significantly higher values of contraction force and contraction/relaxation speed when compared to tissues composed of mutant cardiomyocytes. In terms of contraction force, healthy EHTs contract 81.0% stronger than mutated ones. When compared to the previously mentioned studies conducted by Birket et al., van Dijk et al. and Witjas-Paalberends et al., the decrease in CF generation from the healthy cell line to the mutant one is also observed in the

present EHT platform with a higher order of greatness than 2D single cell CM cultures, possibly due to the scale up from a 2D to a 3D microenvironment and differences in measuring tools and procedures. Furthermore, these 3D cardiac tissues contract with lower force than human cardiac samples most likely due to lack of hiPSC-CMs maturation.

As for contraction speed, mutant EHTs suffered a 76.0% contraction velocity reduction when compared to control EHTs. Furthermore, mutated EHTs also relaxed 80.5% slower in contrast to healthy ones. This reductions in both contraction and relaxation speeds are similar to the ones observed in the experiments with HS and once again, the increase in maximum contraction velocity for the mutated cell line is not consistent with the results obtained in the aforementioned study developed by Cohn et al. (which can again be justified by differences in mutations studied). Nevertheless, the model was able to replicate impaired kinetics of contraction and relaxation.

All of the three previous discussed parameters were lower in the serum-free experiments when compared to the ones conducted with this supplement, for both the healthy and the mutated cell lines (Tables 4.1 and 4.9). However, it is not certain if this decrease was due to the removal of the serum or due to the poor cell quality of the hiPSC-CMs used to generate the EHTs, observed across the three different cultured groups. In the future, it would be beneficial to repeat this experiment to ascertain if the removal of HS exerts a significant impact in EHT culturing and maintenance.

The results for the CT10, CT90, RT10 and RT90 are depicted in Figure 4.14.

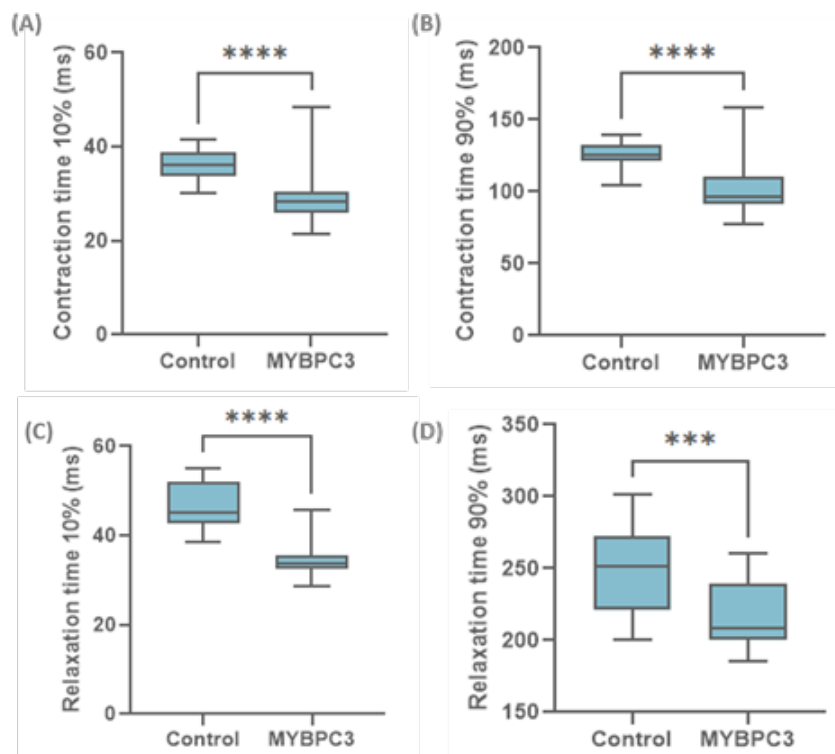


Figure 4.14: Contraction time at (A) 10% and (B) 90% and relaxation time at (C) 10% and (D) 90% for EHTs generated with the FLB (control) and the MYBPC3 mutant cell lines, obtained after 10 days of culturing in CM Low Ins+Low Gluc+TDI+Lact Medium. \*\*\* $p \leq 0.001$ ; \*\*\*\* $p \leq 0.0001$ .

Table 4.10: Contraction/Relaxation time at 10% and 90% obtained for EHTs made with the different cell lines supplemented with CM Low Ins+Low Gluc+TDI+Lact Medium. All the values are in milliseconds.

	<b>Control</b>	<b>MYBPC3</b>
<b>CT10</b>	36.27 ± 0.65	28.91 ± 1.15
<b>CT90</b>	125.0 ± 1.86	101.3 ± 3.59
<b>RT10</b>	46.50 ± 1.07	34.36 ± 0.75
<b>RT90</b>	248.9 ± 6.28	218.8 ± 4.61

Unlike what happens in the experiences with HS supplementation, EHTs made with MYBPC3 mutant CMs took less time to reach contraction and relaxation times, at both percentages.

Figures 4.14-(A) and (B) show that EHTs composed of mutated CMs were 20.3% and 19.0% faster to reach 10% and 90% of contraction, respectively. As for the relaxation parameters (Figures 4.14- (B) and (D)), achieving 10% or 90% of relaxation was 26.1% and 12.1% faster for mutated tissues when compared to healthy ones, respectively.

When compared to the previously mentioned Cohn et al. assay, the EHT platform was not able to replicate impaired relaxation time observed as a consequence of HCM thick-filament mutations, further supporting the need to repeat this experiment.

## 4.2 Drug Induced Heart Failure Model

The second goal of this project was to verify if the platform was able to model heart failure, after long-term exposure of the tissues to different concentrations of norepinephrine.

As mentioned in Section 1.2.4, norepinephrine is a  $\beta_1$  adrenoceptor agonist that produces a short term chronotropic and inotropic response to enhance the heart's "fight-or-flight" response. However, catecholamine overstimulation (due to prolonged SNS activity) contributes to arrhythmias and heart failure development and progression.

Thus, these tissues were cultured in a CM Low Ins+Low Gluc+TDI+Lact Medium and from day 10 to 17, NE was added daily to each well to test the effects of three different drug concentrations, when compared to control tissues: 10  $\mu$ M, 50  $\mu$ M and 100  $\mu$ M (Figure 4.15). HS was not added to the medium, since some proteins in this supplement can bind to drugs and influence functional properties in drug-screening platforms<sup>[34]</sup>.

As explained in Section 3.3, contractile function of EHTs was also monitored 10 days after culturing (prior to drug administration). These measurements are the baseline for tissue behaviour evolution and the differences in obtained parameters before and after drug administration are shown in Appendix D for both experiments and for each condition (control, 10  $\mu$ M, 50  $\mu$ M and 100  $\mu$ M).

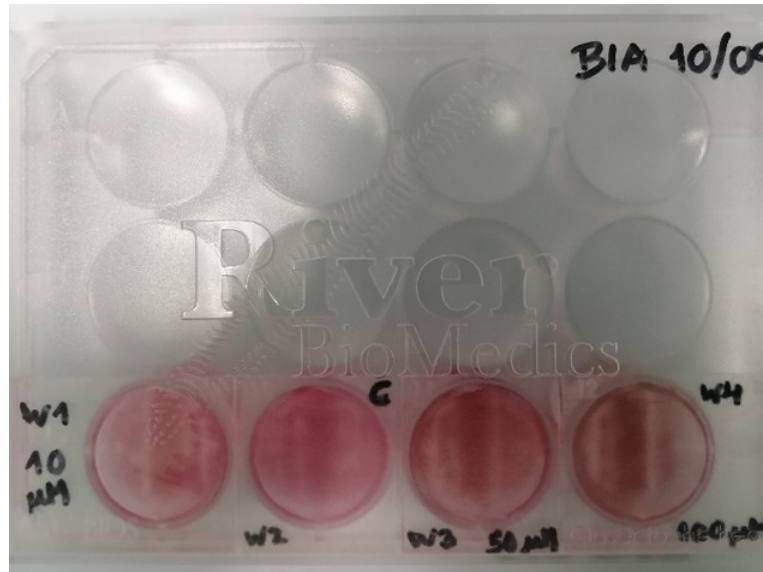


Figure 4.15: Top view of the wells used to culture EHTs in CM Low Ins+Low Gluc+TDI+Lact Medium to study the effects of three different NE concentrations: 10  $\mu\text{M}$ , 50  $\mu\text{M}$  and 100  $\mu\text{M}$ , when compared to control tissues.

The effect of these concentrations was tested in two different occasions, Experiment 1 and Experiment 2. In Experiment 1, comparison of the effects was made between three tissues for each condition ( $n=3$  for all conditions). However, in Experiment 2, 50  $\mu\text{M}$  of NE were tested in only one tissue, since the other two tissues in the well were lost due to tissue malformation, while control conditions and other concentrations were tested in three tissues ( $n=1$  for 50  $\mu\text{M}$  and  $n=3$  for all other concentrations and control tissues). All tissues displayed arrhythmias when compared to control EHTs, regardless of the administrated concentration.

The results obtained for both experiments are presented in the next figures and tables. Results related to force per area for each tissue were not available for these datasets.

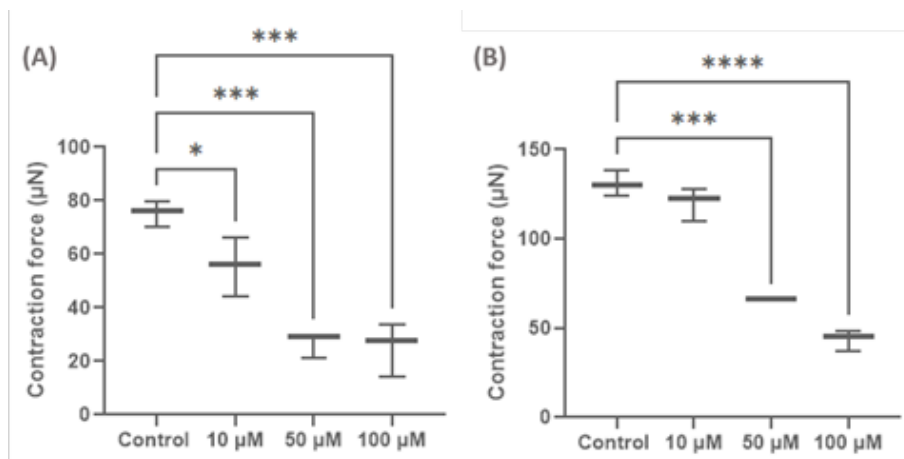


Figure 4.16: Contraction force obtained after incubating the tissues for 7 days with the different drug concentrations (10  $\mu\text{M}$ , 50  $\mu\text{M}$  and 100  $\mu\text{M}$ ) when compared to control tissues, for (A) Experiment 1 and (B) Experiment 2. \* $p \leq 0.05$ ; \*\*\* $p \leq 0.001$ ; \*\*\*\* $p \leq 0.0001$ .

Table 4.11: Contraction force values for EHTs from both experiments. All values are in  $\mu\text{N}$ .

	Experiment 1	Experiment 2
<b>Control</b>	75.38 $\pm$ 2.29	130.9 $\pm$ 3.36
<b>10 <math>\mu\text{M}</math></b>	55.61 $\pm$ 5.26	120.3 $\pm$ 4.37
<b>50 <math>\mu\text{M}</math></b>	26.62 $\pm$ 2.29	66.04 $\pm$ 0.00
<b>100 <math>\mu\text{M}</math></b>	25.20 $\pm$ 4.65	43.83 $\pm$ 2.80

As shown in Figure 4.16 and Table 4.11, there was a decrease in contraction force as tissues were subjected to an increasing drug concentration for both experiments, although the effect of long-term exposure to 10  $\mu\text{M}$  was not as statistically significant as when compared to tissues exposed to 50  $\mu\text{M}$  and 100  $\mu\text{M}$ . For Experiment 1, tissues incubated with 10  $\mu\text{M}$ , 50  $\mu\text{M}$  and 100  $\mu\text{M}$  contract 26.2%, 64.7% and 66.6% slower on average when compared to control, respectively. As for Experiment 2, beating force decreases 8.04%, 49.5% and 66.5% for 10  $\mu\text{M}$ , 50  $\mu\text{M}$  and 100  $\mu\text{M}$  when compared to control tissues.

A study conducted by Tiburcy et al., 2017 with engineered heart myocardium (EHM) tissues generated with PSCs (particularly the embryonic stem cell line HES2-RFP) and human foreskin fibroblasts in serum-free conditions, growing between two flexible holders fabricated with the biocompatible TangoBlack polymer displayed that stimulation with NE for 7 days (concentrations between 0.001-1  $\mu\text{M}$ ) induced contractile dysfunction in the EHMs in a concentration dependent manner, with a evident decrease in contraction force [49]. A study developed by Thomas et al., 1978, in which nineteen patients with different levels of congestive heart failure were tested, displayed that plasma norepinephrine concentration is directly related to the degree of left ventricular dysfunction and the higher this concentration, the greater the contraction force impairment [62].

The present platform was also able to mimic this contractile dysfunction in a concentration dependent manner observed in human patients and in other PSCs-CMs derived models, so it is a valid option to further study the effects of catecholamine overstimulation in CMs and HF progression.

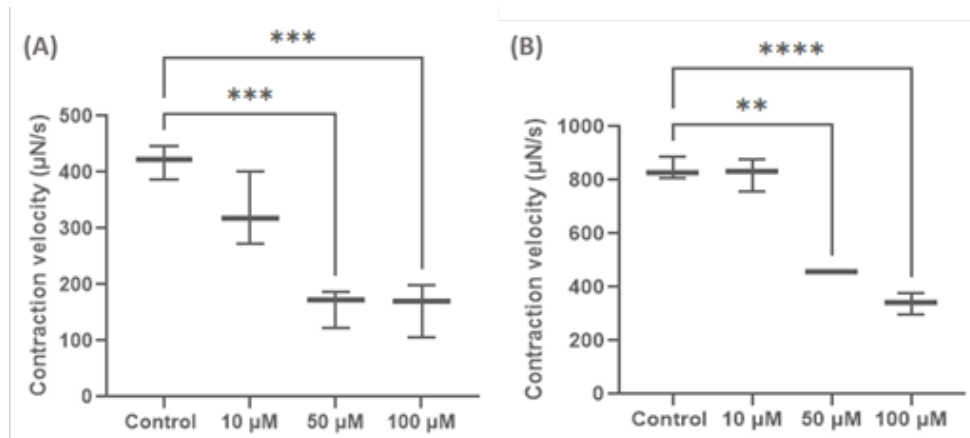


Figure 4.17: Contraction velocity values obtained after incubating the tissues for 7 days with the different drug concentrations (10  $\mu\text{M}$ , 50  $\mu\text{M}$  and 100  $\mu\text{M}$ ) when compared to control tissues, for (A) Experiment 1 and (B) Experiment 2. \*\* $p \leq 0.01$ ; \*\*\* $p \leq 0.001$ ; \*\*\*\* $p \leq 0.0001$ .

Table 4.12: Contraction velocity values for EHTs from both experiments. All values are in  $\mu\text{N/s}$ .

	Experiment 1	Experiment 2
<b>Control</b>	419.1 $\pm$ 14.3	840.6 $\pm$ 20.1
<b>10 <math>\mu\text{M}</math></b>	331.0 $\pm$ 30.7	822.5 $\pm$ 28.8
<b>50 <math>\mu\text{M}</math></b>	161.0 $\pm$ 16.2	457.7 $\pm$ 0.00
<b>100 <math>\mu\text{M}</math></b>	158.0 $\pm$ 22.4	339.9 $\pm$ 18.6

Contraction velocity also diminished as drug concentration increased, but norepinephrine administration only produced significant decreases for concentrations of 50  $\mu\text{M}$  and 100  $\mu\text{M}$  (for 10  $\mu\text{M}$ , tissues contract an average of 27.0% and 2.15% slower than control tissues in Experiments 1 and 2, respectively).

When incubated with 50  $\mu\text{M}$  of the drug, tissues of Experiment 1 contracted 42.8% slower and the one from Experiment 2 contracted 45.5% slower when compared to respective controls. A concentration of 100  $\mu\text{M}$  induced a 51.7% and 59.6% reduction in contraction speed for tissues in Experiment 1 and 2, respectively.

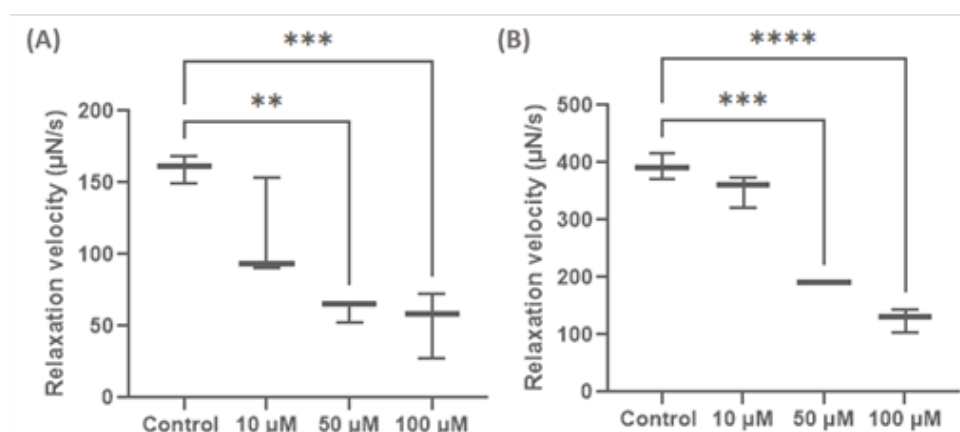


Figure 4.18: Relaxation velocity obtained after incubating the tissues for 7 days with the different drug concentrations (10  $\mu\text{M}$ , 50  $\mu\text{M}$  and 100  $\mu\text{M}$ ) when compared to control tissues, for **(A)** Experiment 1 and **(B)** Experiment 2.  $**p \leq 0.01$ ;  $***p \leq 0.001$ ;  $****p \leq 0.0001$ .

Table 4.13: Relaxation velocity values for EHTs from both experiments. All values are in  $\mu\text{N/s}$ .

	Experiment 1	Experiment 2
<b>Control</b>	159.8 $\pm$ 4.64	392.8 $\pm$ 10.3
<b>10 <math>\mu\text{M}</math></b>	112.2 $\pm$ 16.7	351.7 $\pm$ 13.1
<b>50 <math>\mu\text{M}</math></b>	61.59 $\pm$ 3.64	191.8 $\pm$ 0.00
<b>100 <math>\mu\text{M}</math></b>	52.87 $\pm$ 10.7	126.7 $\pm$ 10.1

Similarly to what happened with contraction velocity, NE only appreciably affected relaxation speed of tissues incubated with a 50  $\mu\text{M}$  and 100  $\mu\text{M}$  concentration (at 10  $\mu\text{M}$ , tissues from Experiment 1 relaxed 40.0% slower than control ones, which was not considered significant given the wide range of obtained values (tissues relaxed at a speed between 90.09 and 153.1  $\mu\text{N/s}$ , as shown in Figure 4.18); tissues from Experiment 2 only relaxed 10.5% slower when compared to respective controls).

For Experiment 1, EHTs exposed to 50  $\mu\text{M}$  and 100  $\mu\text{M}$  achieved a relaxed state 44.4% and 67.5% slower than control EHTs, respectively. Tissues from Experiment 2 subjected to 50  $\mu\text{M}$  and 100  $\mu\text{M}$  of

NE relaxed 51.2% and 67.7% slower when compared to control ones, respectively.

The used EHT platform showed a notable reduction in both contraction and relaxation speed in a concentration-dependent way. Although no articles in literature were found to compare the results obtained for these parameters, the aforementioned study developed by Tiburcy et al. confirmed enhanced cardiomyocyte hypertrophy, reduction of CM viability and eventual death in response to increasing NE concentrations [49], so it is deducible that NE also affects CMs contraction and relaxation velocity.

In the next figures (Figures 4.19 to 4.22) and tables (Tables 4.14 and 4.15) are presented the time that tissues took to achieve 10% and 90% of contraction and relaxation.

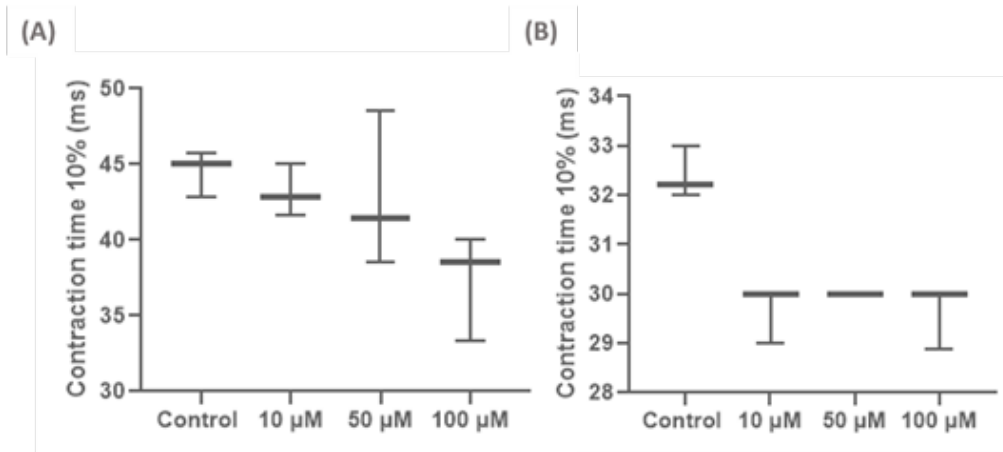


Figure 4.19: Contraction time at 10% obtained after incubating the tissues for 7 days with the different drug concentrations (10 μM, 50 μM and 100 μM) when compared to control tissues, for (A) Experiment 1 and (B) Experiment 2.

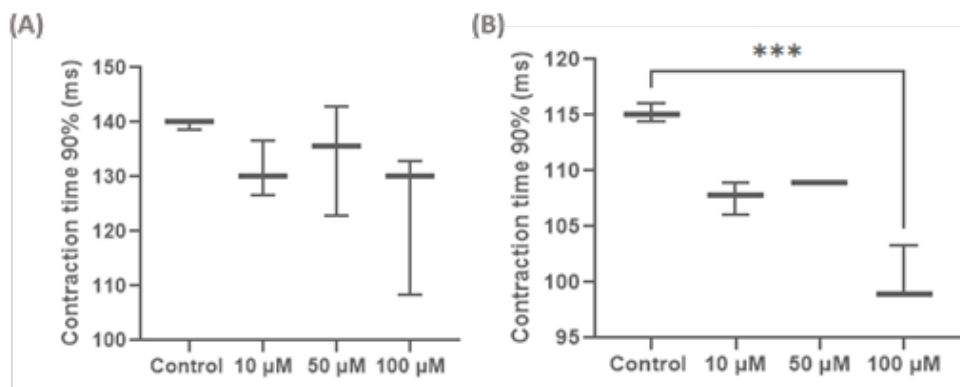


Figure 4.20: Contraction time at 90% obtained after incubating the tissues for 7 days with the different drug concentrations (10 μM, 50 μM and 100 μM) when compared to control tissues, for (A) Experiment 1 and (B) Experiment 2. \*\*\* $p \leq 0.001$ .

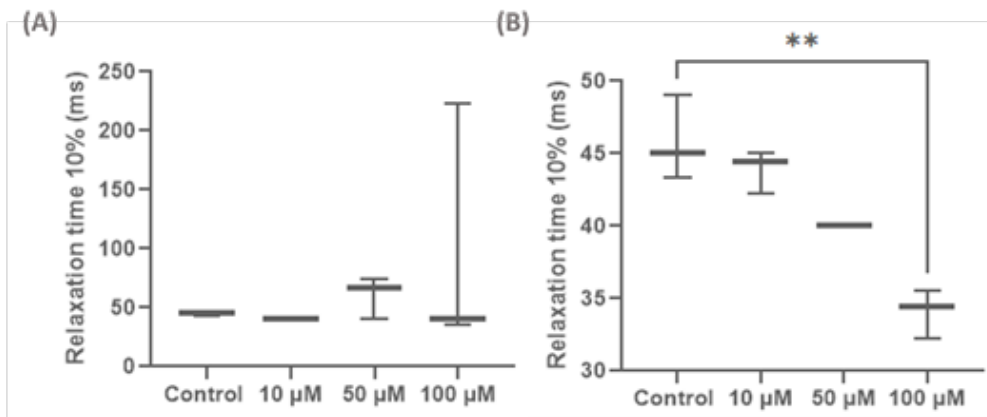


Figure 4.21: Relaxation time at 10% obtained after incubating the tissues for 7 days with the different drug concentrations (10 μM, 50 μM and 100 μM) when compared to control tissues, for **(A)** Experiment 1 and **(B)** Experiment 2. **\*\* $p \leq 0.01$** .

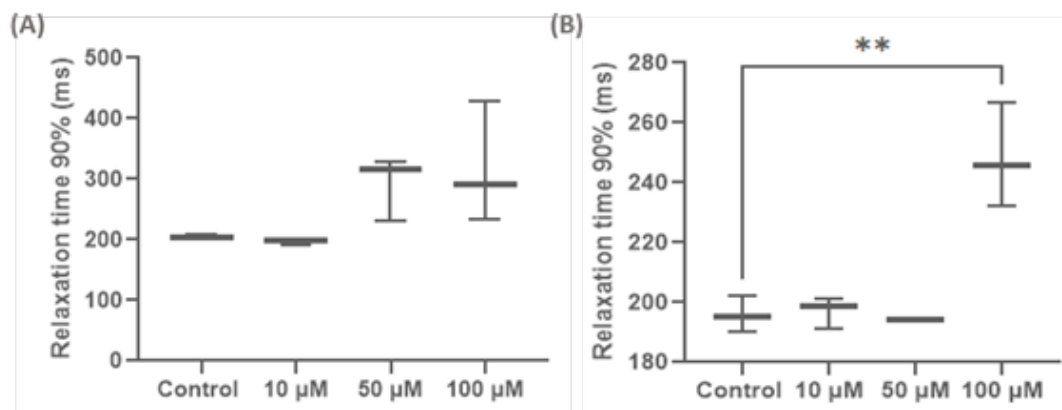


Figure 4.22: Relaxation time at 90% obtained after incubating the tissues for 7 days with the different drug concentrations (10 μM, 50 μM and 100 μM) when compared to control tissues, for **(A)** Experiment 1 and **(B)** Experiment 2. **\*\* $p \leq 0.01$** .

Table 4.14: CT10, CT90, RT10, RT90 values for EHTs from Experiment 1. All values are in milliseconds.

	Experiment 1			
	CT10	CT90	RT10	RT90
<b>Control</b>	44.52 ± 0.70	139.5 ± 0.39	44.52 ± 0.70	204.4 ± 1.74
<b>10 μM</b>	43.17 ± 0.80	131.1 ± 2.40	40.00 ± 0.00	197.1 ± 2.46
<b>50 μM</b>	42.86 ± 2.43	133.8 ± 4.78	60.48 ± 8.53	291.9 ± 24.9
<b>100 μM</b>	37.30 ± 1.65	123.7 ± 6.32	99.44 ± 50.6	317.5 ± 47.1

Table 4.15: CT10, CT90, RT10, RT90 values for EHTs from Experiment 2. All values are in milliseconds.

	<b>Experiment 2</b>			
	CT10	CT90	RT10	RT90
<b>Control</b>	32.41 ± 0.25	115.1 ± 0.37	45.78 ± 1.37	195.7 ± 2.84
<b>10 μM</b>	29.67 ± 0.27	107.6 ± 0.69	43.89 ± 0.69	197.0 ± 2.46
<b>50 μM</b>	30.00 ± 0.00	108.9 ± 0.00	40,00 ± 0.00	194.4 ± 0,00
<b>100 μM</b>	29.63 ± 0.30	34.07 ± 0.80	100.4 ± 1.21	248.1 ± 8.19

As depicted in Figures 4.19, 4.20, 4.21 and 4.22- (A) and presented in Table 4.14, time of contraction and relaxation to 10% or 90% are not significantly influenced by norepinephrine in Experiment 1, regardless of the administrated concentration.

For Experiment 2, CT10 was also quite similar for all conditions (as presented in Table 4.15 and Figure 4.19- (B)), while CT90 only showed a noteworthy average decrease in time of 12.8% for tissues administrated with 100 μM of NE. As for the relaxation parameters, there was no significant difference in values obtained for concentrations of 10 μM and 50 μM when compared to respective controls, but for 100 μM there was a considerable decrease in RT10 of 25.6% and an unusual 26.8% increase in RT90.

Since no results were found in literature for comparison regarding time of contraction and relaxation of cardiomyocytes in catecholamine overstimulation conditions, the exact effect of norepinephrine in these parameters is not certain and it is not known if the model was not able to replicate correctly what happens in patients that suffer from heart failure or if these parameters are not key features to replicate when simulating HF.



## Chapter 5

# Conclusions and Future Perspectives

With the aid of a platform that allowed the generation of fibrin-based 3D cardiac tissues using hiPSC-CMs, successful modeling of hypertrophic cardiomyopathy and chronic-stress induced heart failure was achieved.

By generating tissues with isogenic iPSC-derived cardiomyocytes cell lines, that only differed in a single nucleotide mutation in the MYBPC3 gene, the model allowed to replicate the same contractile dysfunction, particularly in contraction force, that is observed in patients, when comparing human cardiac samples from patients that carry this mutation and healthy ones. This dysfunction was not dependent on experiment conditions, as it was apparent in experiments with and without the supplementation of horse serum.

Experiments without horse serum supplementation also allowed to ascertain, after FACS analysis, that a higher cardiomyocyte content in generated tissues translates into a more significant contraction output, with higher contraction force, contraction velocity and relaxation velocity. Regardless of the cardiomyocyte content in tissues, contraction output was always more significant in healthy tissues when compared to mutated ones, which further supports impairment of contractile function caused by a MYBPC3 mutation.

Since contraction output was higher in experiments conducted with horse serum when compared to serum-free conditions, further experiments may be conducted to assess the exact effect of removing horse serum from supplementation medium, since it is not certain if these disparities were due to the differences in cardiomyocyte content or due to the poor cell quality observed across the three different occasions of culturing tissues with the MYBPC3 mutant cell line. Furthermore, ideal comparison between the different parameters obtained for EHTs generated with the healthy and mutant cell lines would be done with tissues that had a close content of cardiomyocytes, so that the contraction output would be similar, which also supports the need to repeat this experimental setup, with higher CM content in tissues after lactate purification treatment of hiPSC-CMs cultures (this treatment can generate purity yields up to 80-99% in hPSC-CMs <sup>[29]</sup> <sup>[61]</sup> and in this project these purities were not achieved).

The used EHT platform was also able to recreate contractile dysfunction induced by long-term exposure to norepinephrine, in a concentration dependent manner, also observed in patients that suffer from heart failure. In order to improve both of these experiment setups, it would be beneficial to switch the used medium to a fatty acid source, since adult CMs rely mainly on these compounds as energy source and this would help *in vitro* maturation of hPSC-CMs <sup>[63]</sup>.

The absence of effective treatments for both these cardiovascular conditions leads to the urgent need of *in vitro* human models that aid in disease modeling and drug development. This platform was able to replicate key aspects of both HCM and HF, which may help to find their pathomechanisms and new and efficient therapeutics for these diseases.



# Bibliography

- [1] NHS, "Cardiovascular disease," 2018. <https://www.nhs.uk/conditions/cardiovascular-disease/>, last accessed on 13/04/2020.
- [2] W. H. O. (WHO), "Cardiovascular diseases," 2017. [https://www.who.int/health-topics/cardiovascular-diseases/{#}tab=tab\\_{\\_}1](https://www.who.int/health-topics/cardiovascular-diseases/{#}tab=tab_{_}1), last accessed on 13/04/2020.
- [3] E. Wilkins, W. L., K. Wickramasinghe, and B. P, "European Cardiovascular Disease Statistics 2017 edition," *European Heart Network*, 2017.
- [4] A. Timmis, N. Townsend, C. P. Gale, A. Torbica, M. Lettino, S. E. Petersen, E. A. Mossialos, A. P. Maggioni, D. Kazakiewicz, H. T. May, D. De Smedt, M. Flather, L. Zuhke, J. F. Beltrame, R. Huculeci, L. Tavazzi, G. Hindricks, J. Bax, B. Casadei, S. Achenbach, L. Wright, P. Vardas, L. Mimoza, G. Artan, D. Aurel, M. Chettibi, N. Hammoudi, H. Sisakian, S. Pepoyan, B. Metzler, P. Siostrzonek, F. Weidinger, T. Jahangirov, F. Aliyev, Y. Rustamova, N. M. A. Mrochak, P. Lancellotti, A. Pasquet, M. Claeys, Z. Kusljagic, L. D. Hudic, E. Smajic, M. P. Tokmakova, P. M. Gatzov, D. Milicic, M. Bergovec, C. Christou, H. H. Moustra, T. Christodoulides, A. Linhart, M. Taborsky, M. Abdelhamid, K. Shokry, P. Kampus, M. Viigimaa, E. Ryödi, M. Niemela, T. T. Rissanen, J. Y. Le Heuzey, M. Gilard, A. Aladashvili, A. Gamkrelidze, M. Kereselidze, A. Zeicher, H. Katus, K. Bestehorn, C. Tsioufis, J. Goudevenos, Z. Csanádi, D. Becker, K. Tóth, P. J. Hrafnkelsdóttir, J. Crowley, P. Kearney, B. Dalton, D. Zahger, A. Wolak, D. Gabrielli, C. Indolfi, S. Urbinati, G. Imantayeva, S. Berkinbayev, G. Bajraktari, A. Ahmeti, G. Berisha, M. Erkin, A. Saamay, A. Erglis, I. Bajare, S. Jegere, M. Mohammed, A. Sarkis, G. Saadeh, R. Zvirblyte, G. Sakalyte, R. Slapikas, K. Ellafi, F. El Ghamari, C. Banu, J. Beissel, T. Felice, S. C. Buttigieg, R. G. Xuereb, M. Popovici, A. Boskovic, M. Rabrenovic, S. Ztot, S. Abir-Khalil, A. C. Van Rossum, B. J. Mulder, M. W. Elsendoorn, E. Srbinska-Kostovska, J. Kostov, B. Marjan, T. Steigen, O. C. Mjølstad, P. Ponikowski, A. Witkowski, P. Jankowski, V. M. Gil, J. Mimoso, S. Baptista, D. Vinereanu, O. Chioncel, B. A. Popescu, E. Shlyakhto, R. Oganov, M. Foscoli, M. Zavatta, A. D. Dikic, B. Beleslin, M. R. Radovanovic, P. Hlivak, R. Hatala, G. Kaliska, M. Kenda, Z. Frasc, M. Anguita, A. Cequier, J. Muniz, S. James, B. Johansson, P. Platonov, M. J. Zellweger, G. B. Pedrazzini, D. Carballo, H. E. Shebli, S. Kabbani, L. Abid, F. Addad, E. Bozkurt, M. Kayikçioğlu, M. K. Erol, V. Kovalenko, E. Nesukay, A. Wragg, P. Ludman, S. Ray, R. Kurbanov, D. Boateng, G. Daval, V. De Benito Rubio, D. Sebastiao, P. T. De Courtelary, and I. Bardinet, "European society of cardiology: Cardiovascular disease statistics 2019," *European Heart Journal*, vol. 41, no. 1, pp. 12–85, 2020.
- [5] S. Dassanayaka and S. P. Jones, "Recent developments in heart failure," *Circulation Research*, vol. 117, no. 7, pp. e58–e63, 2015.
- [6] Healthline, "What is heart failure?," 2017. <https://www.healthline.com/health/heart-failure>, last accessed on 13/04/2020.

- [7] A. Inamdar and A. Inamdar, "Heart Failure: Diagnosis, Management and Utilization," *Journal of Clinical Medicine*, vol. 5, no. 7, p. 62, 2016.
- [8] EMSWORLD, "CE Article: Diagnosis and Treatment of the Patient With Heart Failure," 2015. <https://www.emsworld.com/206842/ce-article-diagnosis-and-treatment-patient-heart-failure>, last accessed on 17/04/2020.
- [9] E. Kell, S. Wait, E. Harding, and I. Mclister, "A policy brief on heart failure in Europe," tech. rep., 2015.
- [10] A. Liew, V. Vassiliou, R. Cooper, and C. Raphael, "Hypertrophic Cardiomyopathy—Past, Present and Future," *Journal of Clinical Medicine*, vol. 6, no. 12, p. 118, 2017.
- [11] A. H. Association, "Hypertrophic cardiomyopathy (HCM)," 2020. <https://www.heart.org/en/health-topics/cardiomyopathy/what-is-cardiomyopathy-in-adults/hypertrophic-cardiomyopathy>, last accessed on 17/04/2020.
- [12] A. J. Marian and E. Braunwald, "Hypertrophic cardiomyopathy: Genetics, pathogenesis, clinical manifestations, diagnosis, and therapy," *Circulation Research*, vol. 121, no. 7, pp. 749–770, 2017.
- [13] B. J. Maron, E. J. Rowin, and M. S. Maron, "Global burden of hypertrophic cardiomyopathy," *JACC: Heart Failure*, vol. 6, no. 5, pp. 376–378, 2018.
- [14] S. Marston, K. Gehmlich, S. Schlossarek, L. Carrier, *et al.*, "How do mybpc3 mutations cause hypertrophic cardiomyopathy?," *Journal of Muscle Research and Cell Motility*, vol. 33, no. 1, pp. 75–80, 2012.
- [15] A. S. Helms, V. T. Tang, T. S. O'Leary, S. Friedline, M. Wauchope, A. Arora, A. H. Wasserman, E. D. Smith, L. M. Lee, X. W. Wen, *et al.*, "Effects of mybpc3 loss-of-function mutations preceding hypertrophic cardiomyopathy," *JCI Insight*, vol. 5, no. 2, 2020.
- [16] S. J. Van Dijk, D. Dooijes, C. D. Remedios, M. Michels, J. M. Lamers, S. Winegrad, S. Schlossarek, L. Carrier, F. J. Cate, G. J. Stienen, and J. D. Van Velden, "Cardiac myosin-binding protein C mutations and hypertrophic cardiomyopathy haploinsufficiency, deranged phosphorylation, and cardiomyocyte dysfunction," *Circulation*, vol. 119, no. 11, pp. 1473–1483, 2009.
- [17] S. Marston, O. Copeland, A. Jacques, K. Livesey, V. Tsang, W. J. McKenna, S. Jalilzadeh, S. Carballo, C. Redwood, and H. Watkins, "Evidence from human myectomy samples that MYBPC3 mutations cause hypertrophic cardiomyopathy through haploinsufficiency," *Circulation Research*, vol. 105, no. 3, pp. 219–222, 2009.
- [18] A. C. Pereira and J. D. C. Marsiglia, "Hypertrophic Cardiomyopathy: How do Mutations Lead to Disease?," *Arquivos Brasileiros de Cardiologia*, vol. 102, no. 3, pp. 295–304, 2014.
- [19] N. P. Andreas Spannauer, Denise Traxler, Katrin Zlabinger, Alfred Gugerell, Johannes Winkler, Julia Mester-Tonczar, Dominika Lukovic, Claudia Müller, Martin Riesenhuber and M. Gyöngyösi, "Large Animal Models of Heart Failure With Reduced Ejection Fraction (HFrEF)," *Frontiers in Cardiovascular Medicine*, vol. 6, p. 117, 2019.
- [20] L. M. Freeman, J. E. Rush, J. A. Stern, G. S. Huggins, and M. S. Maron, "Feline Hypertrophic Cardiomyopathy: A Spontaneous Large Animal Model of Human HCM," *Cardiology Research*, vol. 8, no. 4, p. 139, 2017.

- [21] L. Citro, S. Naidu, F. Hassan, M. L. Kuppusamy, P. Kuppusamy, M. G. Angelos, and M. Khan, "Comparison of human induced pluripotent stem-cell derived cardiomyocytes with human mesenchymal stem cells following acute myocardial infarction," *PloS One*, vol. 9, no. 12, 2014.
- [22] M. F. Hoes, N. Bomer, and P. van der Meer, "Concise review: the current state of human in vitro cardiac disease modeling: a focus on gene editing and tissue engineering," *Stem Cells Translational Medicine*, vol. 8, no. 1, pp. 66–74, 2019.
- [23] A. Mathur, Z. Ma, P. Loskill, S. Jeeawoody, and K. E. Healy, "In vitro cardiac tissue models: current status and future prospects," *Advanced Drug Delivery Reviews*, vol. 96, pp. 203–213, 2016.
- [24] B. Lo and L. Parham, "Ethical issues in stem cell research," *Endocrine Reviews*, vol. 30, no. 3, pp. 204–213, 2009.
- [25] C. Zuppinger, "3d cardiac cell culture: a critical review of current technologies and applications," *Frontiers in Cardiovascular Medicine*, vol. 6, p. 87, 2019.
- [26] T. Eschenhagen, C. Mummery, and B. C. Knollmann, "Modelling sarcomeric cardiomyopathies in the dish: from human heart samples to ipsc cardiomyocytes," *Cardiovascular Research*, vol. 105, no. 4, pp. 424–438, 2015.
- [27] R. E. Ahmed, T. Anzai, N. Chanthra, and H. Uosaki, "A brief review of current maturation methods for human induced pluripotent stem cells-derived cardiomyocytes," *Frontiers in Cell and Developmental Biology*, vol. 8, p. 178, 2020.
- [28] G. D. Lopaschuk and J. S. Jaswal, "Energy metabolic phenotype of the cardiomyocyte during development, differentiation, and postnatal maturation," *Journal of Cardiovascular Pharmacology*, vol. 56, no. 2, pp. 130–140, 2010.
- [29] S. Tohyama, F. Hattori, M. Sano, T. Hishiki, Y. Nagahata, T. Matsuura, H. Hashimoto, T. Suzuki, H. Yamashita, Y. Satoh, *et al.*, "Distinct metabolic flow enables large-scale purification of mouse and human pluripotent stem cell-derived cardiomyocytes," *Cell Stem Cell*, vol. 12, no. 1, pp. 127–137, 2013.
- [30] X. Yang, M. Rodriguez, L. Pabon, K. A. Fischer, H. Reinecke, M. Regnier, N. J. Sniadecki, H. Ruohola-Baker, and C. E. Murry, "Tri-iodo-L-thyronine promotes the maturation of human cardiomyocytes-derived from induced pluripotent stem cells," *Journal of Molecular and Cellular Cardiology*, vol. 72, pp. 296–304, 2014.
- [31] S. S. Parikh, D. J. Blackwell, N. Gomez-Hurtado, M. Frisk, L. Wang, K. Kim, C. P. Dahl, A. Fiane, T. Tønnessen, D. O. Kryshtal, *et al.*, "Thyroid and glucocorticoid hormones promote functional t-tubule development in human-induced pluripotent stem cell-derived cardiomyocytes," *Circulation research*, vol. 121, no. 12, pp. 1323–1330, 2017.
- [32] T. C. McDevitt, M. A. Laflamme, and C. E. Murry, "Proliferation of cardiomyocytes derived from human embryonic stem cells is mediated via the igf/pi 3-kinase/akt signaling pathway," *Journal of Molecular and Cellular Cardiology*, vol. 39, no. 6, pp. 865–873, 2005.
- [33] R. Chaudhuri, M. Ramachandran, P. Moharil, M. Harumalani, and A. K. Jaiswal, "Biomaterials and cells for cardiac tissue engineering: current choices," *Materials Science and Engineering: C*, vol. 79, pp. 950–957, 2017.

- [34] C. Dambrot, S. R. Braam, L. G. Tertoolen, M. Birket, D. E. Atsma, and C. L. Mummery, "Serum supplemented culture medium masks hypertrophic phenotypes in human pluripotent stem cell derived cardiomyocytes," *Journal of Cellular and Molecular Medicine*, vol. 18, no. 8, pp. 1509–1518, 2014.
- [35] F. Weinberger, I. Mannhardt, and T. Eschenhagen, "Engineering cardiac muscle tissue: a maturing field of research," *Circulation research*, vol. 120, no. 9, pp. 1487–1500, 2017.
- [36] T. Eschenhagen, C. Fink, U. Remmers, H. Scholz, J. Wattchow, J. Weil, W. Zimmermann, H. H. Dohmen, H. Schäfer, N. Bishopric, *et al.*, "Three-dimensional reconstitution of embryonic cardiomyocytes in a collagen matrix: a new heart muscle model system," *The FASEB Journal*, vol. 11, no. 8, pp. 683–694, 1997.
- [37] A. Hansen, A. Eder, M. Bönstrup, M. Flato, M. Mewe, S. Schaaf, B. Aksehirliglu, A. Schwörer, J. Uebeler, and T. Eschenhagen, "Development of a drug screening platform based on engineered heart tissue," *Circulation Research*, vol. 107, no. 1, p. 35, 2010.
- [38] G. Pasirayi, V. Auger, S. M. Scott, P. KSM Rahman, M. Islam, L. O'Hare, and Z. Ali, "Microfluidic bioreactors for cell culturing: a review," *Micro and Nanosystems*, vol. 3, no. 2, pp. 137–160, 2012.
- [39] Z. Li and J. Guan, "Hydrogels for cardiac tissue engineering," *Polymers*, vol. 3, no. 2, pp. 740–761, 2011.
- [40] S. R. Caliari and J. A. Burdick, "A practical guide to hydrogels for cell culture," *Nature Methods*, vol. 13, no. 5, pp. 405–414, 2016.
- [41] C. S. Hughes, L. M. Postovit, and G. A. Lajoie, "Matrigel: a complex protein mixture required for optimal growth of cell culture," *Proteomics*, vol. 10, no. 9, pp. 1886–1890, 2010.
- [42] S. Kattula, J. R. Byrnes, and A. S. Wolberg, "Fibrinogen and Fibrin in Hemostasis and Thrombosis," *Circulation Research*, vol. 107, no. 1, pp. 35–44, 2017.
- [43] S. Masuda and T. Shimizu, "Three-dimensional cardiac tissue fabrication based on cell sheet technology," *Advanced Drug Delivery Reviews*, vol. 96, pp. 103–109, 2016.
- [44] B. Maher, "Tissue engineering: How to build a heart," *Nature*, vol. 499, no. 7456, pp. 20–22, 2013.
- [45] E. Garreta, R. Oria, C. Tarantino, M. Pla-Roca, P. Prado, F. Fernández-Avilés, J. M. Campistol, J. Samitier, and N. Montserrat, "Tissue engineering by decellularization and 3D bioprinting," *Materials Today*, vol. 20, no. 4, pp. 166–178, 2017.
- [46] K. Breckwoldt, D. Letuffe-Brenière, I. Mannhardt, T. Schulze, B. Ulmer, T. Werner, A. Benzin, B. Klampe, M. C. Reinsch, S. Laufer, A. Shibamiya, M. Prondzynski, G. Mearini, D. Schade, S. Fuchs, C. Neuber, E. Krämer, U. Saleem, M. L. Schulze, M. L. Rodriguez, T. Eschenhagen, and A. Hansen, "Differentiation of cardiomyocytes and generation of human engineered heart tissue," *Nature Protocols*, vol. 12, pp. 1177–1197, 2017.
- [47] A. Lymperopoulos, G. Rengo, and W. J. Koch, "Adrenergic nervous system in heart failure: Pathophysiology and therapy," *Circulation Research*, vol. 113, no. 6, pp. 739–753, 2013.
- [48] W. S. Colucci, "The effects of norepinephrine on myocardial biology: Implications for the therapy of heart failure," in *Clinical Cardiology*, vol. 21, pp. 20–24, 1998.

- [49] M. Tiburcy, J. E. Hudson, P. Balfanz, S. Schlick, T. Meyer, M. L. C. Liao, E. Levent, F. Raad, S. Zeidler, E. Wingender, J. Riegler, M. Wang, J. D. Gold, I. Kehat, E. Wettwer, U. Ravens, P. Dierickx, L. W. Van Laake, M. J. Goumans, S. Khadjeh, K. Toischer, G. Hasenfuss, L. A. Couture, A. Unger, W. A. Linke, T. Araki, B. Neel, G. Keller, L. Gepstein, J. C. Wu, and W. H. Zimmermann, "Defined engineered human myocardium with advanced maturation for applications in heart failure modeling and repair," *Circulation*, vol. 135, no. 19, pp. 1832–1847, 2017.
- [50] Y. C. Fu, C. S. Chi, S. C. Yin, B. Hwang, Y. T. Chiu, and S. L. Hsu, "Norepinephrine induces apoptosis in neonatal rat cardiomyocytes through a reactive oxygen species-TNF $\alpha$ -caspase signaling pathway," *Cardiovascular Research*, vol. 62, no. 3, pp. 558–567, 2004.
- [51] E. G. Navarrete, P. Liang, F. Lan, V. Sanchez-Freire, C. Simmons, T. Gong, A. Sharma, P. W. Burrige, B. Patlolla, A. S. Lee, H. Wu, R. E. Beygui, S. M. Wu, R. C. Robbins, D. M. Bers, and J. C. Wu, "Screening drug-induced arrhythmia events using human induced pluripotent stem cell-derived cardiomyocytes and low-impedance microelectrode arrays," *Circulation*, vol. 128, no. 11, pp. S3–S13, 2013.
- [52] D. Mosqueira, J. G. Smith, J. R. Bhagwan, and C. Denning, "Modeling Hypertrophic Cardiomyopathy: Mechanistic Insights and Pharmacological Intervention," *Trends in Molecular Medicine*, vol. 25, no. 9, pp. 775–790, 2019.
- [53] A. Dutsch, P. J. Wijnker, S. Schlossarek, F. W. Friedrich, E. Krämer, I. Braren, M. N. Hirt, D. Brenière-Letuffe, A. Rhoden, I. Mannhardt, T. Eschenhagen, L. Carrier, and G. Mearini, "Phosphomimetic cardiac myosin-binding protein C partially rescues a cardiomyopathy phenotype in murine engineered heart tissue," *Scientific Reports*, vol. 9, 2019.
- [54] Z. Ma, N. Huebsch, S. Koo, M. A. Mandegar, B. Siemons, S. Boggess, B. R. Conklin, C. P. Grigoriopoulos, and K. E. Healy, "Contractile deficits in engineered cardiac microtissues as a result of MYBPC3 deficiency and mechanical overload," *Nature Biomedical Engineering*, vol. 2, pp. 955–967, 2018.
- [55] R. Cohn, K. Thakar, A. Lowe, F. A. Ladha, A. M. Pettinato, R. Romano, E. Meredith, Y. S. Chen, K. Atamanuk, B. D. Huey, and J. T. Hinson, "A Contraction Stress Model of Hypertrophic Cardiomyopathy due to Sarcomere Mutations," *Stem Cell Reports*, vol. 12, no. 1, pp. 71–83, 2019.
- [56] M. Bellin, S. Casini, R. P. Davis, C. D'Aniello, J. Haas, D. Ward-Van Oostwaard, L. G. Tertoolen, C. B. Jung, D. A. Elliott, A. Welling, K. L. Laugwitz, A. Moretti, and C. L. Mummery, "Isogenic human pluripotent stem cell pairs reveal the role of a KCNH2 mutation in long-QT syndrome," *EMBO Journal*, vol. 32, no. 24, pp. 3161–3175, 2013.
- [57] F. L. Crespo, V. R. Sobrado, L. Gomez, A. M. Cervera, and K. J. McCreath, "Mitochondrial reactive oxygen species mediate cardiomyocyte formation from embryonic stem cells in high glucose," *Stem Cells*, vol. 28, no. 7, pp. 1132–1142, 2010.
- [58] M. J. Birket, M. C. Ribeiro, G. Kosmidis, D. Ward, A. R. Leitoguinho, V. van de Pol, C. Dambrot, H. D. Devalla, R. P. Davis, P. G. Mastroberardino, D. E. Atsma, R. Passier, and C. L. Mummery, "Contractile Defect Caused by Mutation in MYBPC3 Revealed under Conditions Optimized for Human PSC-Cardiomyocyte Function," *Cell Reports*, vol. 13, no. 4, pp. 733–745, 2015.
- [59] E. R. Witjas-Paalberends, N. Piroddi, K. Stam, S. J. Van Dijk, V. S. Oliviera, C. Ferrara, B. Scellini, M. Hazebroek, F. J. Ten Cate, M. Van Slegtenhorst, C. Dos Remedios, H. W. Niessen, C. Tesi, G. J. Stienen, S. Heymans, M. Michels, C. Poggesi, and J. Van Der Velden, "Mutations in MYH7

- reduce the force generating capacity of sarcomeres in human familial hypertrophic cardiomyopathy,” *Cardiovascular Research*, vol. 99, no. 1, pp. 432–441, 2013.
- [60] C. Y. Ho, S. M. Day, S. D. Colan, M. W. Russell, J. A. Towbin, M. V. Sherrid, C. E. Canter, J. L. Jefferies, A. M. Murphy, A. L. Cirino, T. P. Abraham, M. Taylor, L. Mestroni, D. A. Bluemke, P. Jarolim, L. Shi, L. A. Sleeper, C. E. Seidman, and E. J. Orav, “The burden of early phenotypes and the influence of wall thickness in hypertrophic cardiomyopathy mutation carriers: Findings from the HCMNet study,” *JAMA Cardiology*, vol. 2, no. 4, pp. 349–464, 2017.
- [61] M. Fuerstenau-Sharp, M. E. Zimmermann, K. Stark, N. Jentsch, M. Klingenstein, M. Drzymalski, S. Wagner, L. S. Maier, U. Hehr, A. Baessler, M. Fischer, and C. Hengstenberg, “Generation of highly purified human cardiomyocytes from peripheral blood mononuclear cell-derived induced pluripotent stem cells,” *PLoS ONE*, vol. 10, no. 5, 2015.
- [62] J. A. Thomas and B. H. Marks, “Plasma norepinephrine in congestive heart failure,” *The American Journal of Cardiology*, vol. 41, no. 2, pp. 233–243, 1978.
- [63] R. H. Slaats, V. Schwach, and R. Passier, “Metabolic environment in vivo as a blueprint for differentiation and maturation of human stem cell-derived cardiomyocytes,” *Biochimica et Biophysica Acta (BBA) - Molecular Basis of Disease*, vol. 1866, no. 10, 2020.

## Appendix A

# Appendix A: Preparation of the CM High Gluc+TDI Medium

To perform the experiments, batches of 1000 mL of CM High Gluc Medium were prepared previously. All its components are described in Table A.1 and are added without a specific order except for the sodium hydrogen carbonate, which should be added lastly, in order to bring the final concentration of sodium to 148 mM. The working solutions used were BSA (Bovine Serum Albumin) (10% in IMDM) and ascorbic acid-2P (5 mg/mL in water).

Table A.1: Formulation of the CM High Gluc Medium with all its components discriminated, along with suppliers for ordering and the quantities to add for a final volume of medium of 1000 mL.

Component	Supplier	For 1L (1000 mL)
DMEM	Sigma-Aldrich ®	8.3 g
D(+)-Glucose	Millipore ®	2.73 g
Sodium pyruvate	Thermo Fisher	5 mL
Sodium 3-hydroxybutyrate	Sigma-Aldrich ®	0.024 gr
L-Carnitine hydrochloride	Sigma-Aldrich ®	0.1 gr
Creatine monohydrate	Sigma-Aldrich ®	0.15 gr
Taurine	Sigma-Aldrich ®	0.626 gr
Phenol red	Sigma-Aldrich ®	0.011 gr
Distilled water	Thermo Fisher	961 mL
Trace elements A (1x)	Cellgro	1 mL
Trace elements B (1x)	Cellgro	1 mL
Trace elements C (1x)	Cellgro	1mL
Chemically defined lipid concentrate (1x)	Thermo Fisher	10 mL
GlutaMAX™ supplement (1x)	Thermo Fisher	10 mL
1-Thioglycerol ( $\alpha$ -MTG)	Sigma-Aldrich ®	39 $\mu$ L (of undiluted stock)
Insulin-Transferin-Selenium Ethanolamine (ITS-X) (0,1x)	Thermo Fisher	1 mL
Ascorbic acid-2P	Sigma-Aldrich ®	10 mL
Penicillin-Streptomycin (0.5x)	Thermo Fisher	5 mL
Sodium hydrogen carbonate	Millipore ®	3.7 gr
BSA (Bovine Serum Albumin)	Bovostar	2.5 gr

After adding and mixing all the components, NaOH (working solution of 5M) should be added to bring

the final pH of the medium to physiological relevant values (7.3-7.4). Afterwards, the medium undergoes sterile filtration using a Stericup-GV sterile vacuum filtering (Millipore ®), with a pore of 0.22 µm. The medium is then aliquoted and kept at -20 °C for long-term usage or at -4 °C for short-term usage.

T3 hormone is only supplemented to the medium before experiments at a dilution of 1:15000 (v/v) of a 1.5 mM stock (Sigma-Aldrich ®), as well as dexamethasone at a dilution of 1:10000 (v/v) of a 1 mg/mL stock (Tocris) and long R3 insulin like-growth factor-1, known as IGF-1 at a dilution of 1:10000 (v/v) of a 10 nM stock (Sigma-Aldrich ®).

Onwards, the medium is referred to as CM High Gluc+TDI Medium, with a final glucose concentration of 15 mM.

## Appendix B

# Appendix B: Preparation of the CM Low Ins+Low Gluc+TDI+Lact Medium

Batches of 1000 mL of CM Low Ins Medium were prepared prior to experiments. This medium is comprised by the components specified in Table B.1 and are added without a specific order apart from the sodium hydrogen carbonate, which should be added lastly to bring the final concentration of sodium to 148 mM. The working solutions used were BSA (Bovine Serum Albumin) (10% in IMDM) and ascorbic acid-2P (5mg/mL in water).

Table B.1: Formulation of the CM Low Ins Medium with all its components discriminated, along with suppliers for ordering and the quantities to add for a final volume of medium of 1000 mL.

Component	Supplier	For 1L (1000 mL)
DMEM	Sigma-Aldrich ®	8.3 g
Sodium pyruvate	Thermo Fisher	5 mL
Sodium 3-hydroxybutyrate	Sigma-Aldrich ®	0.024 gr
L-Carnitine hydrochloride	Sigma-Aldrich ®	0.1 gr
Creatine monohydrate	Sigma-Aldrich ®	0.15 gr
Taurine	Sigma-Aldrich ®	0.626 gr
Phenol red	Sigma-Aldrich ®	0.011 gr
Distilled water	Thermo Fisher	961 mL
Trace elements A (1x)	Cellgro	1 mL
Trace elements B (1x)	Cellgro	1 mL
Trace elements C (1x)	Cellgro	1mL
Chemically defined lipid concentrate (1x)	Thermo Fisher	10 mL
GlutaMAX™ supplement (1x)	Thermo Fisher	10 mL
1-Thioglycerol ( $\alpha$ -MTG)	Sigma-Aldrich ®	39 $\mu$ L (of undiluted stock)
Insulin-Transferin-Selenium Ethanolamine (ITS-X) (0.01x)	Thermo Fisher	100 $\mu$ L
Ascorbic acid-2P	Sigma-Aldrich ®	10 mL
Penicillin-Streptomycin (0,5x)	Thermo Fisher	5 mL
Sodium hydrogen carbonate	Millipore ®	3.7 gr
BSA (Bovine Serum Albumin)	Bovostar	2.5 gr

After adding and mixing all the components, a working solution of 5M of NaOH should be added to bring the final pH of the medium to physiological relevant values (7.3-7.4). The medium then under-

goes sterile filtration using a Stericup-GV sterile vacuum filtering (Millipore®), with a pore of 0.22 µm. Afterwards, the medium is aliquoted and kept at -20°C for long-term usage or at -4°C for short-term usage.

Since the lactate should be stored from 2 to 8°C, this component is only supplemented to the medium before experiments (7.18 µL of lactate/10 mL of medium), as well as the following components: T3 hormone at a 1:15000 dilution (v/v) of a 1.5 mM stock (Sigma-Aldrich®); dexamethasone at a dilution of 1:10000 (v/v) of a 1 mg/mL stock (Tocris); long R3 insulin like-growth factor-1, also known as IGF-1 at a dilution of 1:10000 (v/v) of a 10 nM stock (Sigma-Aldrich®); glucose at a dilution of 1:100 (v/v) of a 450 mM stock (Millipore®), so that the final glucose concentration is 4.5 mM. Onwards, the medium is referred to as CM Low Ins+Low Gluc+TDI+Lact Medium.

## Appendix C

# Appendix C: Calculation Formula for Contraction Force Based on Pillar Deflection

For each EHT contraction, post deflection ( $\delta$ ) was found from the difference between the maximum and minimum distance between the pillars (the maximum distance happens when the tissue is fully relaxed and the minimum when the tissue is fully contracted). This deflection was used to ascertain the force of contraction, by using the following formula:

$$F = \frac{3\pi ER^4}{2a^2(3L - a)}\delta \quad (\text{C.1})$$

In this formula,  $F$  is the contraction force,  $E$  represents the elastic modulus of the PDMS,  $a$  is the height of the tissue in the pillar and  $L$  and  $R$  are the length and radius of the PDMS cantilever, respectively.



## Appendix D

# Appendix D: Drug Induced Heart Failure Assay- Measurements for Tissues from Experiments 1 and 2 before and after incubation with norepinephrine

As previously explained, tissues were measured on day 10 (prior to drug administration) and on day 17 (after 7 days of daily drug administration). The first measurements are the base line to see how tissue behaviour evolves over time. The results are expressed in the next figures and tables.

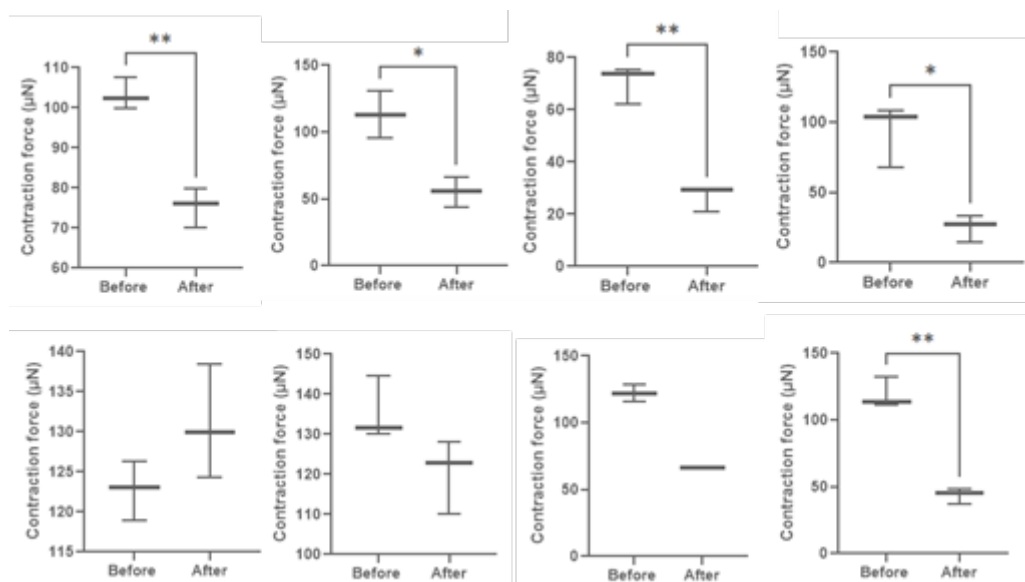


Figure D.1: Contraction force obtained 10 days after culturing (**before**) and after incubating the tissues for 7 days with norepinephrine (**after**). From left to right, the graphs depict Control, 10 µM, 50 µM and 100 µM tissues, from Experiment 1 (top row) and Experiment 2 (bottom row). \* $p \leq 0.05$ ; \*\* $p \leq 0.01$ .

Table D.1: Contraction force values of tissues from Experiments 1 and 2, before and after daily drug administration for 7 days. All values are in  $\mu\text{N}$ .

	Experiment 1		Experiment 2	
	Before	After	Before	After
<b>Control</b>	103.3 $\pm$ 1.86	75.38 $\pm$ 2.29	122.7 $\pm$ 1.76	130.9 $\pm$ 3.36
<b>10 <math>\mu\text{M}</math></b>	113.1 $\pm$ 8.30	55.61 $\pm$ 5.26	135.5 $\pm$ 3.78	120.3 $\pm$ 4.37
<b>50 <math>\mu\text{M}</math></b>	70.50 $\pm$ 3.49	26.62 $\pm$ 2.29	122.2 $\pm$ 4.63	66.04 $\pm$ 0.00
<b>100 <math>\mu\text{M}</math></b>	93.22 $\pm$ 10.5	25.20 $\pm$ 4.65	119.0 $\pm$ 5.40	43.83 $\pm$ 2.80

For Experiment 1, differences in tissues contraction force prior to drug administration and after 7 days of daily incubation become progressively higher as NE concentration increases, since CF decreases 26.9%, 50.4%, 62.5% and 73.7% for control, 10  $\mu\text{M}$ , 50  $\mu\text{M}$  and 100  $\mu\text{M}$  concentrations, respectively. For Experiment 2, control tissues contraction force increased 6.57%, while after daily exposure to 10  $\mu\text{M}$ , 50  $\mu\text{M}$  and 100  $\mu\text{M}$ , tissues suffered a decrease in CF of 11.2%, 42.9% and 63.0%, respectively.

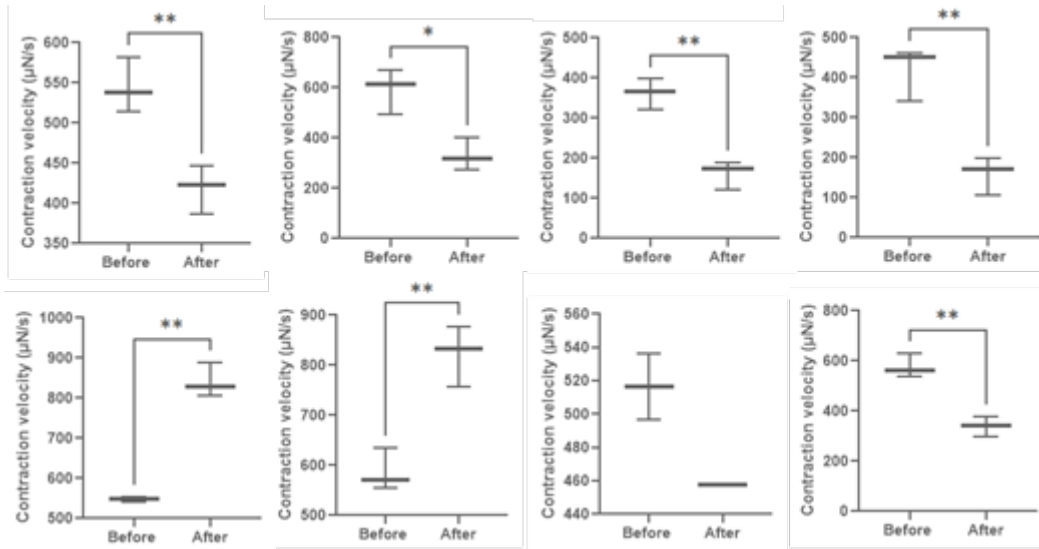


Figure D.2: Contraction velocity obtained 10 days after culturing (**before**) and after incubating the tissues for 7 days with norepinephrine (**after**). From left to right, the graphs depict Control, 10  $\mu\text{M}$ , 50  $\mu\text{M}$  and 100  $\mu\text{M}$  tissues, from Experiment 1 (top row) and Experiment 2 (bottom row). \* $p \leq 0.05$ ; \*\* $p \leq 0.01$ .

Table D.2: Contraction velocity values of tissues from Experiments 1 and 2, before and after daily drug administration for 7 days. All values are in  $\mu\text{N/s}$ .

	Experiment 1		Experiment 2	
	Before	After	Before	After
<b>Control</b>	545.2 $\pm$ 16.2	419.1 $\pm$ 14.3	548.0 $\pm$ 3.32	840.6 $\pm$ 20.1
<b>10 <math>\mu\text{M}</math></b>	592.7 $\pm$ 41.9	331.0 $\pm$ 30.7	587.0 $\pm$ 20.0	822.5 $\pm$ 28.8
<b>50 <math>\mu\text{M}</math></b>	362.0 $\pm$ 18.0	161.0 $\pm$ 16.2	516.6 $\pm$ 14.0	457.7 $\pm$ 0.00
<b>100 <math>\mu\text{M}</math></b>	418.0 $\pm$ 31.4	158.0 $\pm$ 22.4	575.9 $\pm$ 22.5	339.9 $\pm$ 18.6

As for contraction speed, there was also a significant reduction for tissues in all conditions in Experiment 1: when compared to base line measurements, there was a 22.9%, 43.7%, 55.9% and 62.8% decrease in CV for control, 10  $\mu\text{M}$ , 50  $\mu\text{M}$  and 100  $\mu\text{M}$  tissues, respectively. For Experiment 2, there was

an unusual increase in CV for control EHTs and the ones subjected to 10  $\mu\text{M}$  of norepinephrine (53.3% and 40.1%, respectively). For a 50  $\mu\text{M}$  drug concentration, tissues beat 7.86% slower and the ones subjected to a 100  $\mu\text{M}$  concentration beat 40.8% slower than prior to drug administration.

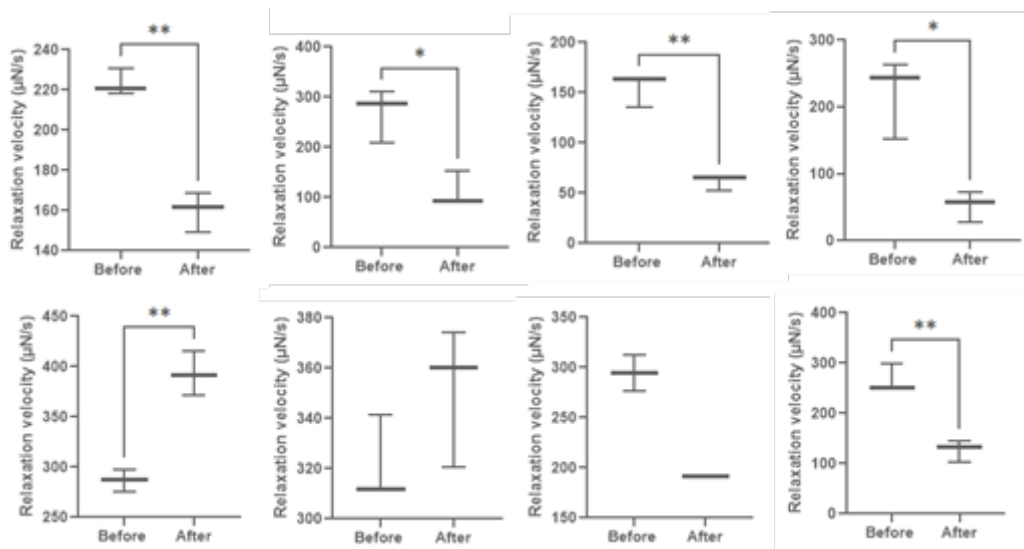


Figure D.3: Relaxation velocity obtained 10 days after culturing (**before**) and after incubating the tissues for 7 days with norepinephrine (**after**). From left to right, the graphs depict Control, 10  $\mu\text{M}$ , 50  $\mu\text{M}$  and 100  $\mu\text{M}$  tissues, from Experiment 1 (top row) and Experiment 2 (bottom row). \* $p \leq 0.05$ ; \*\* $p \leq 0.01$ .

Table D.3: Relaxation velocity values of tissues from Experiments 1 and 2, before and after daily drug administration for 7 days. All values are in  $\mu\text{N/s}$ .

	Experiment 1		Experiment 2	
	Before	After	Before	After
<b>Control</b>	223.3 $\pm$ 3.10	159.8 $\pm$ 4.64	286.8 $\pm$ 5.35	392.8 $\pm$ 10.3
<b>10 <math>\mu\text{M}</math></b>	269.0 $\pm$ 25.0	112.2 $\pm$ 16.7	321.6 $\pm$ 8.00	351.7 $\pm$ 13.1
<b>50 <math>\mu\text{M}</math></b>	154.5 $\pm$ 7.86	61.59 $\pm$ 3.64	294.2 $\pm$ 12.8	191.8 $\pm$ 0.00
<b>100 <math>\mu\text{M}</math></b>	219.8 $\pm$ 27.7	52.87 $\pm$ 10.7	267.7 $\pm$ 12.9	126.7 $\pm$ 10.1

Experiment 1 relaxation velocity values follow the trend of previously discussed parameters and there is a notable decline of speed to achieve a relaxed state: 28.4%, 57.7%, 60.2 and 76.8% for control, 10  $\mu\text{M}$ , 50  $\mu\text{M}$  and 100  $\mu\text{M}$  conditions, respectively.

As for Experiment 2, EHTs incubated with 50  $\mu\text{M}$  and 100  $\mu\text{M}$  of NE exhibit the expected decrease in relaxation speed (30.5% and 52.5%) when compared to prior to drug administration values. However, control EHTs and the ones incubated with 10  $\mu\text{M}$  of drug achieved a relaxed state 36.9% and 9.3% faster when compared to base line measurements.

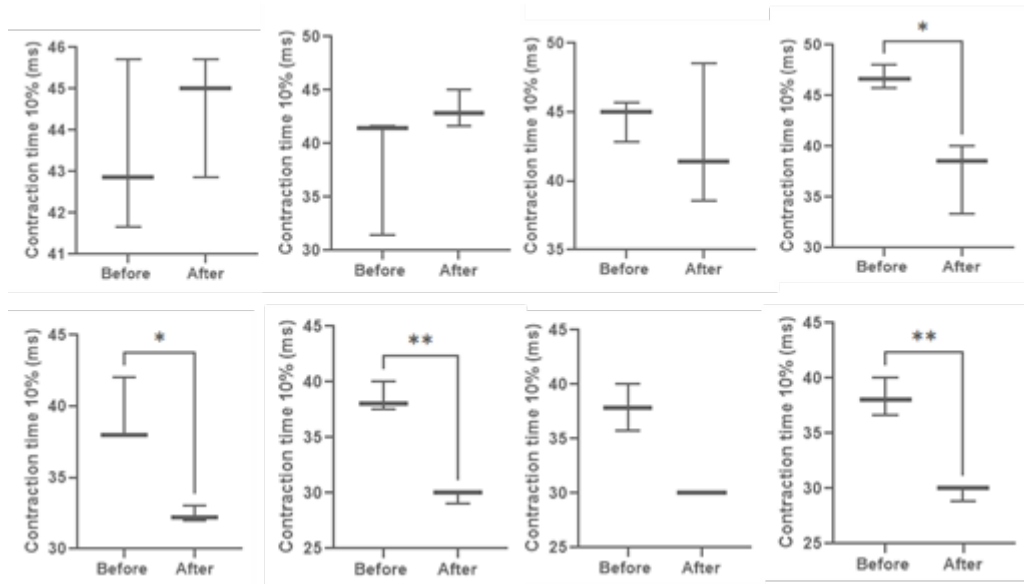


Figure D.4: Contraction time at 10% obtained 10 days after culturing (**before**) and after incubating the tissues for 7 days with norepinephrine (**after**). From left to right, the graphs depict Control, 10  $\mu\text{M}$ , 50  $\mu\text{M}$  and 100  $\mu\text{M}$  tissues, from Experiment 1 (top row) and Experiment 2 (bottom row). \* $p \leq 0.05$ ; \*\* $p \leq 0.01$ .

Table D.4: CT10 values of tissues from Experiments 1 and 2, before and after daily drug administration for 7 days. All values are in milliseconds.

	Experiment 1		Experiment 2	
	Before	After	Before	After
<b>Control</b>	43.41 $\pm$ 0.98	44.52 $\pm$ 0.70	39.33 $\pm$ 1.09	32.41 $\pm$ 0.25
<b>10 <math>\mu\text{M}</math></b>	38.18 $\pm$ 2.75	43.17 $\pm$ 0.80	38.50 $\pm$ 0.62	29.67 $\pm$ 0.27
<b>50 <math>\mu\text{M}</math></b>	44.52 $\pm$ 0.70	42.86 $\pm$ 2.43	37.86 $\pm$ 1.52	30.00 $\pm$ 0.00
<b>100 <math>\mu\text{M}</math></b>	46.79 $\pm$ 0.54	37.30 $\pm$ 1.65	38.22 $\pm$ 0.79	29.63 $\pm$ 0.30

Concerning the CT10 parameter, Experiment 2 tissues exhibited the expected decrease in time to get to 10% of contraction for all conditions, although the decrease is not particularly relevant (17.4%, 22.9%, 16.0% and 22.4% for control, 10  $\mu\text{M}$ , 50  $\mu\text{M}$  and 100  $\mu\text{M}$  conditions, respectively). In Experiment 1, EHTs incubated with 50  $\mu\text{M}$  and 100  $\mu\text{M}$  of NE also suffered a slight CT10 reduction (3.41% and 20.2%), while control and 10  $\mu\text{M}$  EHTs showed a small increase in this parameter (2.67% and 14.7%).

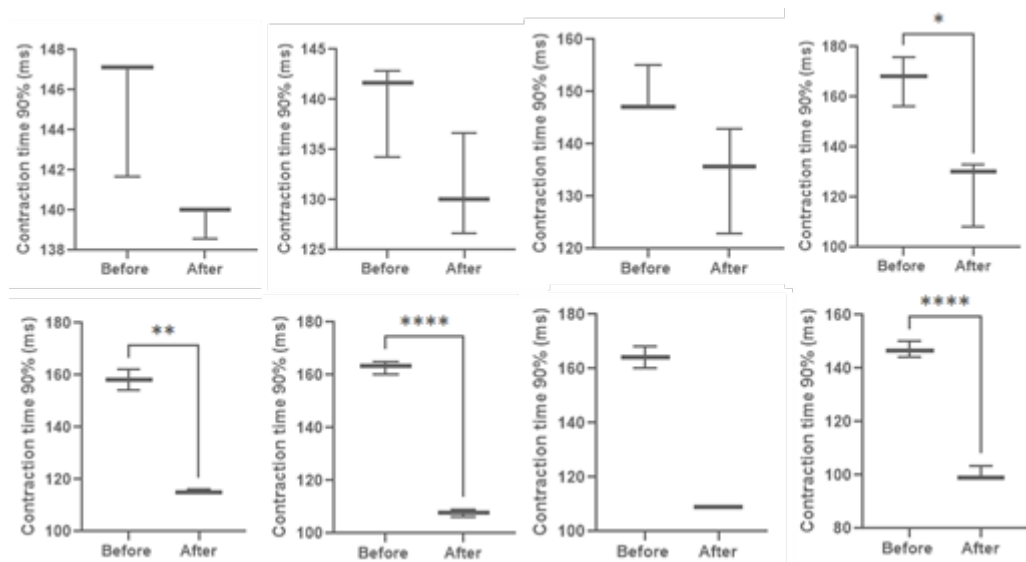


Figure D.5: Contraction time at 90% obtained 10 days after culturing (before) and after incubating the tissues for 7 days with norepinephrine (after). From left to right, the graphs depict Control, 10  $\mu$ M, 50  $\mu$ M and 100  $\mu$ M tissues, from Experiment 1 (top row) and Experiment 2 (bottom row). \* $p \leq 0.05$ ; \*\* $p \leq 0.01$ ; \*\*\*\* $p \leq 0.0001$ .

Table D.5: CT90 values of tissues from Experiments 1 and 2, before and after daily drug administration for 7 days. All values are in milliseconds.

	Experiment 1		Experiment 2	
	Before	After	Before	After
<b>Control</b>	145.3 $\pm$ 1.49	139.5 $\pm$ 0.39	158.0 $\pm$ 1.89	115.1 $\pm$ 0.37
<b>10 <math>\mu</math>M</b>	139.6 $\pm$ 2.19	131.1 $\pm$ 2.40	162.8 $\pm$ 1.20	107.6 $\pm$ 0.69
<b>50 <math>\mu</math>M</b>	149.8 $\pm$ 2.14	133.8 $\pm$ 4.78	164.0 $\pm$ 2.83	108.9 $\pm$ 0.00
<b>100 <math>\mu</math>M</b>	166.7 $\pm$ 4.70	123.7 $\pm$ 6.32	146.9 $\pm$ 1.42	100.4 $\pm$ 1.21

When it comes to contraction time at 90%, all tissues from both experiments showed a reduction for this parameter: when compared to base line measurements, there was a 3.95%, 6.07%, 10.6% and 25.9% average decrease in CT90 for control, 10  $\mu$ M, 50  $\mu$ M and 100  $\mu$ M tissues of Experiment 1, respectively; for Experiment 2, control, 10  $\mu$ M, 50  $\mu$ M and 100  $\mu$ M EHTs exhibited a 27.1%, 33.9%, 31.9% and 31.6% average decrease, respectively.

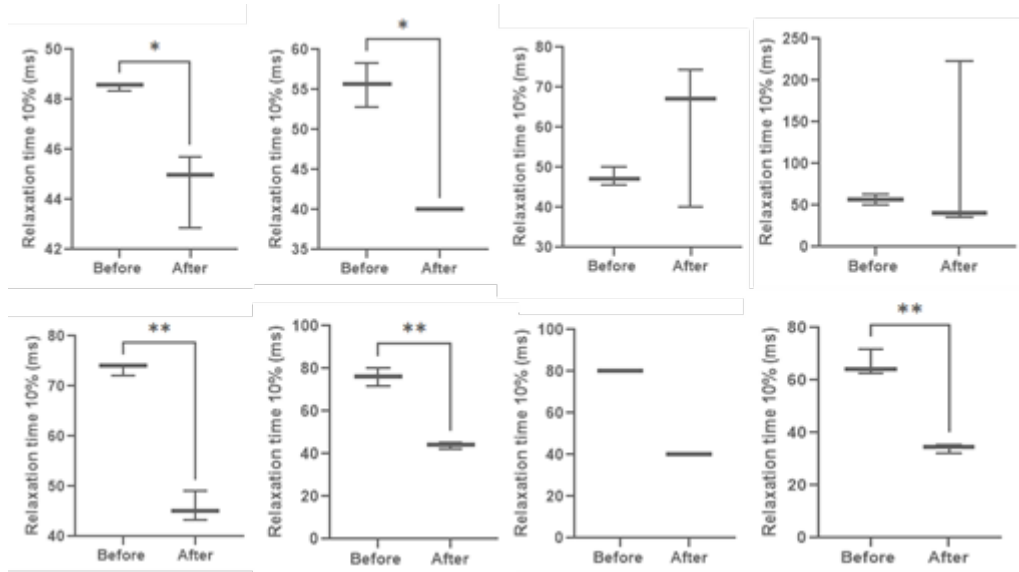


Figure D.6: Relaxation time at 10% obtained 10 days after culturing (**before**) and after incubating the tissues for 7 days with norepinephrine (**after**). From left to right, the graphs depict Control, 10  $\mu$ M, 50  $\mu$ M and 100  $\mu$ M tissues, from the Experiment 1 (top row) and Experiment 2 (bottom row). \* $p \leq 0.05$ ; \*\* $p \leq 0.01$ .

Table D.6: RT10 values of tissues from Experiments 1 and 2, before and after daily drug administration for 7 days. All values are in milliseconds.

	Experiment 1		Experiment 2	
	Before	After	Before	After
<b>Control</b>	48.49 $\pm$ 0.06	44.52 $\pm$ 0.70	73.33 $\pm$ 0.54	45.78 $\pm$ 1.37
<b>10 <math>\mu</math>M</b>	55.63 $\pm$ 1.29	40.00 $\pm$ 0.00	75.89 $\pm$ 1.96	43.89 $\pm$ 0.69
<b>50 <math>\mu</math>M</b>	47.62 $\pm$ 1.03	60.48 $\pm$ 8.53	80.00 $\pm$ 0.00	40.00 $\pm$ 0.00
<b>100 <math>\mu</math>M</b>	56.51 $\pm$ 3.03	99.44 $\pm$ 50.6	66.06 $\pm$ 2.32	34.07 $\pm$ 0.80

Tissues incubated with 50  $\mu$ M and 100  $\mu$ M of norepinephrine from Experiment 1 showed an average increase of 28.2% and 90.7% in RT10, respectively (this last increase is extremely high due to an outlier value of 223.3 ms when compared to two other tissue close values: 35 ms and 40 ms) when compared to base line measurements. Besides these two cases, all other tissues from both experiments, for all conditions, exhibited a decrease in the time to achieve 10% of relaxation: 37.6%, 42.0%, 50.0% and 48.3% for control, 10  $\mu$ M, 50  $\mu$ M and 100  $\mu$ M tissues of Experiment 2, respectively and 8.18% and 28.0% for control and 10  $\mu$ M EHTs of Experiment 1, respectively.

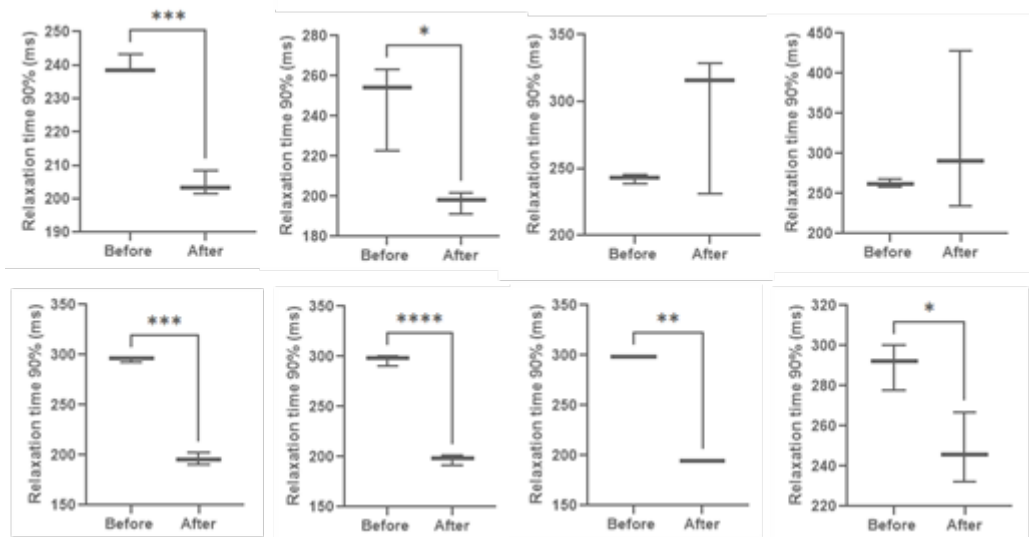


Figure D.7: Relaxation time at 90% obtained 10 days after culturing (**before**) and after incubating the tissues for 7 days with norepinephrine (**after**). From left to right, the graphs depict Control, 10  $\mu\text{M}$ , 50  $\mu\text{M}$  and 100  $\mu\text{M}$  tissues, from the Experiment 1 (top row) and Experiment 2 (bottom row). \* $p \leq 0.05$ ; \*\* $p \leq 0.01$ ; \*\*\* $p \leq 0.001$ ; \*\*\*\* $p \leq 0.0001$ .

Table D.7: RT90 values of tissues from Experiments 1 and 2, before and after daily drug administration for 7 days. All values are in milliseconds.

	Experiment 1		Experiment 2	
	Before	After	Before	After
<b>Control</b>	240.2 $\pm$ 1.30	204.4 $\pm$ 1.74	294.7 $\pm$ 1.09	195.7 $\pm$ 2.84
<b>10 <math>\mu\text{M}</math></b>	246.8 $\pm$ 10.0	197.1 $\pm$ 2.46	296.0 $\pm$ 2.49	197.0 $\pm$ 2.46
<b>50 <math>\mu\text{M}</math></b>	242.1 $\pm$ 1.54	291.9 $\pm$ 24.9	298.3 $\pm$ 0.20	194.4 $\pm$ 0.00
<b>100 <math>\mu\text{M}</math></b>	262.7 $\pm$ 2.27	317.5 $\pm$ 47.1	289.8 $\pm$ 5.38	248.1 $\pm$ 8.19

Similarly to what happened to RT10, EHTs from Experiment 1 exposed to 50  $\mu\text{M}$  and 100  $\mu\text{M}$  of NE exhibited a 20.7% and 20.4% average increase in time to achieve 90% of relaxation, while control EHTs and the ones exposed to 10  $\mu\text{M}$  suffered a 14.9% and 19.6% reduction in this parameter.

As for Experiment 2, all tissues reached 90% of relaxation slower when compared to prior to drug administration values (33.6%, 33.4%, 34.9% and 14.1% for control, 10  $\mu\text{M}$ , 50  $\mu\text{M}$  and 100  $\mu\text{M}$  tissues, respectively).